The Pennsylvania State University

The Graduate School

College of Engineering

NUMERICAL MODEL FOR ISOBARIC STEAM HEATING OF INITIALLY SATURATED

PACKED BEDS

A Dissertation in

Agricultural and Biological Engineering

by

Haijun Wu

Submitted in Partial Fulfillment
of the Requirements
for the Degree of

Doctor of Philosophy

December 2009

The dissertation of Haijun Wu was reviewed and approved* by the following:

Paul N Walker
Professor of Agricultural and Biological Engineering.
Dissertation Advisor
Chair of Committee

Virendra M Puri
Distinguished Professor of Agricultural and Biological Engineering

Paul H Heinemann
Professor of Agricultural and Biological Engineering

Savas Yavuzkurt
Professor of Mechanical Engineering

Roy E Young
Professor of Agricultural and Biological Engineering
Head of the Department of Agricultural and Biological Engineering

*Signatures are on file in the Graduate School

ABSTRACT

Pressurized-steam segmented-flow aseptic processing (PSAP) is a novel technology being developed to process particulate foods, e.g. mushrooms, soybeans, beans, peas, apple slices, corn, etc. For the commercial application of this system, it is essential to model the heat and mass transfer, steam distribution and penetration in the heating of those foods. Models will be helpful in adjusting the segmented-flow aseptic processing system in order to process different particulate foods in this system. Such capability can bring great benefits to the food and agricultural industry of the Commonwealth of Pennsylvania and beyond.

For modeling purposes, each segmented unit in PSAP was simplified to be a packed bed. Glass beads with 2, 3, and 5 mm diameter were used to simulate the particulate foods. In preliminary experiments, a capillary fringe (CF) was observed, which was a region with 100% water saturation existing at the bottom of packed beds after vertical drainage. CF prevented steam from penetrating the whole bed and slowed down the heating, which is a negative effect.

Four major heat transfer mechanisms were important in this research: conduction, convection, condensation, and steam penetration. Although many researchers have modeled these processes, there was no applicable, integrated model available for predicting the temperature changes in the packed beds with the same scenario as in PSAP. The overall objective of this research was to develop a numerical model to simulate the heat and mass transfer in packed beds during isobaric steam heating so that the maximum bed depth can be determined, with which the temperature distribution from top to bottom of packed bed is still uniform.

Firstly, the characteristics of packed beds were studied. Although different sizes of glass beads have different particle densities and bulk densities, the porosity turned out to be the same, 0.46, for each size of glass beads. The sphericities were 0.989, 0.991, and 0.992 for 2, 3, and 5 mm glass beads, respectively, suggesting ideal spheres of the glass beads. The measurement of static holdup showed that at 1 cm above upper boundary of capillary fringe in packed beds, static holdup decreased rapidly from 0.46 to 0.024, while above that elevation it remained almost constant at 0.24. Under low water flux, the water flow velocity (parent velocity) in packed bed had positive polynomial relationship with dynamic holdup. Under high water flux, the relationship between dynamic holdup and water flow velocity was assumed to be linear, based on the literature. The capillary fringe thickness were 2.4, 1.4, 0.6 cm for 2, 3, and 5 mm glass beads, respectively, under atmospheric pressure. Less thickness of capillary fringe was expected for packed beds at high temperature due to the decreased surface tension of water.

A PSAP simulator was designed and built, and steam heating experiments were performed to investigate the temperature histories in packed beds with different bed depths and particle diameters. By modifying the experimental setup, temperature and weight changes in packed beds in steam heating were simultaneously measured. The general trend of temperature change of packed bed in steam heating was that the elevations from top to bottom were heated in order, and the bottom portion, CF, was heated much slower than other elevations. Further studies showed that with the decrease of particle diameter and increase of bed height, it took longer time for CF to reach a target accomplished temperature fraction (ATF).

The overall scheme for developing the numerical model was to divide the unsaturated flow zone (UFZ) and CF into N and M finite layers, in which the energy and

mass balances were developed. Finite difference method was used to develop this numerical model, which was programmed and solved in an Excel spreadsheet. Model validation showed that after calibration of two parameters the one-dimensional numerical model performed well in predicting temperature and mass change, local porosity and liquid holdup and lethality, etc, in each layer.

A comparison of heating time versus bed depth showed that the predicted and observed data had the same trend and were close to each other, which doubly confirmed that the model works well.

TABLE OF CONTENTS

LIST OF FIGURES

LIST OF TABLES

NOMENCLATURE

A   = surface area, m^2; heat transfer area, m^2

Ac   = cross-sectional area of packed bed, m^2

A_{ve} = surface area of volume-equivalent sphere, m^2

Bi   = Biot number

c   = condensation coefficient constant,

c_p = specific heat, J/(kg·K)

D   = mass diffusivity, m^2/s

D_{AB} = mass diffusivity between species A and B, m^2/s

d   = diameter, m

E_{incon} = energy flow by conduction, J

E_{inma} = energy inflow with mass flow, J

E_{outcon} = energy outflow by conduction, J

E_{outma} = energy outflow with mass flow, J

Eo   = Eötvös number,

F   = mass flow speed, m/s

Fo   = Fourier number,

g   = acceleration of gravity, (m/s^2)

h   = convection coefficient, W/(m^2·K)

h_a = condensation coefficient, W/(m^2·K)

h_{fg} = enthalpy of vaporization, J/kg

H_{fg} = latent heat of steam, J/kg

H_{fg}' = modified latent heat of steam, J/kg

H   = height, m

H_u = height of unsaturated flow zone (UFZ), m

I = diameter along the intermediate axe of the particle, m

j = diffusive mass flux relative to mass average velocity, kg/s·m^2

k = thermal conductivity, W/(m·K)

k_f = thermal conductivity of fluid, W/(m·K)

L = length, m; Long axes, m

L_c = characteristic length, m

m = mass, kg

m_A = mass fraction of species A

N = total layers of unsaturated flow zone

n = layer number in unsaturated flow zone

O = observed data

P = predicted data

q'' = heat flux, W/m^2

$\bar{q}$ = generated heat, W

Q = Energy (in UFZ), J

R_p = radius of a sphere, m

r = radial distance, m

s = saturation (percentage of liquid volume per void volume), dimensionless

T(x, y, z) = scalar temperature field, K

t = time, s

t_{step} = time step, s

T_a = ambient temperature, K

T_g = temperature of steam, K

T_i = initial temperature, K

T_{cush} = current temperature in each shell of solid particle, K

T_{lav} = average liquid film temperature, K

T_{presh} = predicted temperature in each shell of solid particle, K

T_w = wall temperature, K

T_∞ = ambient temperature, K

T^* = function of dimensionless head

V_t = total volume of packed bed, m^3

V_f = fluid volume, m^3

V_v = void space volume, m^3

W = volume of mass, m^3/s

w = mass flow speed, m/s

x, y, z = coordinate system

Greek Symbol

α = thermal diffusivity, m^2/s

β_{dy} = dynamic liquid holdup

β_s = static liquid holdup

β_t = total liquid holdup

δ = thickness of liquid film

ε = porosity

θ = polar angle, rad

θ_i = temperature difference between initial temperature and ambient

temperature, K

θ_t	= temperature difference between transient and ambient temperature, K
θ_c	= dimensionless temperature of center
Φ	= dimensionless heat transfer rate
ϕ	= azimuthal angle, rad; degree of true sphericity
λ	= volume fraction
σ	= surface tension, N/m
ρ	= mass density, kg/m^3
ρ_b	= bulk density, kg/m^3
ρ_s	= solid density, kg/m^3
ρ_m	= mixed density, kg/m^3
μ	= root of a transcendental equation; dynamic viscosity, kg/(s·m)

Subscripts

CF	= capillary fringe
con	= conduction
cond	= condensation
ef	= effective
f	= fluid
fl	= liquid film
g	= gas/steam
l	= liquid
in	= inflow

ini   = initial

L   = layer

lav   = average value (temperature, mass, etc.) of liquid film

low   = lower boundary

m   = layer number in capillary fringe

out   = outflow

p   = particle

s   = solid

sh   = shell

st   = stored

up   = upper boundary

Superscript

j   = time step

p   = power number

Abbreviation

ATF   = accomplished temperature fraction

CF   = capillary fringe

CFD   = computational fluid dynamics

CFT   = capillary fringe thickness

DH   = dynamic holdup

FD   = finite difference

FDM   = finite difference method

FEM = finite element method

ID = inside diameter

OD = outside diameter

PDF = partial differential equation

PSAP = pressurized-steam segmented-flow aseptic processing

RMSE = root mean square error

RTD = residence time distribution

SD = standard deviation

SH = static holdup

UFZ = unsaturated flow zone

UTF = unaccomplished temperature fraction

ACKNOWLEDGEMENTS

Dedicated to

my wife Du Wen

and my daughters Selina and Emma

for their unconditional love and support

CHAPTER 1

INTRODUCTION

Aseptic processing is a technology of continuous food sterilization, cooling, and subsequent filling of the food product into sterilized containers or packages under sterile conditions. Segmented-flow is a processing method in which the processing flow is divided into discrete elements so no mixing of particles occurs between upstream and downstream elements, hence, in segmented-flow every unit has the same time of processing.

Pressurized-steam segmented-flow aseptic processing (PSAP) is the integration of steam infusion and segmented-flow method to aseptic processing. It is a novel technology developed to process particulate food materials, e.g. mushrooms, soybeans, beans, peas, apple slices, corn, etc. (Anderson and Walker, 2005). PSAP utilizes high temperature, short time (HTST) processing conditions, eliminates a separate blanching step, eliminates the unnecessary packaging of water and promotes the use of bag-in-box and other versatile aseptic packaging methods (Anderson, 2006). As shown in Figure **1-1**, the raw food particles after preprocessing are conveyed through a tube where the particles are first submerged in water and then carried through a saturated steam environment. The water minimizes the amount of air that enters with the particles and prohibits steam from exiting as the food enters. Once food particles are moved from the water at the lower portion of the sterilization chamber, they are heated under pressure directly with condensing steam—a process commonly called steam infusion. The incline of the conveyor and the presence of flights doubly ensure that no particle advances faster —or slower—than the conveyor itself (Anderson and Walker, 2005), so

the food particles move at a fixed speed, which can be adjusted by the speed of the conveyor motor, through the heating and holding section on the conveyor belt until commercial sterilization is reached. Food particles next fall from the conveyor into the vertical tube filled with counter-flow chilled water, and finally drop through a pressure lock to the packaging unit.
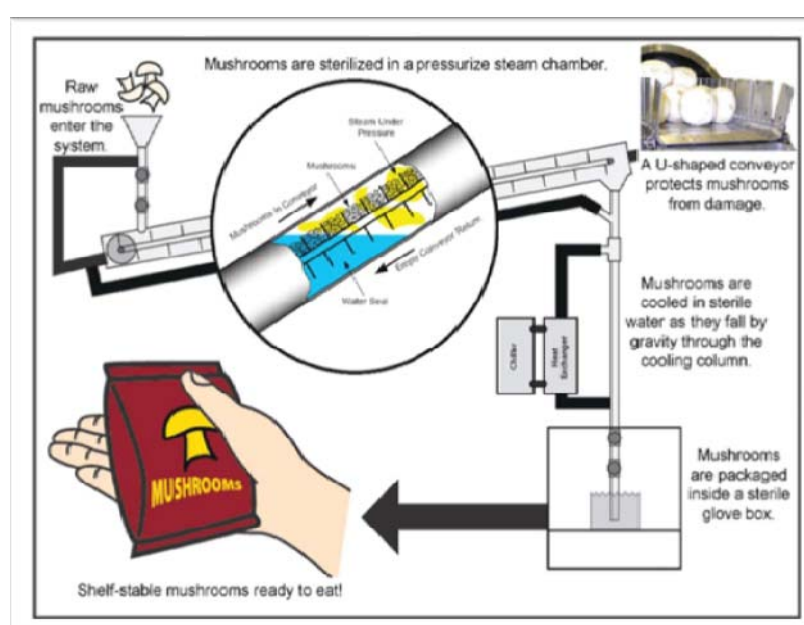
Figure **1-1**: Segmented-flow aseptic processing system (Anderson, 2006).

PSAP is an innovative way to allow particulate foods to be processed aseptically with obvious advantages compared to traditional, continuous aseptic processing and conventional canning processing (Walker and Beelman, 2002). The primary advantage of segmented-flow aseptic processing is the ability to control residence time precisely in a continuous process – whether that process is holding, heating, or cooling.

Anderson (2006) and Oner (2007) have proven for mushrooms and apples, respectively, that segmented-flow aseptic processing gave better yield and quality than

conventional canning. Their research was conducted using a pilot scale processing system as shown in Figure **1-1**.

When this technology is applied commercially, it will be important to maximize the throughput for a given food and size processor. Different foods have different properties (e.g. food particle size, specific heat, bed porosity, etc.) and behave differently in steam processing. For each different food, hence, the operational condition of full-scale production, such as residence time, temperature in food particles and food bed, bed depth, steam pressure, flow rate, feed rate and packaging system should all be adjusted to achieve commercial sterilization and optimal food quality. Among these parameters, bed depth would be the most complex and important determinative factor for the performance of steam in the system. In other words, at what bed depth do particles at the top, bottom or middle of the bed heat more slowly than particles at other elevations. Thus, it was mandatory to investigate and model the heat and mass transfer in packed beds of food particles in a steam environment to determine and understand the effect of bed depth.

Although steam is commercially employed to sterilize and blanch food products, there was a lack of readily available data that can be used with confidence to simulate packed bed heating of particulate food by pressurized steam. The overall goal of this research was to develop and validate a mathematical model of heat and mass transfer inside the packed beds so the optimum bed depth could be determined. The model would be helpful in adjusting the segmented-flow aseptic processing system to process different particulate foods in this system.

CHAPTER 2

LITERATURE REVIEW

This literature review introduces the readers to continuous aseptic processing, conventional canning processing, and recent studies on modeling of heat and mass transfer within food particles and within packed beds.

2.1 Conventional Canning System

Thermal processing is sometimes defined as the heat treatment of packaged foods to bring about microbiological safety. Much of the analysis of thermal processing has been developed for foods placed in glass or metal containers. Often the container is a cylindrical metal can made from thin tin-plated steel or aluminum, and is heated by steam. This process is often referred to as 'canning' (Smith, 2003).

Despite the widespread popularity of canned foods, the major limitation of canning is in the quality of the final products. Since food is not a good conductor of heat, excess temperature needs to be applied to the container's surface for a long enough period of time to guarantee sufficient heat at the center, or "cold spot", in order to destroy all organisms that cause spoilage and disease. This method of preserving by 'canning,' causes foods to lose juices, texture, flavor, and nutrients. The cost of energy is also a significant problem of the total cost of processing canned foods, especially heating and cooling, which are two unit operations where energy consumption is substantial. Another shortcoming for canned food is the low yield, the productivity per unit time, with batch processing.

2.2 Continuous Aseptic Processing

Aseptic processing is a technology of continuous food sterilization, cooling, and subsequent filling of the food products in sterilized containers or packages under sterile conditions. The major advantages of aseptic processing include less damage to the processed product, improved product quality, reduced packaging cost and energy consumption, and ready adaptability to automatic control (Liu, 1994).

The thermal death time F is the total time required to accomplish a stated reduction in a population of vegetative cells or spores (Singh and Heldman, 2001). It should be noted that thermal death time F decreases as temperature increases, hence, high temperatures inactivate microorganisms more rapidly than lower temperatures. High temperature, short time (HTST) systems are predominantly used to commercially sterilize liquid foods. With shortened processing time, quality degradation can be minimized while still achieving the commercial sterilization.

In a continuous processing system, residence time is defined as the time period for which a differential volume of food resides within the holding tube. The purpose of a "holding tube" is to retain the food product at certain temperature within the aseptic system for the minimum period of time required. In a conventional holding tube not all differential volumes have the same residence time, even for homogeneous liquids, and so the residence time is represented as a distribution of residence times (Anderson, 2006).

Since virtually all the particles have a longer residence time than the minimum, then virtually all the particles will be overcooked, as shown in Figure **2-1** .
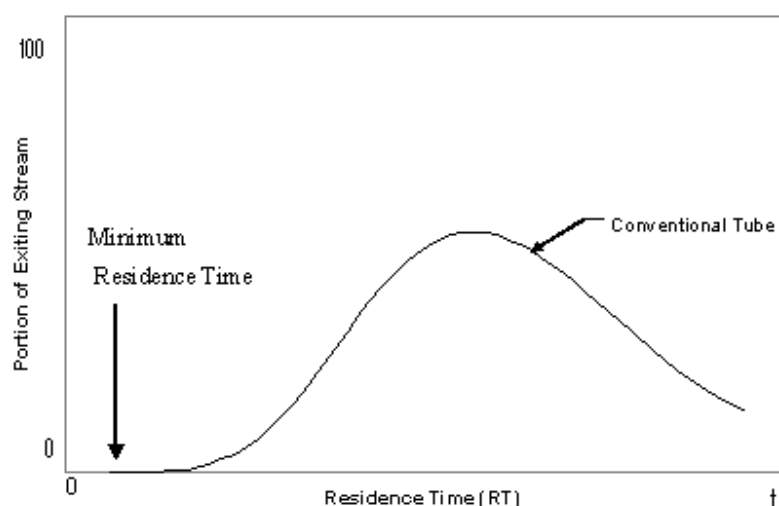
Figure **2-1**: Residence time distribution of particles in a conventional holding tube (from Walker and Beelman, 2002).

In the U.S, the lack of practical technology for predicting or controlling the residence time of particles in the holding tube of the food processing system has prevented continuous aseptic processing of foods from commercial application (Walker and Beelman, 2002). Several researchers have investigated the residence time distribution (RTD) in continuous processing system. For example, Alhamdan and Sastry (1997) studied RTD of particle food flowing in a holding tube, as affected by particle shape, particle concentration, particle type, fluid viscosity, and bulk flow rate. Abdelrahim (1997) investigated RTD of meat and carrot cubes in the holding tube of a commercial pilot scale aseptic processing system using a full factorial design. However, all these studies only focused on describing and predicting the RTD of particulates in the holding tube but failed to provide a practical technology for controlling the residence time distribution of particles in aseptic processing systems.

Per the Food and Drug Administration (FDA), currently only the time that the food is within the holding tube can be counted as the lethality time for microorganisms in a

conventional aseptic processing system. The reason for excluding the time in heat exchangers is that the residence time of both fluid and particle elements are highly variable in these units (Walker and Beelman, 2002). However, the segmented-flow controls the residence time in tubular heat exchanger. If FDA could approve that using segmented-flow heating allows the residence time in the heat exchangers to be counted toward microbial lethality, the food quality would be further improved by further shortening thermal treatment time while still achieving commercial sterility (Walker and Beelman, 2002).

2.3 Segmented Flow Aseptic Processing

Segmented-flow is achieved by installing a series of barriers into the processing flow. Particles are trapped between the barriers so that the residence time of the particles is the same and is controlled by the speed of the barriers (Walker and Beelman, 2005). Segmented flow can precisely control the residence time through the entire aseptic processing operation, though most of the advantages still come from controlling the residence time in the holding tube. The segmented-flow device (U.S. Patent No. 6,457,513) is a technology invented at Pennsylvania State University specifically for the aseptic processing of low acid foods (pH>4.6) with large particles, such as mushrooms, potatoes, green beans, beef stews, and macaroni and cheese (Walker and Beelman, 2002). Such a segmented-flow system provides precise control of residence time of particles in a continuous process by allowing food to travel through the sterilization system at a prescribed rate. A complete pressurized-steam segmented flow aseptic processing system is shown in Figure **2-2**.
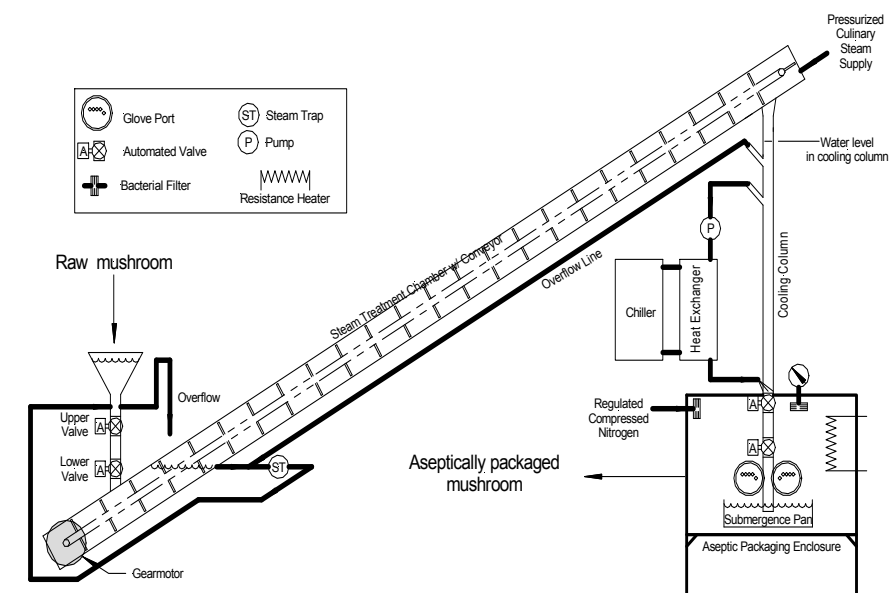
Figure **2-2**: Conceptual design of aseptic mushroom processing system (from Anderson, 2006).

As shown in Figure **2-2**, vacuum hydrated food particles enter the sterilization chamber submerged in water through two three-inch sanitary ball valves. The water prohibits air from entering the system. Computer controls are used to cyclically open and close the valves to feed food particles into the sterilization chamber (Anderson, 2006). Once falling into the water at the lower portion of the chamber, food particles are trapped into a U-shaped cross-section conveyor which was designed to support food particles from the bottom and sides and prevent the food particles from contacting the tube wall. Food particles are carried on through the sterilization chamber by the conveyor which is driven by an adjustable speed motor at the bottom of sterilization chamber.

Once food particles are carried out of water at the lower portion of the inclined sterilization chamber, they are heated under pressure directly with saturated condensing steam. Pressurized saturated steam can provide much higher and more uniform heat transfer rate than hot liquid water, so the processing time is shortened to minimize the

damages of color, texture, and flavor of food particles by heat. Food particles are moved at a fixed speed on the conveyor belt both in the heating and holding sections; the steam temperature and belt speed are adjusted appropriately to render food particles commercially sterile. At the end of the inclined sterilization chamber, food particles fall from the conveyor into the counter-flow, direct-contact water cooling section which is constructed as a pressurized, vertical column of chilled water. A double-valve system, identical to that used for product entry, is used to transfer cool, processed food particles from the pressurized cooling column into the sterile glove box at atmospheric pressure where manual packaging occurred.

Anderson (2006) configured this system successfully to be capable of aseptically processing and packaging mushrooms and similar particle materials easily susceptible to mechanical damage. When compared to conventionally canned mushrooms, aseptically processed yield (weight basis) increased 6.1% (SD=2.9%) and 6.6% (SD=2.2%), whiteness (L) improved 3.1% (SD=1.9%) and 4.7% (SD=0.7%), color difference (ΔE) improved 6.0% (SD=1.3%) and 8.5% (SD=1.5%), and texture improved 3.9% (SD=1.7%) and 4.6% (SD=4.2%), for whole and sliced mushrooms, respectively. The overall result proved that the segmented flow aseptic processing obtained superior quality over conventionally canned mushrooms. The processing time designed for this aseptic processing was based on the temperature penetration experiments using microbiological kinetics of *Clostridium sporogenes* spores.

Based on the mushroom research of Anderson (2006), Oner (2007) investigated the processing results of apple slices using both PSAP and conventional canning. Compared to conventionally canned apple slices, aseptically processed yield (weight basis) increased 14.5% and 12.5%, whiteness improved 1.8% and 4.2%, color

difference improved 2.01% and 4.57% and texture improved 45.4% and 80.7%, for

mean and mean plus 2 standard deviation times, respectively.

In summary, pressurized-steam segmented flow aseptic processing system is a

novel technology for aseptically processing of particulate foods. Walker and Beelman

(2002; 2005) summarized the advantages of segmented-flow aseptic processing

compared to conventional canning as follows:"

1. Segmented flow provides a shorter and more precisely controlled cooking time to minimize overcooking and, thereby, to increase quality and value of processed foods.

2. Reduces shrinkage and weight loss results from reduced cooking during processing.

3. Replaces blanching and retort cooking units into a single processing unit. Traditionally, some foods are blanched before being placed in cans and cooked. With segmented flow the foods are placed in containers after cooking so the cooking step also serves the blanching function.

4. Reduces processing energy and water consumption because blanching may be eliminated.

5. Allows packaging material alternatives such as plastic pouches, bag-in-box, and bag-in-drum. With segmented flow aseptic processing the food container does not move through the cooking process and so containers other than cans and jars can be used. Plastic pouches or similar alternatives can be considered. This is a big benefit particularly in food service applications where there are disposal and safety issues with metal cans and glass jars.

6. Allows packaging in large containers such as 450 kg totes for further processing applications. Such large containers are not practical in conventional canning because the long heating and cooling time would result in severe overcooking. In segmented flow processing, the problem is avoided because the product is heated and cooled outside the container.

7. Allows packaging with minimal liquid. In canning processing, virtually all the voids must be filled with liquid to maximize heat transfer. But in segmented flow aseptic processing much of this liquid can be recycled or discarded after cooking to reduce package weight and to minimize handling and shipping costs.

8. Increases the profitability of the food industry. The main benefit will be a superior shelf-stable food product which will sell for a premium price. Substantial energy and water cost savings will also result as described above.

9. Is transferable and applicable to other Pennsylvania fruit and vegetable crops. Like for any process, the technique must be optimized for each food to get maximum benefit.

10. And, like canning, segmented flow processing can be scaled to any size production line, e.g. 4500 kg/hr."

2.4 Heat and Mass Transfer through Packed Beds in Segmented-Flow Aseptic Processing

In the food industry, fully-cooked products are a rapidly increasing portion of total product sales, with pre-cooked, refrigerated products projected to account for 80% of the industry's growth by the year 2005. Therefore, thermal processes are increasingly important in determining the safety and quality of retail products. The design and operation of these processes also influence the productivity, which is an important economic factor for the industry. In order to analyze and improve these processes, considerable previous investigations have focused on simulation of heat penetration and moisture diffusion in food products under various thermal conditions.

Heating (i.e. for drying, cooking or sterilization) and cooling (i.e. chilling and cold storage) are common thermal processes in the food industry. These thermal-processing techniques are widely used to improve quality and safety of food products, such as to reduce the microbial population, inactivate enzymes, reduce the product moisture, modify the functionality of certain compound, and extend shelf life of the products.

The first step in understanding heat transfer is to define what heat is and how it diffuses through a single body or is transferred from one body to another (Welti-Chanes et al., 2004). The temperature gradient is the driving force in heat transfer processes

(Otero and Sanz, 2003). Heat transfer plays a central role in all thermal processing of food products. Studying and understanding the heat transfer mechanism in high-pressure food processing can lead to better control for avoiding under- or over-processing.

Four major heat transfer mechanisms were important in this project: conduction, convection, condensation, and steam penetration. The steam penetrates the packed bed from top and bottom and heats the particles while condensing into water. The resulting condensate then flows down from upper elevations to lower elevations coating the particles with a flowing layer of water. The heat transfer from steam to the water layer is by condensation, while the transfer of heat within the water layer and the transfer of heat within the particulate foods, from the outer layer to the center of beans occur by convection and conduction, respectively.

In PSAP as shown in Figure **2-2**, every segmented unit is essentially identical and subjected to the same treatment. Moreover, the food particles move through the steam environment on a conveyor and it is most cost effective to put a thick bed of particles on the conveyor so that large quantities of food particles can be processed with given size machine. For modeling purposes the food particles in every segment can be treated to be a packed bed unit.

A packed bed is a hollow tube, pipe, or other vessel filled with a packing material to create a porous bed. Packed beds are extensively used for catalytic reactors, separation processes, or distillation processes in chemical engineering or process industries. The term packed bed refers to a condition for which the position of the particles is fixed. In contrast, a fluidized bed is one for which the particles are in motion due to advection with the fluid. As an analog of packed beds, porous media refers to

"solids" with "holes", i.e. presenting connected void spaces, distributed – randomly or quite homogeneously – within a solid matrix.

2.4.1 Heat and Mass Transfer inside Food Particles

Conduction of heat takes place from the liquid film/particle interface to the center of the particle after the steam has condensed on the surface of the particle. The principles of thermal processing of solid foods are based on heat and moisture exchanges between a solid food body and the medium flow. Heat transfer through a solid is normally described by Fourier's law as shown in Eq. **2.1** and moisture transfer is generally modeled by Fick's law of mass diffusion which is show in Eq. **2.2**:

$$q'' = -k\nabla T = -k(i\frac{\partial T}{\partial x} + j\frac{\partial T}{\partial y} + k\frac{\partial T}{\partial z}) \qquad\qquad \textbf{2.1}$$

$$j_A = -\rho_A D_{AB}\nabla m_A \qquad\qquad \textbf{2.2}$$

where q'' is the heat flux, k is the thermal conductivity, ∇ is the three-dimensional del operator, $T(x, y, z)$ is the scalar temperature field, j is mass flux, ρ_A is mass density of species A, D_{AB} is mass diffusivity between species A and B, and m_A is mass fraction of species A.

The problem of transient heat transfer dominated this project, because the temperature at each point of packed bed would begin to change when the packed bed is exposed to steam environment until a quasi-steady state is reached. A simple, yet common, transient conduction problem is one for which a solid experiences a sudden change in its thermal environment. If temperature gradients within the solid may be

neglected, a comparatively simple approach, termed the lumped capacitance method, may be used to determine the variation of temperature with time:

$$t = \frac{\rho_s V c_p}{hA} \ln \frac{\theta_i}{\theta_t}$$

2.3

where ρ_s is solid density (kg/m^3), V is total volume of solid (m^3), c_p is specific heat (J/kg·K), A is surface area (m^2). $\theta_i = T_i - T_\infty$ is the temperature difference (K) between initial temperature (T_i) and infinite temperature (T_∞); $\theta_t = T - T_\infty$ is temperature difference between transient temperature (T) and infinite temperature (T_∞).

The lumped capacitance method, however, is appropriate only if the following condition is satisfied (Incropera and Dewitt, 2002):

$$Bi = \frac{hL_c}{k} < 0.1$$

2.4

where h = convection coefficient,

L_c = characteristic length.

k= conductivity of object

In most of the cases in food engineering, however, the temperature gradient inside food particles is not negligible. The general form of the 3-D heat diffusion equation in Cartesian coordinates is

$$\frac{\partial}{\partial x}\left(k\frac{\partial T}{\partial x}\right) + \frac{\partial}{\partial y}\left(k\frac{\partial T}{\partial y}\right) + \frac{\partial}{\partial z}\left(k\frac{\partial T}{\partial z}\right) + \overline{q} = \rho c_p \frac{\partial T}{\partial t}$$

2.5

where *x, y, z* is coordinate system, $\overline{q}$ is generated heat, ρ is density, c_p is specific heat, *T* is temperature and *t* is time. This equation, usually known as the heat diffusion equation, provides the basic tool for heat conduction analysis. It is often possible to work

with simplified versions of Eq. **2.6** if the thermal conductivity is a constant and no energy generation:

$$\frac{\partial^2 T}{\partial x^2} + \frac{\partial^2 T}{\partial y^2} + \frac{\partial^2 T}{\partial z^2} = \frac{1}{\alpha}\frac{\partial T}{\partial t}$$

2.6

where $\alpha = k / \rho c_p$ is the thermal diffusivity.

In spherical coordinates the general form of the heat flux vector and Fourier's law is

$$\frac{1}{r^2}\frac{\partial}{\partial r}\left(kr^2\frac{\partial T}{\partial r}\right) + \frac{1}{r^2\sin^2\theta}\frac{\partial}{\partial\theta}\left(k\frac{\partial T}{\partial\phi}\right)$$
$$+ \frac{1}{r^2\sin\theta}\frac{\partial}{\partial\theta}\left(k\sin\theta\frac{\partial T}{\partial\theta}\right) + \overline{q} = \rho c_p\frac{\partial T}{\partial t}$$

2.7

where r, ϕ, θ, are spherical coordinates (shown in Figure **2-3**).
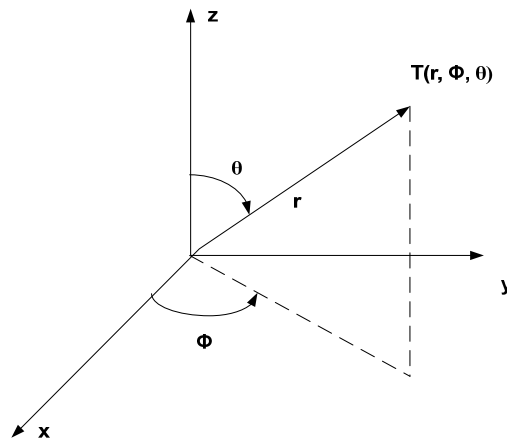
Figure **2-3**: Heat conduction in spherical coordinates.

Heat and mass transfer in particulate foods/spheres subjected to thermal processing is well known, and a very large collection of data for physical,

physicochemical, and thermal properties of foods have been published. The pioneer

research of Lenz and Lund (1973) presented the heat/hold solution for spheres of food

given by Eq. **2.8** and mass average temperature (Carslaw and Jaeger, 1959) given by

Eq. **2.9**, assuming isotropic behavior for the products being considered.

$$[(T - T_i)/(T_a - T_i)] - [(\langle T \rangle - T_i)/(T_a - T_i)] = [(T - \langle T \rangle)/(T_a - T_i)] =$$
$$\frac{2}{\pi \rho} \sum_{n=1}^{\infty} \sum_{k=1}^{\infty} \exp(-\alpha_n^2 Fo_t - k^2 \pi^2 Fo_\tau) \sin(\alpha_n \rho)[(\alpha_n^2 + 1)/\alpha_n^2][(-1)^k / k] \qquad \textbf{2.8}$$
$$[(\sin(\alpha_n - k\pi)/\alpha_n - k\pi) - (\sin(\alpha_n + k\pi)/\alpha_n + k\pi)]$$

$$[(\langle T \rangle - T_i)/(T_a - T_i)] = 1 - (6/\pi^2) \sum_{k=1}^{\infty} (1/k^2) \exp(-\pi^2 k^2 Fo_\tau) \qquad \textbf{2.9}$$

where

T = temperature at a given point

T_a = ambient temperature

T_i = Initial temperature

<T> = mass average temperature

$(T_a-T)/(T_a-T_i)$ = unaccomplished temperature

$(T-T_i)/(T_a-T_i)$ = accomplished temperature

$(Ts-<T>)/(T_s-T_i)$ = unaccomplished mass average temperature

$(<T>-T_i)/(T_s-T_i)$ = accomplished mass average temperature

r = radial distance to a desired point

R_p= radius of a particle

ρ = r/R

k = thermal conductivity

Fo_t = holding Fourier number = kt/R^2

Fo_τ = heating Fourier number = kτ/R^2

t = holding time

τ = heating time

α = roots of the equation.

These equations (Eq. **2.8** and Eq. **2.9**) were programmed on computer and the results used to establish charts for predicting temperatures as a function of heat/hold time.

Similar to Lenz and Lund's research (1993), Dincer (1994) investigated the unsteady heat transfer of spherical fruit to air flow. Assuming (i) unsteady conditions existed; (ii) the rate of heat transfer in the radial direction of the spherical product was much less than in any other directions; (iii) the spherical product was homogeneous and isotropic. (iv) the initial temperature and water content of the product were uniform; (v) the temperature and thermophysical properties of the cooling medium were constant; (vi) the thermal conductivity, thermal diffusivity and specific heat were constant, the dimensionless center temperature distribution and the heat transfer rate, respectively, were given as

$$\theta_c = \sum_{n=1}^{\infty} \left[(2Bi \sin \mu_n)/(\mu_n - \sin \mu_n \cos \mu_n) \right] \exp\left(-\mu_n^2 Fo\right) \qquad \textbf{2.10}$$

$$\Phi = \sum_{n=1}^{\infty} \left[\left(6Bi^2\right)/\mu_n^2 \left(\mu_n^2 + Bi^2 - Bi\right)\right]\left[1 - \exp\left(-\mu_n^2 Fo\right)\right]. \qquad \textbf{2.11}$$

where θ_c = Dimensionless temperature of center, Φ = Dimensionless heat transfer rate, *Bi* = Biot number, Fo = Fourier number, and μ is root of a transcendental equation which was given as

$$\mu_n \cot g\mu_n = (1 - Bi). \qquad \textbf{2.12}$$

Particulate foods usually have neither a regular form nor isotropic behavior, which makes the modeling of these processes difficult or impractical. Moreover, some particular features of food such as non-uniform evaporation of water, crust formation or closing or opening of pores, are of such complexity that it makes the modeling of these processes even more difficult or impracticable. Nevertheless, some of these drawbacks have been overcome and the modeling of several specific practical situations is possible, mainly due to the development of knowledge of empirical relations that properly suit these specific processes (Welti-Chanes et al., 2004). Present-day numerical analytical techniques, such as the finite element method (Huan et al., 2003; Ikediala et al., 1996; Puri and Anantheswaran, 1993; Wang and Sun, 2002;), finite difference method (Akterian and Fikiin, 1994; Califano and Zaritzky, 1993; Chau and Gaffney, 1990; Erdogdu et al., 2003; Kim and Teixeira, 1997; Mohamed, 2003; Sheen et al., 1993; Sun and Zhu, 1999), finite volume method/computational fluid dynamics (Ghani et al., 1999; Scott and Richardson, 1997), allowed the modeling of situations characterized by non-uniform thermal properties that change with time, temperature and location. Moreover, an irregular shaped body may be divided into several parts and each small part is then assumed to be regular shape. The reviews of finite difference method, finite element method, finite volume method/computational fluid dynamics, and numerical modeling in the food industry were given by Welt et al. (1997), Puri and Anantheswaran (1993), Scott and Richardson (1997), and Wang and Sun (2003).

In summary, heat and mass transfer inside food particles has been studied for decades, and numerical methods are useful for estimating the thermal behavior of foods under complex but realistic conditions such as variation in initial temperature, non-linear and non-isotropic thermal properties, irregular-shaped bodies and time dependent boundary conditions (Puri and Anantheswaran, 1993).

2.4.2 Condensation and Convection

Condensation occurs when the temperature of a vapor is reduced below its

saturation temperature. In industrial equipment, the process commonly results from

contact between the vapor and a cool surface. The latent energy of the vapor is released,

heat is transferred to the surface, and the condensate is formed (Incropera and DeWitt,

2002). If the surface is wettable with the condensate, a continuous condensate film

forms on the surface and filmwise condensation occurs. Conversely, if the surface is not

wettable with the condensate, a series of condensate droplets form on the surface (i.e.,

dropwise condensation occurs) (Faghri and Zhang, 2006). In PSAP, the vacuum

hydration and material handling are adapted to reduce or eliminate air in the intercellular

and extracellular spaces of foods. Therefore, the surface of each particle is wetted and

surrounded by water, and filmwise condensation takes place when steam meets the

particle surface.

Few practical models were available for film condensation on the surface of

granular foods, and most of the research found in the literature focused on film

condensation on the surface of a plate or tube. The pioneer work was on plates and was

reported by Nusselt (Incropera and DeWitt, 2002), who formulated the problem in terms

of simple force and heat balances within the condensate film. The average value of the

heat-transfer coefficient, $\bar{h}$, for laminar flow on vertical plate can be obtained as:

$$\bar{h} = 0.943 \left[\frac{\rho_f(\rho_f - \rho_g)gh_{fg}k_f^3}{L\mu_f(T_g - T_w)} \right]^{1/4} \qquad \textbf{2.13}$$

where:

L = the length of the plate,

g = acceleration of gravity,

h_{fg} = enthalpy of vaporization,

k_f = thermal conductivity of fluid,

μ_f =dynamic viscosity of fluid,

ρ_f = density of condensed fluid,

ρ_g = density of steam,

T_g = Temperature of steam,

T_w = Temperature of wall.

For laminar film condensation on horizontal tubes, Nusselt obtained the relation as follows (Holman, 1997):

$$\bar{h} = 0.725 \left[\frac{\rho(\rho - \rho_v)gh_{fg}k_f^3}{\mu_f d(T_g - T_w)} \right]^{1/4}$$ **2.14**

where d is the diameter of the tube and other symbols are as described for Eq. **2.13**. The analysis of Popiel and Boguslawski (1975) showed that Eq. **2.14** could be used for a single isothermal sphere if the constant was changed to 0.825.

In Nusselt's model for condensation on a vertical plate, the effects of inertia forces and energy convection were not taken into account. An improvement on Nusselt's analysis was made by Rohsenow (1956). He included energy convection in the heat balance, while continuing to neglect the inertia forces. Sparrow and Gregg (1959) reformulated the problem in terms of boundary layer theory, including both convection and inertia. They showed that the effect of the inertia forces on heat transfer was fully negligible for Prandtl numbers of 10 or greater and was quite small even for a Prandtl number of one.

The first results of calculations of heat transfer at film condensation on the sphere were given by Dhir and Lienhard (1971). They used Nusselt's theory and

developed the general expression for the heat transfer coefficient on plane and axisymmetric bodies in nonuniform gravity. Subsequently, Yang (1973) presented the results of numerical solution of momentum and energy equations, describing a thin layer of condensate in the form of laminar film running downward over the sphere. He considered two cases. The first case included both the inertia forces and heat convection, and the second one excluded the inertia forces. Dhir (1975) investigated an experimental study of quasi-steady laminar film condensation of steam on single copper spheres with 1.90, 2.54, and 3.17 cm in diameters. The data were compared with the steady-state predictions of Dhir and Lienhard (1971) and Yang (1973). Next, Hu and Jacobi (1992) investigated flowing vapor which condensed onto a copper sphere. More recently, Hu (2005) investigated the condensation heat transfer of an isothermal sphere with high velocity of the vapor flow. The research pointed out that under high vapor velocity the laminar condensate flow theories were not accurate. The observed mean Nusselt number was obviously higher than that determined for low velocity.

2.4.3 Steam Penetration through Packed Bed

Condensing steam is a multiphase system because phase change is involved. Multiphase systems in which a packed bed of solid particles are permeated by gas, liquid or both, are among the most widely used in a variety of industrial activities. Examples are packed distillation and rectification columns, absorption and scrubbing equipment, trickle bed catalytic reactors, biological filters for waste water treatment, reactors with immobilized enzymes, oil shale retorts, adsorption columns for separation of noxious contaminants, preparative gas and liquid chromatography columns, nuclear pebble bed reactors, metallurgical equipment such as blast furnaces and agglomeration

machines, hydrogen accumulators on the basis of intermetallides, reactors for oxidation of organic contaminants in waste gases and exhaust gases of motor vehicles, heat exchangers, water cooling towers, and others (Stanek, 1994).

Heat transfer plays a crucial role in determining the performance of packed beds in thermal processing or high-pressure processing and has therefore been a subject of numerous investigations over the past few decades. These studies addressed fluid-packed particle heat transfer, transient response of packed beds, and various effective parameters under the unsteady-state including effective axial and radial thermal conductivities, wall to fluid heat transfer coefficient and overall heat transfer coefficient. Specchia and Baldi (1977) examined the pressure drop and liquid holdup for concurrent downward two-phase flow in packed beds. Good correlations of these parameters either for non-foaming or foaming systems were obtained by considering two main hydrodynamic regimes, a poor and a high interaction regime. Beasley and Clark (1984) investigated the transient response of a packed bed thermal storage unit. A 2-D finite-difference model was developed to predict the two-dimensional transient response of both solid and fluid phases. The research utilized air as the working fluid, and no phase change was involved. More recently, Crone et al. (2002) presented an analytical model for the description of multicomponent and multiphase flows with phase change in porous media. The heating steam was injected into a vertical column initially filled with glass beads, humid air and water (Figure **2-4**). The model assumed that during the steam injection, a condensation front was established, and the multiphase flow thus could be divided into five regions according to the values of the intensive variables of state. Later on Bergins et al. (2005) provided the analytical solution for this model and experiments were performed for modeling validation. The research showed that the Ergun-Equation (Ergun, 1952), including the inertial term, must be taken into consideration; otherwise the

heating times are underestimated significantly. In contrast to these approaches, the new model presented in this dissertation started from vertical drainage of packed beds, and focused on how the steam was prevented from penetrating the packed beds by capillary fringe (CF). The description of the heat transfer from the gas phase to the solid was the main goal of the modeling.
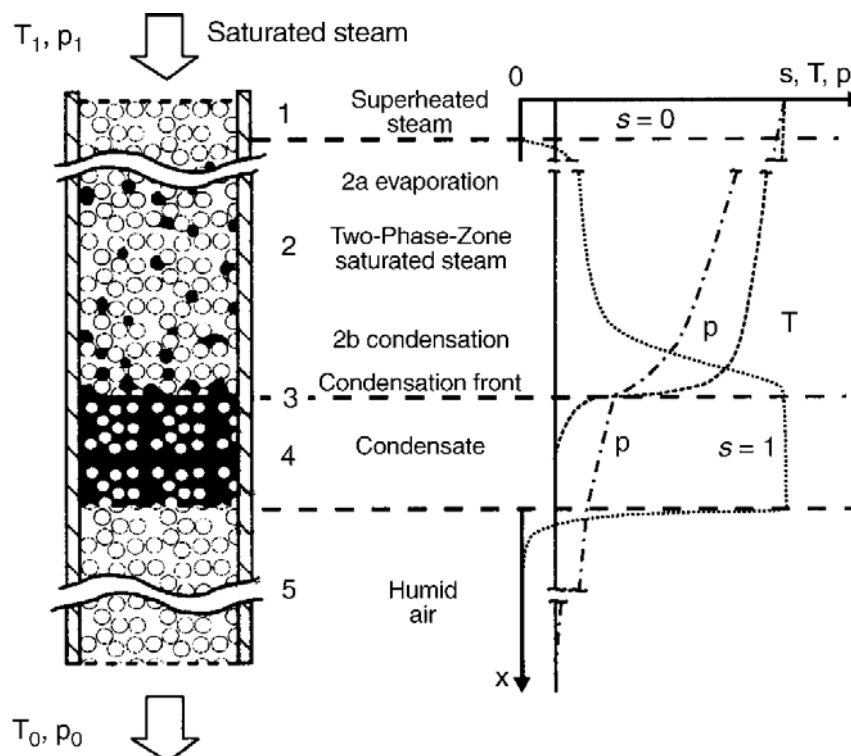
Figure **2-4**: Heating of a porous medium with steam (Crone et al., 2002)

In food engineering, it would be very desirable to assure homogeneous conditions of pressure and temperature during treatments to optimize the quality of the products from organoleptic and safety point of view. A thick packed bed will not be effective if the particles at the bottom, middle, and top of the bed are not heated at the same rate. Preliminary experiments revealed that blanching was sufficiently uniform from top to bottom for any reasonable thickness of particles unless the particles were small

enough to form a thick capillary fringe (CF). The packed beds of foods were initially

submerged under water in a pressurized-steam chamber. While the packed bed was

lifted from water to steam environment, water drained vertically and was replaced by

saturated steam and the resulting condensed water. Although most of water in the void

space of packed beds drained out in a short of time, some stayed in the space between

particles due to the liquid surface tension. A phenomenon called capillary fringe (CF)

thus occurs, as shown in Figure **2-5**.

In soil science, the CF refers to the subsurface layer, for example, in which

groundwater seeps up from a water table by capillary pressure to fill pores (Figure **2-6**).

The water table is the dividing line in the soil profile separating the unsaturated zone, in

which pore spaces are filled by a combination of water and gases, from the saturated

zone, in which essentially all pores are filled with groundwater (Trautmann and Porter,

2009). When a liquid–vapor interface is curved, a pressure difference develops across it

due to surface tension. The pressure on the convex side of the interface is higher than

that on the concave side and the pressure difference is defined as the capillary pressure,

ΔP (Hilden and Trumble, 2003). The capillary pressure of a liquid occupying some

fraction of the pore space between solid particles creates the CF which can be found in

both liquid drainage and infiltration into porous media.

Mixture of air
and solid
particles

Approximate
upper boundary
Capillary Fringe

Pore space was filled with
water

Water drained out
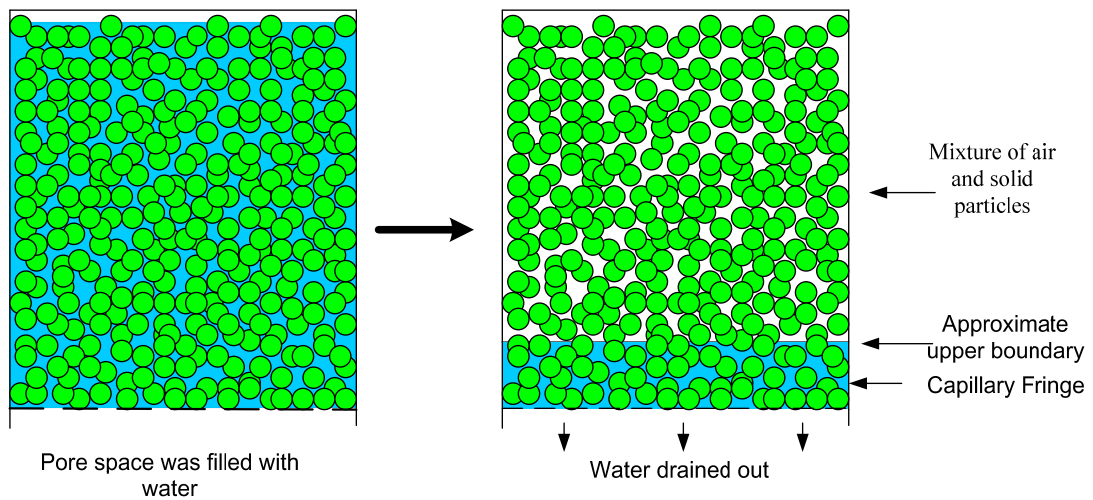
Figure **2-5**: Observation of capillary fringe after vertical drainage.

Water Content

Soil Surface

Vadose Zone

Unsaturated Zone

Depth

Capillary Fringe

Water Table

Ground Water
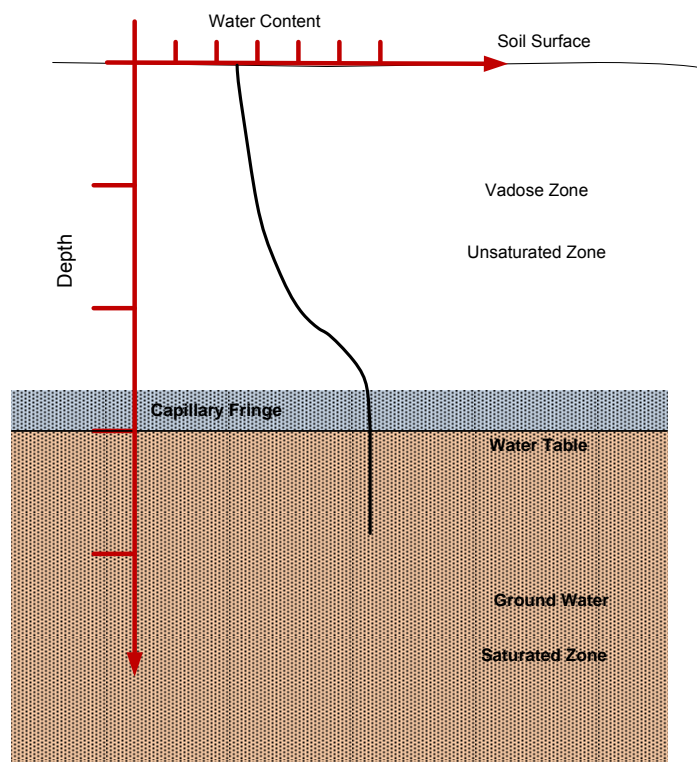
Saturated Zone

Figure **2-6**: Capillary fringe between vadose zone and saturated zone in soil.

The existence of CF, however, was a negative factor for the performance of the steam in this research because the saturated liquid in CF prevented steam from penetrating the packed bed, which slowed down the heating process. Preliminary experiments revealed that the heating of CF was much slower than upper part of the packed bed. Hence in this research, the major concern was to investigate how the CF prevented the steam from penetrating the whole packed bed.

2.4.4 Vertical Drainage in Packed Beds

Multiphase flow in packed bed in PSAP involves vertical drainage as well as steam flow. It is very important to derive the theory of the movement of water in packed beds because water flow interacts with steam flow and affects the heat and mass transfer from steam to solid particles. The flow of water in the vertical column can be divided into the following steps:

1. The packed column is saturated with water initially.

2. Free drainage starts by gravitational forces, and water table in the packed bed drains to lower horizons. Before the water table reaches the upper boundary of CF, which exists at the bottom of packed column, saturated flow occurs below the water table, and unsaturated flow above it.

3. Saturated flow stops after water table reaches CF, then packed column is dominated by unsaturated flow.

Thus, this drainage problem can be treated as one-dimensional unsteady mass transfer with both saturated and unsaturated flow. The flux of water in porous media is given by Darcy's Law. Determined experimentally, Darcy's law is analogous to Fourier's

law in the field of heat conduction, Ohm's law in the field of electrical networks, or Fick's law in diffusion theory:

$$q = -K\left(\frac{\partial \varphi}{\partial z} - 1\right)$$ **2.15**

where q is the flux (m/s), K the hydraulic conductivity (m/s), φ the pressure head (m), z the coordinate.

Although the simulation of the movement of water through porous media is a topic encountered in many applications of advanced engineering mathematics, e.g. hydrogeology, groundwater pollution, design and safety of earth dams, soil science, chemical engineering, etc, the studies of free drainage of water through vertical packed beds initially saturated with water were not common. This was due to the fact that analytical solutions of the governing differential equations in most cases were impossible, even when rigid simplifications were accepted (Kastanek, 1971).

Youngs (1960) presented an equation to describe the yield of liquid at a given time from a freely draining column of initially saturated porous material in a gravitational field by using a "capillary tube model". This model considered the void space in porous materials as many capillary tubes of radius *r* and length *L* initially full of liquid, and the total drainage was the sum of liquid draining out from the individual capillary tubes. Fujioka and Kitamura (1964) studied the water potential distribution in soils when the water was draining from a vertical soil column into the atmosphere as shown in Figure **2-7**.
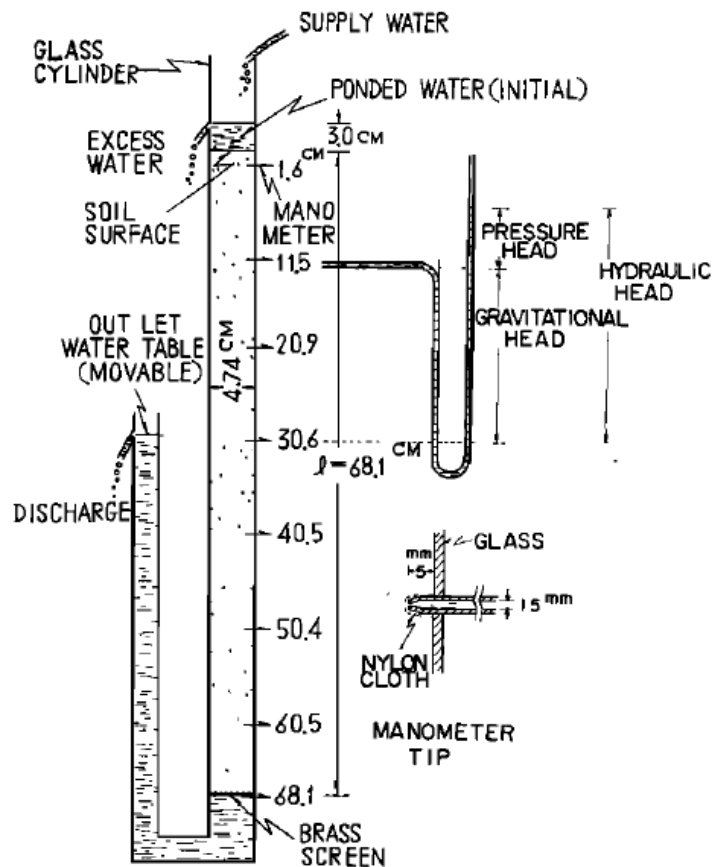
Figure **2-7**: Schematic sketch of apparatus for studying water potential in soil (from Fujioka and Kitamura,1964).

For the non-steady state when the water table disappears from the soil surface and is falling in the vertical soil column, the time required for the descent of a water table was given as (Fujioka and Kitamura,1964)

$$t = L^2 T^* / D \qquad \textbf{2.16}$$

where L is the height of column, T^* the function of dimensionless head, D the mass diffusivity. The total discharge Q at the time t from the outlet of the column was calculated by the following equation

$$\frac{Q}{Q_\infty} = \frac{1}{2} - \frac{16}{\pi} \sum_{m=0}^{\infty} \frac{(-1)^m}{(2m+1)^3} \exp\left[-\left(\frac{2m+1}{2}\pi\right)^2 T\right]$$
2.17

where Q is the cumulative outflow at time t, Q_∞ the cumulative outflow when $t \to \infty$.

Similar to Fujioka and Kitamura's equation, Raats and Gardner (1974) presented an analytical solution to water drainage in unsaturated zone of soil, as shown below.

$$\frac{Q}{Q_\infty} = 1 - \frac{32}{\pi^3} \exp-\left(\frac{\pi^2}{4} \frac{Dt}{L^2}\right)$$
2.18

where Q is the cumulative outflow at time t, Q_∞ the cumulative outflow when $t \to \infty$, D the diffusivity, t time, and L the column length. The disadvantage of the analytical solution shown in Eq. **2.18** is that it is restrictive to certain initial and boundary conditions and the medium properties.

The computer-based numerical approach allows problems of a complex nature that simulate field conditions to be readily solved. In general, the differential equations representing the flow in one or more directions are solved by finite difference techniques using computer. For one-dimensional flow in the vertical direction, the governing equation can be given as by Darcy's Law

$$\frac{\partial \theta}{\partial t} = \frac{\partial}{\partial z}\left(K \frac{\partial h}{\partial z}\right) + \frac{\partial K}{\partial z}$$
2.19

where:

θ = the volumetric water content, cm^3/cm^3,

t = time, s,

K = hydraulic conductivity, cm/s,

h = pressure head, cm,

z = vertical ordinate positive upward, cm,

The soil water diffusivity is defined as

$$D(\theta) = K(\theta)/C(\theta)$$ **2.20**

where

$$C(\theta) = d\theta/dh$$ **2.21**

is the specific water capacity. By combining Eq. **2.19** and Eq. **2.20**, Eq. **2.21** can be written as

$$\frac{\partial \theta}{\partial t} = \frac{\partial}{\partial}\left(D(\theta)\frac{\partial \theta}{\partial z}\right) - \frac{\partial K(\theta)}{\partial z}$$ **2.22**

Due to the strong nonlinear nature of Eq. **2.22**, there exists no general analytical solution. Haverkamp et al. (1977) summarized and compared six finite-difference schemes for solving Eq. **2.22** in terms of execution time, accuracy, and programming considerations.

The change of water content of packed bed at different locations in PSAP, however, is more complicated than isothermal flow of water into nonswelling unsaturated soil as studied by Haverkamp et al. (1977). Besides the flowing of water, heat and mass transfer from steam to liquid and solid particles occur at the same time, which makes the flow nonisothermal. Moreover, the infiltration model, such as presented by Haverkamp et al. (1977), does not consider the existence of a capillary fringe. Therefore, a new model is needed for the unique situation in PSAP.

2.5 Characteristics of Packed Beds

2.5.1 Sphericity

Man-made solid particles like glass beads are not perfectly spherical. A variety of empirical factors have been proposed to describe nonspherical shapes of particles.

Sphericity is the degree to which the shape of a particle approaches that of a sphere (Bates and Jackson, 1980). Sphericity could be thought of as the degree of equality of the three orthogonal axes.

Wadell (1933) proposed the "degree of true sphericity" defined as

$$\phi = \frac{A_{ve}}{A_p}$$ **2.23**

where ϕ is sphericity, A_{ve} is the surface area of volume-equivalent sphere, and A_p is the surface area of particle. For a true sphere, the sphericity is thus equal to 1. For nonspherical particles, the sphericity is always less than 1. The drawback of the sphericity is that it is difficult to obtain the true surface area of an irregular particle thus it is difficult to determine ϕ directly (Yang, 2003). Sphericity may also be more simply approximated by (Dockal, 2009)

$$\phi = \sqrt[3]{\frac{LIS}{L^3}}$$ **2.24**

where *L, I, S* are the long, intermediate, and short axes of the grain.

2.5.2 Density

Density is defined as mass per unit volume. There are three types of densities of foods, namely, solid density, particle density, and bulk density. The values of these different types of densities depend on how the pore spaces present in a food material are considered (Singh and Heldman, 2001).

If the pore spaces within food particles are disregarded, or there are none, the solid density equals the particle density. Particle density accounts for the presence of internal pores in the food particles. This density is defined as a ratio of the actual mass of a particle to its actual volume (Singh and Heldman, 2001). Glass beads have little or no internal pore spaces so particle density is equal to solid density. Bulk density is defined as the mass of particles occupied by a unit volume of bed.

2.5.3 Porosity

Porosity (ε) is defined as the ratio of extracellular void space in the bulk volume of packed beds:

$$\varepsilon = \frac{V_v}{V_b} \qquad \qquad \textbf{2.25}$$

where V_v is the void volume and V_b is the bulk volume, respectively, of the packed bed. Note that porosity can be calculated from the bulk density (ρ_b) and particle density (ρ_p):

$$\varepsilon = 1 - \frac{\rho_b}{\rho_p} \qquad \qquad \textbf{2.26}$$

2.5.4 Liquid Holdup and Liquid Saturation

Liquid holdup is an important hydrodynamic parameter in the characterization of packed beds, and has enjoyed considerable attention in the literature (Klerk, 2003). Liquid holdup is less common in research for low mass flux (<0.5 kg/(m^2·s)), but is of importance in modeling heat and mass transfer of steam condensate flow in PSAP.

Liquid holdup and liquid saturation are both used in the description of liquid retention in packed beds. Liquid holdup refers to the liquid volume per bulk volume, while liquid saturation refers to the liquid volume per void volume (Klerk, 2003). The description of liquid holdup is a further refined by the following terms:

1. Internal holdup: is the liquid holdup contained inside a porous particle in the packed bed. For nonporous particles such as glass beads there is no internal liquid holdup.

2. External holdup: is the liquid holdup not contained in particles in the packed bed. For nonporous particles such as glass beads, the external liquid holdup will be the same as the total liquid holdup.

3. Residual holdup: is the part of the external liquid holdup that remains in the packed bed after the packed bed is completely wetted and then fully drained (Figure **2-8**).

4. Dynamic holdup (DH): is also called operating holdup, which represents the liquid which flows in packed bed and will drain from the packing and is also a measure of the liquid flowing through the packing when the column is in operation (Shulman et al., 1955). DH is the part of the external liquid holdup which can be collected at the bottom of the column after a sudden shutoff of the liquid feed (Figure **2-8**).

5.   Static holdup (SH): is the internal liquid holdup plus the residual liquid

holdup. For a bed of nonporous particles, static holdup and residual

holdup are the same.
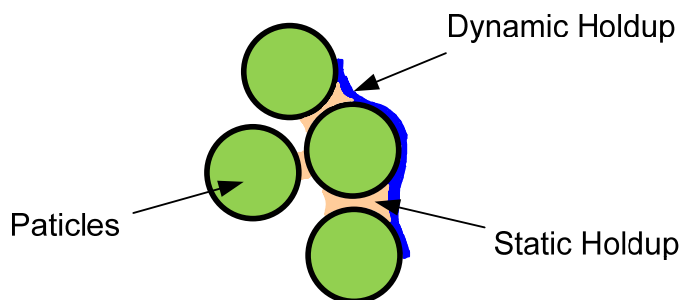
Figure **2-8**: Static holdup and dynamic holdup in packed bed.

For glass beads, SH equals residual holdup, and the total liquid holdup is equal

to the sum of SH and DH. SH and DH are the important parameters in this project.

Degree of saturation expresses the volume of water present in the packed bed

relative to the volume of pores, and is given as

$$s = \frac{V_f}{V_v} \qquad\qquad \textbf{2.27}$$

where V_f and V_v are the liquid volume in the pores and the volume of pores, respectively.

Therefore, 100% saturation means the pore space is fully filled with liquid.

2.5.4.1 Static Holdup (SH)

SH has been well studied in the chemical engineering literature. Shulman et al.

(1955) first pointed out that the total liquid holdup in a packed bed is made up of static

and dynamic holdup. Total liquid holdup can be determined by the difference between

the dry and irrigated column weight, while DH could be found by collecting the liquid

draining from the column after interruption of input liquid. SH can then be determined by the difference between the total holdup and DH. Schubert et al. (1986) presented experimental methods for measuring the SH, but there is substantial disagreement between SH determined by draining and step decrease in tracer methods. These methods are described in a later section.

A widely used expression for predicting SH is the empirical correlation (Saez and Carbonell, 1985):

$$\beta_{stat} = \frac{1}{20 + 0.9Eo} \qquad \textbf{2.28}$$

where *Eo* is Eötvös number, which is the dimensionless ratio determined from gravity *g*, surface tension σ, fluid density ρ_f and particle density d_p:

$$Eo = \frac{\rho_f g d_p^2}{\sigma} \qquad \textbf{2.29}$$

However, Eq. **2.28** is only an approximate representation of the physical observations because the experimental data were widely scattered. More recently, Saez et al. (1991) investigated the SH using better controlled experiments. They used randomly packed-beds of spherical particles, and possible impurities at the solid surface (glass) were removed to ensure that the contact angle is close to zero. Under these controlled conditions, the following relationship was found between static holdup and Eötvös number

$$\beta_{stat} = \frac{0.11}{1 + Eo}. \qquad \textbf{2.30}$$

The correlation in Eq. **2.30** suggests that the maximum SH is 0.11 because Eötvös number is larger than 0. This may be true for average SH, which is calculated by

$$\beta_{stat} = \frac{V_r}{V_t}$$
<div align="right">**2.31**</div>

where V_r is the volume of residual water after the packed bed is fully wetted and completed drained, V_t is the total volume of packed bed. However, the local SH (at given elevation, the ratio of residual water to the controlled volume) may be variable from the top to the bottom of packed bed due to the capillary pressure. At the region right above CF, the value of local SH is between the porosity (maximum value of static holdup) and average SH, which is higher than 0.11.

2.5.4.2 Dynamic Holdup (DH)

There have been two major approaches to measure DH in the literature: draining method (Elgin and Weiss, 1939; Shulman et al., 1955); and tracer method (Schubert et al., 1986; Kushalkar and Pangarkar, 1990; Sater and Levenspiel; 1966).

Elgin and Weiss (1939) measured DH for four different types of packing in a 3 inch diameter glass column by draining method. The flowing medium was a mixture of air and water at different mixing rates. The research shows that at zero gas flow rate, liquid holdup varies linearly with water flow rate except at very low rates.
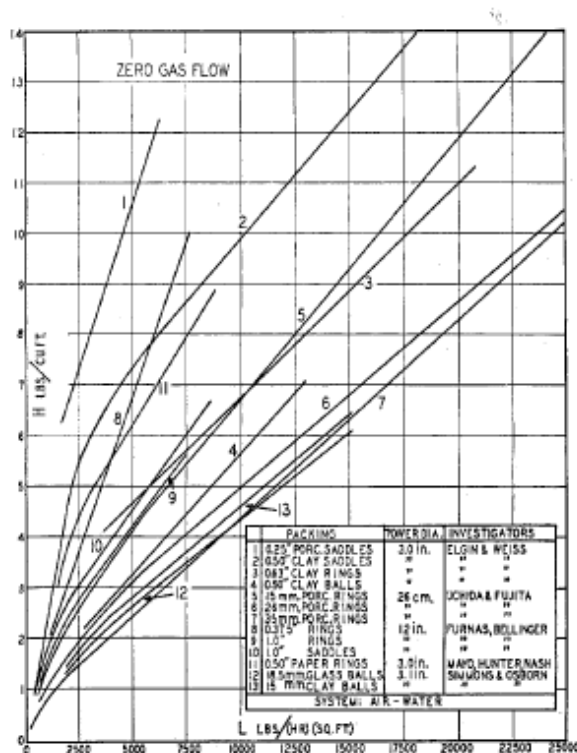
Figure **2-9**: Effect of water rate on holdup in various packings with no gas flowing (From Elgin and Weiss, 1939).

Shulman et al. (1955) measured total, static and dynamic holdup for packed beds, and used their holdup data to successfully explain the significant differences observed when gas-phase mass transfer rates were measured by absorption and vaporization methods, respectively.

The draining method requires the interruption of flow by simultaneously cutting off the liquid inlet and the outlet to the column. Van Swaaij et al. (1969) proposed to use impulse tracer technique to measure holdup and residence time distribution in the liquid phase. They showed that the draining method and tracer method give equivalent DH values and that the entire liquid holdup is accessible to the tracer. However, it has been argued that the response to an impulse input may not include SH due to the fact that the short-lived tracer does not stay long enough in the packing to cause interaction with the

static holdup (Schubert et al., 1986; Kushalkar and Pangarkar, 1990; Sater and Levenspiel, 1966). Hence several researchers have instead used a step decrease tracer approach to study static and dynamic holdup (Schubert et al., 1986; Kushalkar and Pangarkar, 1990; Sater and Levenspiel; 1966).

With new numerical modeling techniques such as computational fluid dynamics (CFD), a better qualitative understanding and a more accurate quantitative description of fluid flow in packed beds are available. CFD is a method that is becoming popular in the modeling of flow systems in many fields. Yin et al. (2002) presented measured results of liquid holdup distribution in a 0.6 m column packed with 25.4 mm stainless steel rings with the gamma ray tomography. With the CFD approach, they found that the liquid holdup distribution was not uniform and that the liquid distributor design had a significant effect on the holdup distribution. The good agreement between simulation results and experimental data indicated the CFD based model proposed in the study could accurately simulate the flow characteristics in randomly packed columns.

2.5.5 Capillary Fringe Thickness (CFT)

Capillary fringe (CF) is the thin zone formed at the bottom of a packed column with essentially 100% water saturation after gravity drainage stops. Capillary pressure is a well known phenomenon that describes the force which can move pore water from lower elevation to higher elevation—or prevents some water at a high elevation from moving to a low elevation. Preliminary study in this project revealed that CF is a key factor for the performance of steam in a packed bed, which prevents steam from completely penetrating the packed column. Hence, the heating of CF is slower than other parts of the packed bed.

As illustrated in Figure **2-5**, on the left at time<0 the pore space in a packed bed is filled with water, then at time=0, water begins to drain out by gravity through a screen at the bottom of the packed bed. The CF remaining after drainage results from a balancing of the gravitational and the capillary forces. Gravitational forces act to pull water downward, while capillary forces act to retain water in the pore space. Eventually the gradient in the capillary forces will balance the gradient in the gravitational forces, and the water in the packed bed will be at equilibrium, causing the drainage to cease (DiCarlo, 2003).

Similar to CF, capillary rise is a well known soil phenomenon that describes the movement of pore water from lower elevation to higher elevation driven by the hydraulic head gradient acting across the curved pore air/pore water interface.

The CFT/capillary rise depends on fluid properties and on the packed bed properties, in terms of medium type and uniformity of pore sizes. The pore size is an analogy to capillary tube diameter. The smaller is the inner diameter of a capillary tube, the greater is the rise of water. Many researchers have investigated the capillary rise in packed bed/porous media (Lago and Araujo, 2001; Lu and Likos, 2004; Kramer, 1998; Washburn, 1921; Yang et al., 1988). All of these studies focused on the rising of water from lower to higher elevation, but studying the thickness of CF after drainage of a packed bed was less common. The simplest phenomenon of capillary rise is the rise of a liquid in a capillary tube, and the height of liquid is given by the equation

$$H_c = \frac{2\sigma \cos\theta}{\gamma R}$$

2.32

where H_c = height of capillary rise, σ= surface tension, θ=contact angle between fluid and tube, γ = specific weight of liquid, and R = tube radius. However, in a randomly packed column of glass beads, the contact angle θ varies. Lago and Araujo (2001)

provided equations for estimating the average height of capillary rise in a packed bed was

$$H_c \cong \frac{2.703\sigma}{\rho_l g D_p}$$ **2.33**

where ρ_l = liquid density; g = gravitational acceleration; and D_p = particle diameter.

2.6 State-of-the-Art

Similar to the food columns in PSAP system, packed beds are extensively used in the chemical and process industries as reactors, separators, dryers, filters, and heat exchangers. Heating of packed beds with pressurized steam in PSAP is a highly complex reaction system involving fluid flow, steam penetration and condensation, heat conduction and convection, etc. Although some potential approaches for modeling heat and mass transfer of two phase flow are identifiable, for example, the model provided by Bergins et al. (2005), none of the currently available models for prediction of temperature changes and lethality were directly applicable to PSAP. Existing heat transfer models can not satisfy the practical needs due to the over-simplifications involved with the models. The heat-transfer coefficient on the surface of different particulate foods, the heat-transfer coefficient in beds of different particulate foods, and the conduction coefficient within different particulates in aseptic processing have received scant consideration. Moreover, to combine different properties of fluid, solid, and vapor into modeling of heat and mass transfer in PSAP needs a detailed theoretical investigation. Further study is needed to gain a deeper understanding of the heat transfer from steam to particulate foods in PSAP in order to design optimal systems flows and to set the optimal operation conditions in the future.

CHAPTER 3

GOALS AND OBJECTIVES

The literature review presents pressurized steam segmented-flow aseptic processing, a novel technology in which particulate foods are divided into discrete packed beds and processed in a steam environment while allowing good control of the residence time. Studying and understanding the mechanisms of heat transfer in packed bed processed by steam is essential for the optimal application of the technology of segmented-flow aseptic processing to the food industry.

3.1 Research Goals

The overall goal of this research was to develop a numerical model to predict the heat and mass transfer in a pressurized-steam segmented-flow aseptic processing system, by which the optimum bed depth could be determined to obtain uniform product temperature distribution from top to bottom of the packed bed. Based on this goal, the characteristics of packed beds, such as static and dynamic holdup, saturated and unsaturated flow rate of liquid, condensation heat transfer from steam to water film in capillary fringe, condensation heat transfer from steam to capillary fringe, heat transfer with mass transfer, convection heat transfer from liquid to solid particles, temperature distribution along vertical direction of packed bed, and weight change of system under steam processing were studied.

3.2 Objectives

The research objectives to achieve the overall goal were to :

1. Design and build a PSAP simulator in which packed beds are heated with saturated steam by simulating a segmented unit in PSAP.
2. Experimentally investigate the temperature histories at different elevations of packed beds.
3. Analyze the data from Objective 2 and use to determine the slowest heated elevation in packed beds.
4. Study the characteristics of packed beds such as static holdup, height of capillary fringe, bulk density and specific density.
5. Investigate the relationship between dynamic holdup and liquid flow in packed beds.
6. Model the fluid flow in packed beds with finite-difference method based on the results in Objective 5.
7. Measure the temperature history at different elevation in capillary fringe under steam processing.
8. Model the heat and mass transfer in capillary fringe based on the data from Objective 7.
9. Develop a numerical model for the whole system which is capable of predicting the heat and mass transfer from steam to liquid and solid particles at different elevations of packed beds.
   Validate and calibrate the numerical model in Objective 9.

CHAPTER 4

CHARACTERISTICS OF PACKED BEDS

In this chapter, the properties of packed bed are discussed, including particle diameter, particle density, bulk density, packed bed porosity, static liquid holdup, dynamic liquid holdup, capillary fringe thickness, and vertical drainage. These properties are very important for studying the performance of the packed bed in the heating process by pressurized steam, and are key parameters for the modeling of heat and mass transfer in packed bed.

4.1 Materials and Methods

Three sizes of glass beads (Jaygo Inc., Union, NJ) were tested for different properties: 2, 3, and 5 mm diameter, and were used throughout the project. Except when specified, all tests were conducted in Food Processing Lab (Agricultural and Biological Engineering, Pennsylvania State University, University Park, PA) with average temperature of 25°C ± 3°C and relative humidity less than 40%.

4.1.1 Diameter and Sphericity

Thirty glass beads of each nominal size, 2 mm, 3 mm, and 5 mm, were picked randomly without replacement and three axial diameters (x, y, z) for each bead were measured using a digital caliper. The values of x, y, z for each bead were used to calculate the sphericity.

4.1.2 Density and Porosity

Particle density was measured with Quantachrome Multipycnometer model MVP-2 (Quantachrome Co., Boynton Beach, FL). For each size of glass beads four replications were performed. Glass beads were randomly selected for measurement. All tests were conducted in an environment-controlled laboratory with average temperature of 22°C ± 3°C and relative humidity less than 40%. Operational procedure of Quantachrome Multipycnometer is shown in Appendix A.

Bulk density was calculated by measuring the mass of beads in a 1 L graduated cylinder and dividing mass by volume. For each size of glass beads three replications were performed. Porosity was calculated with Eq. **2.1**.

4.1.3 Static Holdup (SH)

Packed beds were created in polycarbonate column having 10.2 cm OD, 9.5 cm ID and 50 cm height. A stainless steel screen with US mesh size 14 (14 x 14 openings per inch square, opening size 1.30 x 1.30 mm, wire diameter 0.51 mm) was set on the bottom. Three nominal diameters of glass beads were tested: 2 mm, 3 mm, and 5 mm.

The experiment procedure for SH measurement was as follows:

1) Randomly select one size of glass beads from the 3 sizes.

2) Randomly pack the polycarbonate cylinder with 1, 2, or 5 kg (dry weight) of glass beads.

3) Submerge the column into a bucket filled with tap water. The tap water temperature was 10-17ºC.

4) Pull the packed column out of water and lean the cylinder at 45 degree angle (Figure **4-1**) so that the water in CF can flow down along the wall quickly.

5) Allow the packed bed to drain for 30 minutes, and record the weight of wet packed bed.

Measurements were made for bead masses of 1, 2 and 5 kg for each of the three bead sizes with three replications.
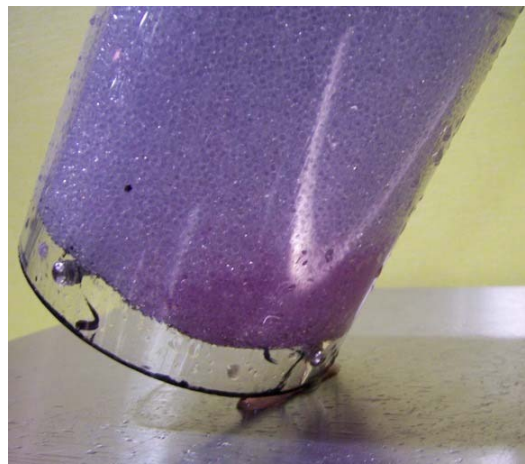
Figure **4-1**: Most of water drains out by leaning the packed bed. Water is colored with red ink for demonstration only.

4.1.4 Dynamic Holdup (DH)

A water-flow method was used to measure the DH in packed bed which is different from draining method and tracer method. A flowmeter (Gilmont®, Barrington, IL) was calibrated beforehand. The flowmeter and a manual control nozzle were installed on the top of a polycarbonate cylinder. Water spraying out of the nozzle and falling through the cylinder was collected in a container. The same polycarbonate cylinder and screen

were used as in measurement of SH. A balance was used to suspend the nozzle and

the cylinder and its packed bed as shown in Figure **4-2**. All three bead sizes were tested.
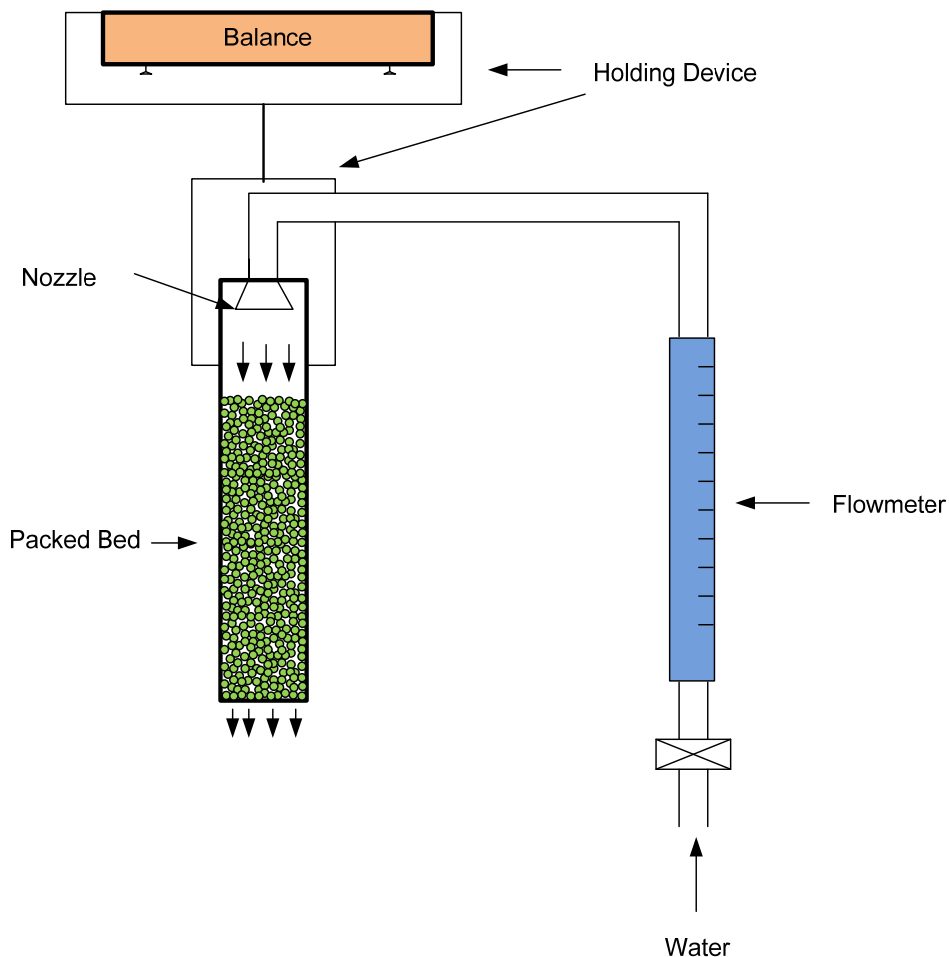
Figure **4-2**: Experimental setup for measuring dynamic liquid holdup.

The experiment steps for measuring DH are described as below:

A. Weigh dry glass beads and fill into cylinder.

B. Open the valve to the maximum to fully wet the glass beads in cylinder.

C. Close water valve. CF can be observed at the bottom of packed bed.

Keeping the cylinder vertical and untouched, tare the balance (This operation

can exclude the SH from the measurement so only DH was observed).

D. Set the flow rate to 5, 10, 15, 20, 25, 30, 35, 40, 45, 50, 55 and 60

(flowmeter scale units), in order, and record the balance reading for each

flow rate after reaching steady reading.

Tests were completed in random order for all three bead sizes, each with bead

weights of 1.0, 1.5, 2.0, 2.5, 3.0 and 3.5 kg, all in random order and with three replicates.

4.1.5 Capillary Fringe Thickness (CFT)

The same polycarbonate cylinder and screen were used for measuring CFT as in

experiments of static and dynamic liquid holdup. Since CFT is independent of bed height

it was not necessary to test different heights of packed bed. In this experiment, 4 kg (36

cm height) dry weight is used for testing all sizes of glass beads.

The packed bed was submerged into water so that the glass beads became fully

wet. Then the column was pulled out of the water and was set vertically for 30 minutes to

allow water drain totally; then CFT was measured (Figure **4-3**).
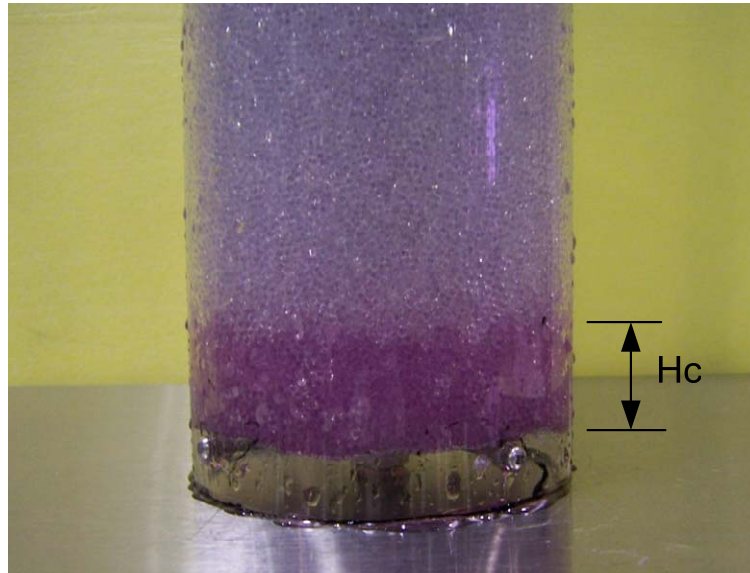
Figure **4-3**: Measurement of capillary fringe thickness after vertical drainage. Hc is the capillary fringe thickness. Water is colored with red ink for demonstration only.

4.1.6 Mass Transfer during Drainage

The weight change of packed bed during drainage was measured with a digital scale, as shown in Figure **4-4**. Packed beds with different bead masses (3 kg and 5 kg) and with different diameters (2, 3, and 5 mm) were tested. The packed bed was held by the digital scale, which was suspended by a long rope. The digital scale data were recorded using LabView (National Instruments, Austin, TX) program (Figure **4-5**).
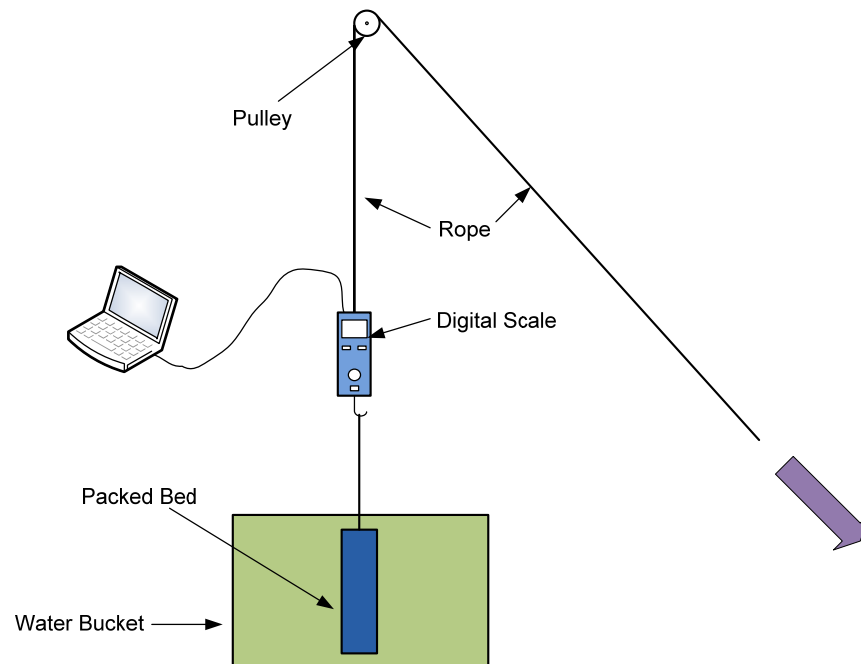
Figure **4-4**: Experimental setup for measuring weight change during drainage.
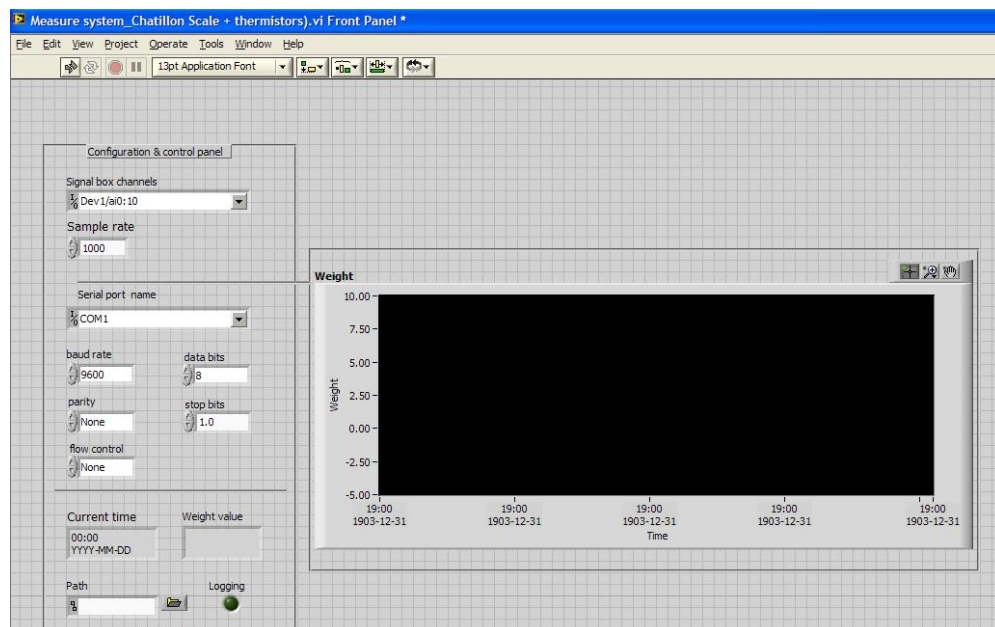
Figure **4-5**: Control panel of LabView program for measuring weight using digital scale.

To run the experiment, first the packed bed was fully dropped into a big bucket filled with tap water at temperature of 17ºC ± 3ºC. After the data collection was begun, the packed bed was pulled out of water with steady force by rope, and was held stationary. The dynamic weight of water in packed bed was calculated by subtracting weights of polycarbonate cylinder and dry glass beads. Three replications were done for each weight and each size of glass beads.

4.2 Results and Discussion

4.2.1 Diameter and Sphericity

The average diameter and sphericity of the each size of glass beads are summarized in Table **4-1**. The result shows that the diameters of the three sizes of glass beads are 1.91 mm, 2.90 mm, and 4.92 mm. The sphericities are 0.989 for 2 mm, 0.991 for 3 mm, and 0.992 for 5 mm.

Table **4-1**: Summary of average diameters and sphericities for different sizes of glass beads.

Bead Diameter	Diameter			Sphericity		
	Average Diameter (mm)	SD*	CoV**(%)	Average Sphericity	SD*	CoV**(%)
2 mm	1.91	0.020	1.02	0.989	0.007	0.68
3 mm	2.90	0.024	0.76	0.991	0.005	0.50
5 mm	4. 92	0.027	0.55	0.992	0.005	0.47

* Standard Deviation
** Coefficient of Variance

4.2.2 Density and Porosity

Table **4-2** shows the data of particle density, along with SD and CoV for different sizes of glass beads. The mean value of particle density decreases with the increase of particle size, which is also illustrated in Figure **4-6**.

Table **4-2**: Particle density (kg/m^3) of different sizes of glass beads.

Bead Size	2 mm	3 mm	5 mm
Trial 1	2923.7	2888.6	2837.3
Trial 2	2927.7	2864.2	2835.6
Trial 3	2887.4	2912.5	2845.0
Trial 4	2873.5	2862.0	2863.5
Mean	2903.1	2881.8	2845.4
SD	26.78	23.74	12.77
CoV(%)	0.92	0.82	0.45
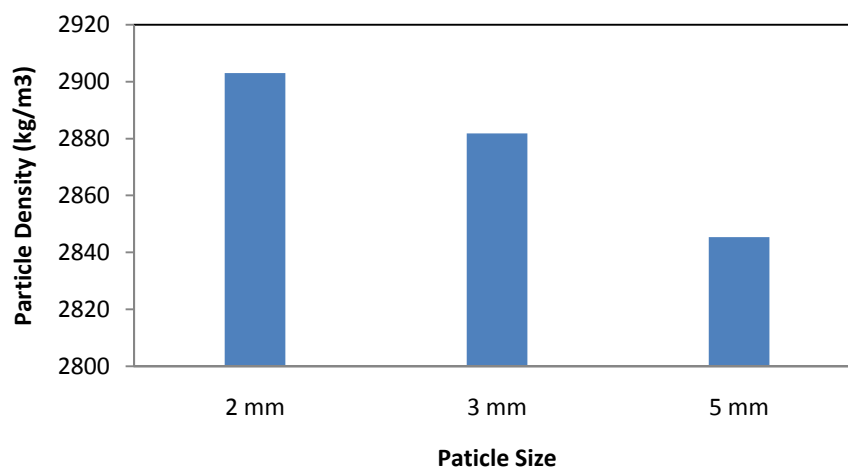
Figure **4-6**: Mean particle density from different sizes of glass beads.

One-way analysis of variance (ANOVA) was used to compare the particle densities from different sizes of glass beads. Except where specified, all the statistical analysis in this research were performed using Minitab software (Release 14, Minitab Inc,

State College, PA). Before ANOVA was performed, normality was examined using a probability plot. The result (Figure **4-7**) shows that the assumption of normal distribution for all particle densities from different sizes is appropriate with 95% confidence interval. Table 4-3 shows the result of one-way ANOVA. The null hypothesis is that all particle densities from the different sizes have the same mean value. The p-value for ANOVA is 0.014<0.05. So the null hypothesis is rejected, indicating that not all of particles have the same particle density. Figure **5-2** also shows that the particle densities between 2 mm and 5 mm, are significantly different, while between 2 mm and 3 mm, and between 3 mm and 5 mm, the particle densities are not significantly different.
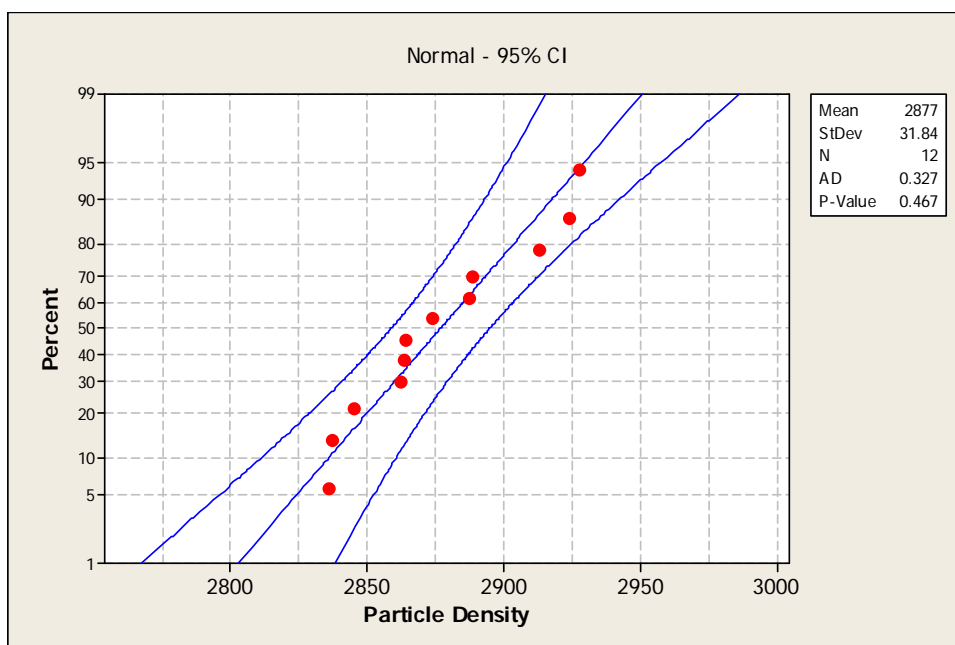
Figure **4-7**: Probability plot of particle densities from different sizes.

Table **4-3**: Descriptive result of one-way ANOVA: particle density versus diameter.

```
Source     DF     SS    MS     F      P
Diameter    2   6819  3409  7.08  0.014
Error       9   4332   481
Total      11  11151

S = 21.94   R-Sq = 61.15%   R-Sq(adj) = 52.52%


                          Individual 95% CIs For Mean Based on Pooled StDev
Level  N    Mean  StDev    +---------+---------+---------+---------
2 mm   4  2903.1   26.8                          (--------*-------)
3 mm   4  2881.8   23.7                  (--------*-------)
5 mm   4  2845.3   12.8      (-------*--------)
                          +---------+---------+---------+---------
                          2820      2850      2880      2910
```
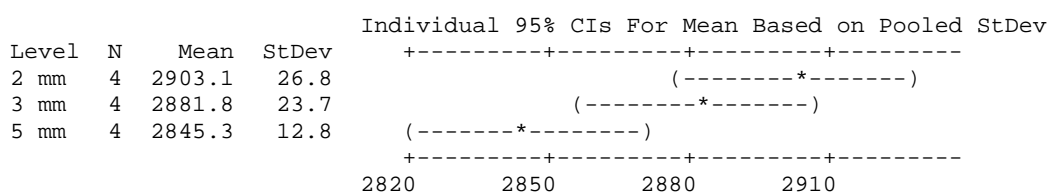
The bulk densities from different sizes of particles are summarized in Table **4-4**. It can be seen that the bulk density decreases with increase of particle diameter, which has the same trend with particle density. The one-way ANOVA statistical analysis illustrated that not all bulk densities for different sizes of glass beads are the same, because p-value is 0.000<0.05, the null hypothesis was rejected (Table **B-1**).

Table **4-4**: Bulk density of glass beads of different sizes.

Bead Size	2 mm	3 mm	5 mm
Trail 1 (kg/m^3)	1565.0	1560.0	1531.6
Trail 2 (kg/m^3)	1572.0	1564.0	1542.0
Trail 3 (kg/m^3)	1562.9	1561.2	1541.5
Trail 4 (kg/m^3)	1566.2	1545.6	1537.4
Mean (kg/m^3)	1566.5	1556.7	1538.1
SD	3.91	8.24	4.80
CoV(%)	0.25	0.53	0.31

Porosity was calculated with Eq. **2.1**. The final results are shown in Figure **4-8**. The figure indicates that packed beds each with different sizes of particles have the same porosity. This result is consistent with the theory of packed bed porosity. For a packed bed with infinite radial length filled with ideal spheres, the theoretical porosity is the same no matter what the particle diameter.
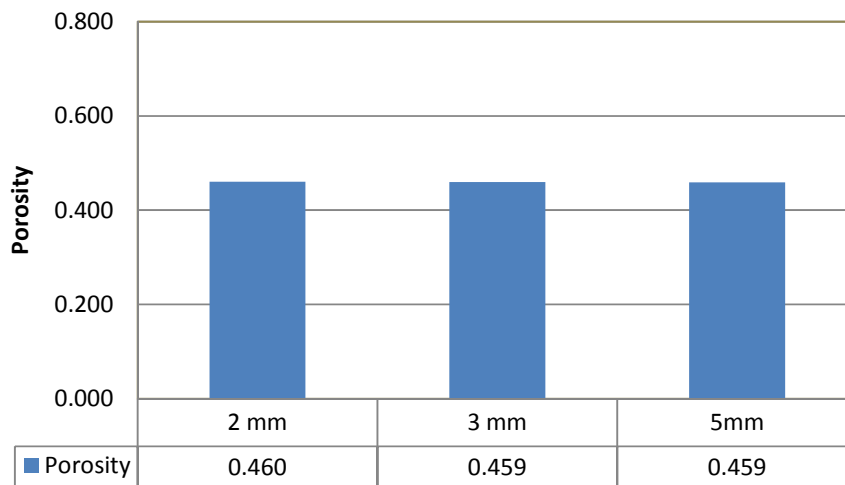
Figure **4-8**: Porosity of packed beds from 3 different sizes of glass beads.

4.2.3 Static Liquid Holdup

The weight-based SH (W/W) was first calculated by mass-difference method to eliminate the effect of CF. The mass-difference method calculated the average liquid holdup based on the liquid and bed weight difference by subtracting the bottom portion of packed bed

$$\beta_s = \frac{m_2 - m_1}{M_2 - M_1} \qquad \textbf{4.1}$$

where m and M are the net weight of liquid and total weight of packed beds after drainage, respectively, subscript 1 and 2 are for different weights. For example, if 1 kg and 5 kg dry packed beds contain 0.0015 kg and 0.005 kg water respectively, the static holdup is (0.005-0.0015)/(5-1)= 0.0014 kg/kg. Volumetric static holdup (SH) is calculated by converting the mass difference in numerator and denominator, respectively, into volume

$$\beta_s = \frac{(m_2 - m_1)/\rho_f}{(M_2 - M_1)/\rho_b},$$

4.2

with ρ_f and ρ_b being fluid density and packed bed bulk density, respectively. In this

dissertation, SH refers to volumetric static hold up if not specifically stated.

The experimental results for SH are listed in Table **4-5**. The original data for

each trial are presented in Appendix B from Table **B-2** to Table **B-4**.

Table **4-5**: SH in packed beds with different sizes of glass beads.

Bead Size	D_{pd}/D_p*	(5-1)**kg			(5-2)*** kg			Average
		SH (V/V)	SD	CoV (%)	SH (V/V)	SD	CoV (%)	SH (V/V)
2 mm	47.5	0.027	0.0007	2.53	0.024	0.0012	5.23	0.025
3 mm	31.7	0.030	0.0013	4.33	0.029	0.0005	1.73	0.029
5 mm	19.0	0.030	0.0007	2.45	0.030	0.0017	5.72	0.030

* ratio of bed diameter over particle diameter.
** SH based on mass difference between 5 kg and 1 kg.
*** SH based on mass difference between 5 kg and 2 kg.

It can be seen from the table above, for 5 mm glass beads, the two values of SH

by subtracting different "base weight" from the bottom of packed bed are no different.

For 3 mm glass beads, the two values have no significant difference: static holdup 0.030

for subtracted base weight 1 kg and 0.029 for subtracted base weight 2 kg. For 2 mm

glass beads, the SH is slightly different, 0.027 for subtracted base weight of 1 kg and

0.025 for subtracted base weight of 2 kg, respectively. Statistical analysis was performed

to determine whether the difference between the two calculation methods is significant.

Because the two sets of data (subtracted base weight 1 kg and 2 kg, respectively, from 5

kg) are not independent, paired t-test was performed and the result was shown in

Table **B-5**. The p-value in paired t-test was $0.009 < 0.05$, so the null hypothesis was

rejected with the conclusion that with 95% confidence the SH by subtracting different

weights from 5 kg packed bed of 2 mm glass beads is not the same. This is probably

caused by the greater SH gradient ($\nabla\beta_s / \nabla Y$, Y is elevation). This suggests that a more

accurate way is needed to describe the SH in packed beds from smaller particles,

therefore, another experiment was performed to investigate the local SH at different

elevations of 2, 3 and 5 mm glass beads.

Using the same experimental apparatus illustrated in Figure **4-4**, the SH was

measured with different amounts of glass beads by changing the weight of particles from

0.5 kg to 5 kg. SH was calculated by noting the final net weight of water sustained in

packed bed after vertical drainage. A typical vertical drainage curve is presented in

Figure **4-9**. 3 mm glass beads were tested, and all other experimental conditions are the

same as described in Section **4.2.3**.
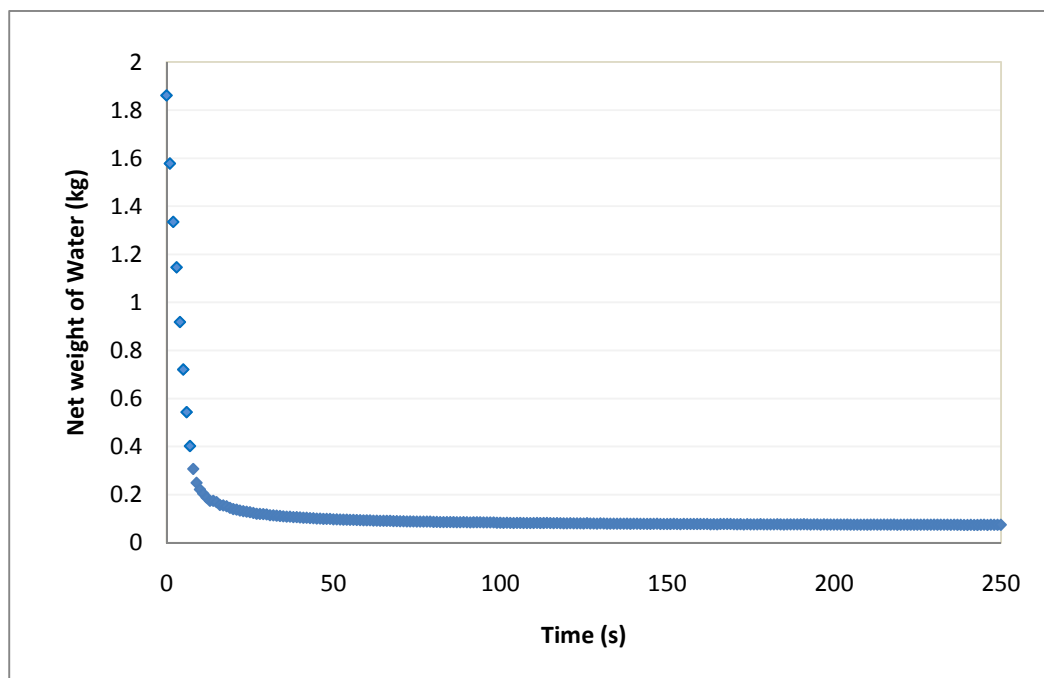
Figure **4-9**: Typical curve of vertical drainage in packed beds. This result is for 3 mm glass beads and 27 cm bed depth.

Figure **4-10** illustrates the residual holdup distribution from bottom to top of packed bed. It shows that above the CF, the SH decrease sharply from 0.46 to 0.02. Since CF is always saturated with water but unsaturated flow zone (UFZ) above CF has variable SH, it was desirable to establish a function between elevation and static holdup to be used for different height and particle size. The fitted line shown in Figure **4-11** was obtained from the equation

$$\beta_{stat} = 0.330 \exp\left[-57.51(H - Hc)\right] + 0.024 \qquad \textbf{4.3}$$

where β_s is the SH, H the elevation from bottom of bed, and H_c the CF thickness. For comparison, the experimental data are also shown in Figure **4-11** by plotting SH versus elevation. It can be seen from Figure **4-11** that for elevations above 10 cm from CF, the SH is almost constant, while between upper boundary of CF and elevation of 10 cm (from CF), SH changes rapidly. Figure **4-12** presents the plot between observation and prediction, in which R-square was 0.99 suggesting an excellent model presented by Eq. **4.3**.

Figure **4-10**: Variable residual liquid holdup distributed from top to bottom of packed bed.

Figure **4-11**: Experimental and predicted data of SH above CF.
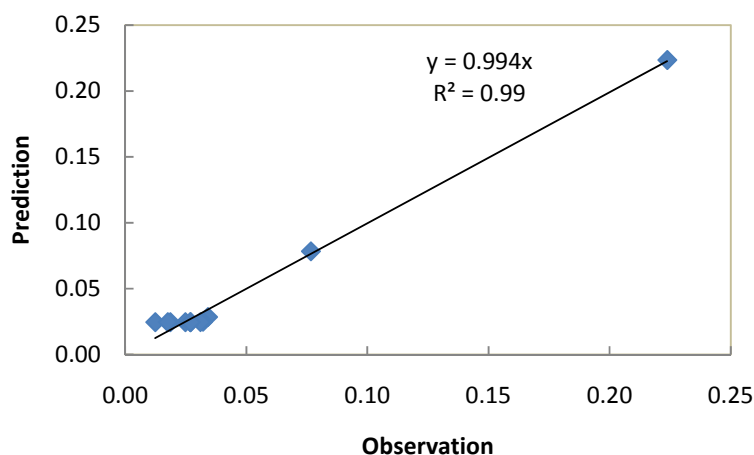
Figure **4-12**: Plot of observation versus prediction of SH in packed bed.

4.2.4 Dynamic Holdup (DH)

Water sprayed out of the nozzle as shown in Figure **4-2** can not cover the upper surface of the packed bed perfectly. According to Radcliffe and Rasmussen (2002), water redistribution occurs. That is, after a certain vertical distance the flowing water is evenly distributed across the cross-sectional area. To eliminate the region of water redistribution, total holdup of a "base" packed bed was subtracted from that of deeper packed bed. For 5 mm glass beads, the base weight is 2.0 kg. For 2 mm and 3 mm glass beads, the base weight is 1.0 kg.

Figure **4-13** illustrates the DH versus superficial velocity of water for different weight-difference of packed bed.

Hold-up 5mm glassbeads
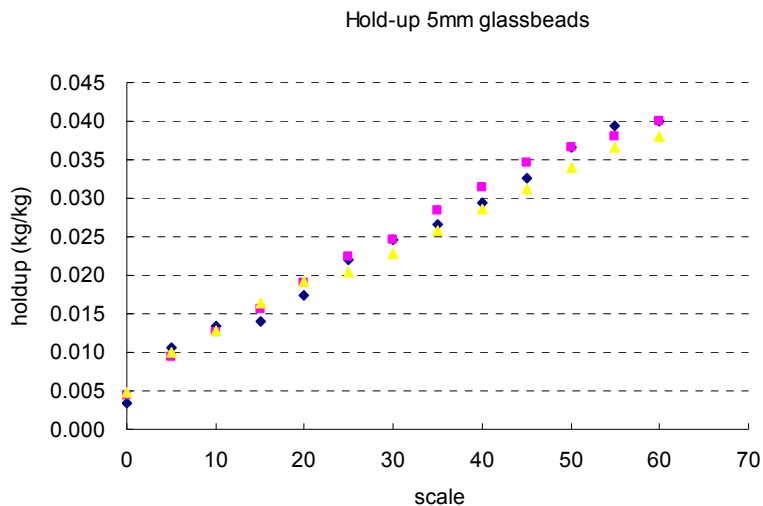
Figure **4-13**: Dynamic liquid holdup of packed bed with 5 mm glass beads at different superficial velocities and subtracted bed weights.

Statistical analysis was performed to determine whether the data for the three bead masses are significantly different. The ANCOVA output is presented in **B.3** showing that the null hypothesis can not be rejected so that homogeneity of different curves is concluded. Therefore, the three data sets can be averaged to one single curve.

DH was also measured for 2 mm and 3 mm glass beads, respectively. Shown in Figure **4-14** and Figure **4-15** are the curves of the dynamic liquid holdup based on weight difference for 2 mm and 3 mm glass beads, respectively. Statistically there was no difference between curves, so all individual curves were combined to single curve by taking the average.
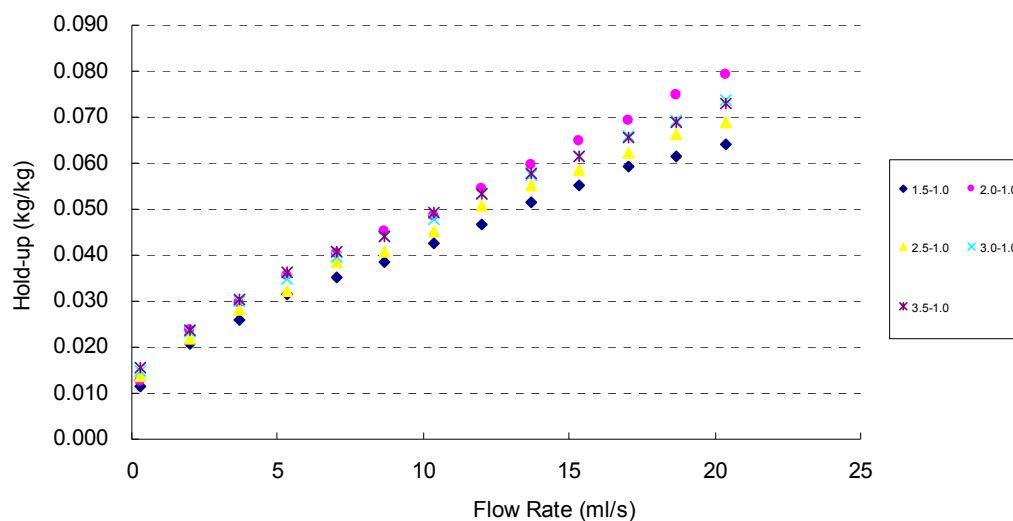
Figure **4-14**: Dynamic liquid holdup of packed bed from 2 mm glass beads at different superficial velocities and subtracted bed weights.
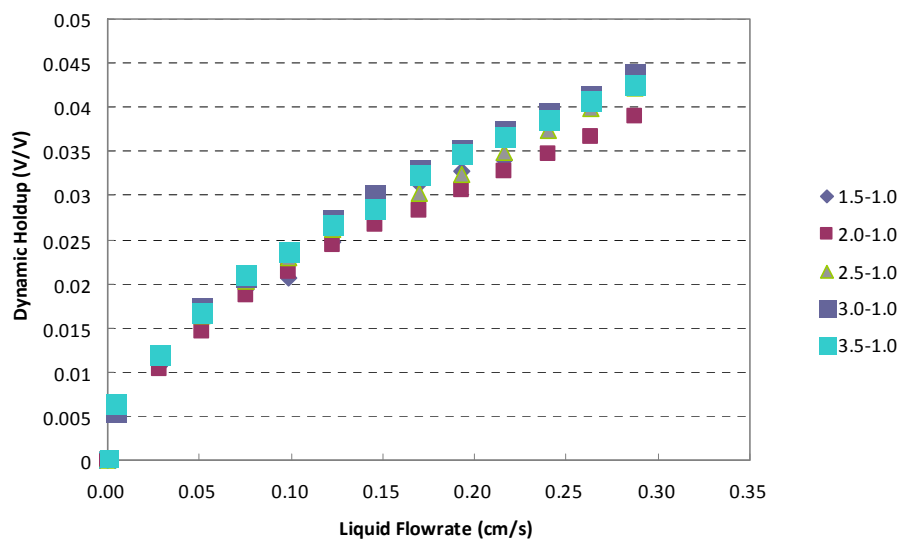
Figure **4-15**: Dynamic liquid holdup of packed bed from 3 mm glass beads at different superficial velocities and subtracted bed weights.

The resulting DH curves for the three bead sizes (Figure **4-16**) illustrate a positive relationship between the two variables. The maximum water flow velocity experimentally tested through the packed beds was 0.6 cm/s which was restricted to the maximum water flow rate in the flowmeter. However, the saturated drainage velocity in packed bed ranges from 3.5 cm/s to 10.5 cm/s, for 2 to 5 mm glass beads (data obtained from vertical drainage experiment in 4.3.3). For the water flow velocity through packed beds above 0.6 cm/s, the DH could not be measured due to the upper limit of water flowmeter. However, according to Elgin and Weiss (1939), liquid holdup varies linearly with water flow velocity except at very low rates, as illustrated in Figure **2-9**. Therefore, linear relationship between DH and water flow velocity was assumed for water flow velocity above 0.6 cm/s.
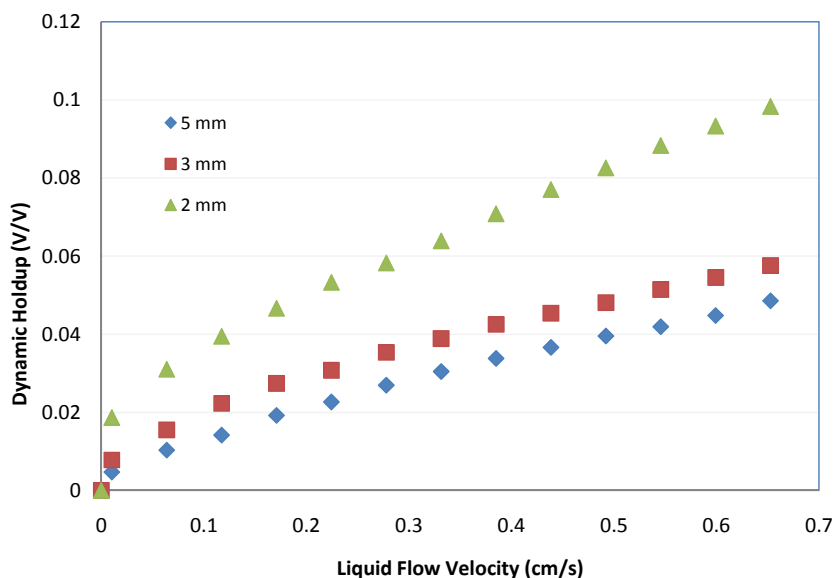
Figure **4-16**: Experimental result of dynamic holdup versus superficial velocity.

From Figure **4-17** to Figure **4-19**, water flow velocity was plotted against DH for each size of glass beads. At lower water flow velocity, a second order polynomial equation was obtained as the trendline, which is illustrated in blue points. While with higher flow rate, a straight line was predicted (orange straight line in Figure **4-17** to Figure **4-19**).
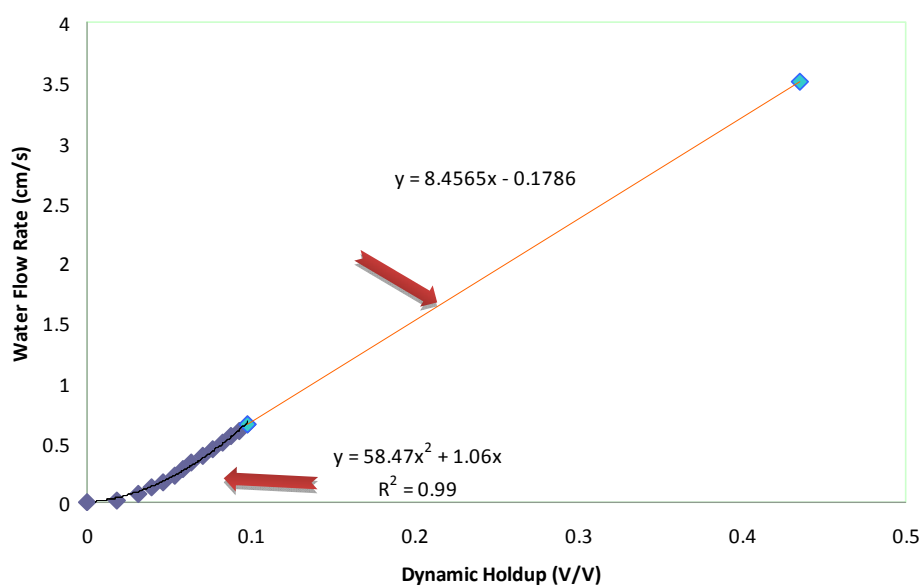
Figure **4-17**: Measured and predicted relationship between water flow velocity and dynamic holdup for 2 mm glass beads.
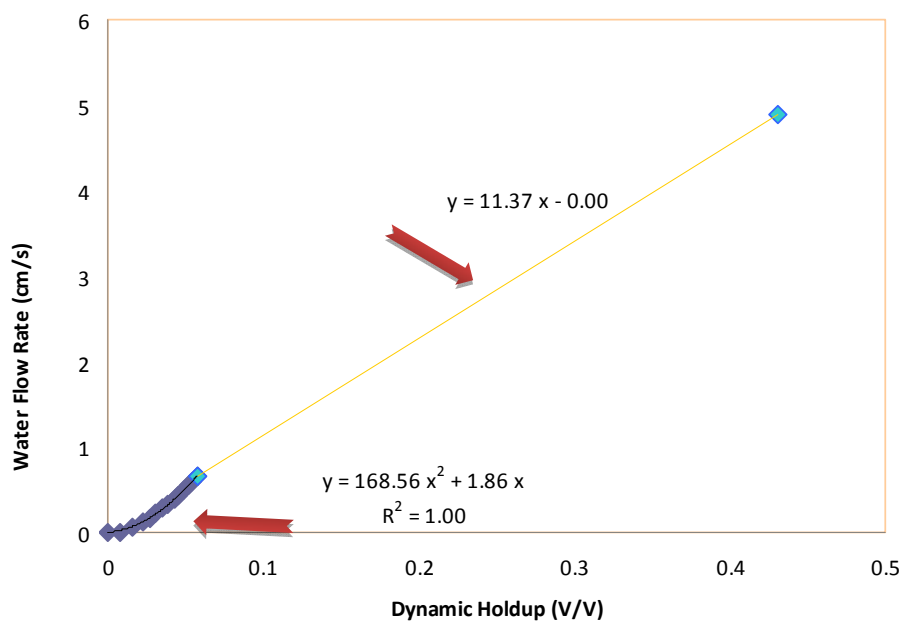
Figure **4-18**: Measured and predicted relationship between water flow velocity and dynamic holdup for 3 mm glass beads.
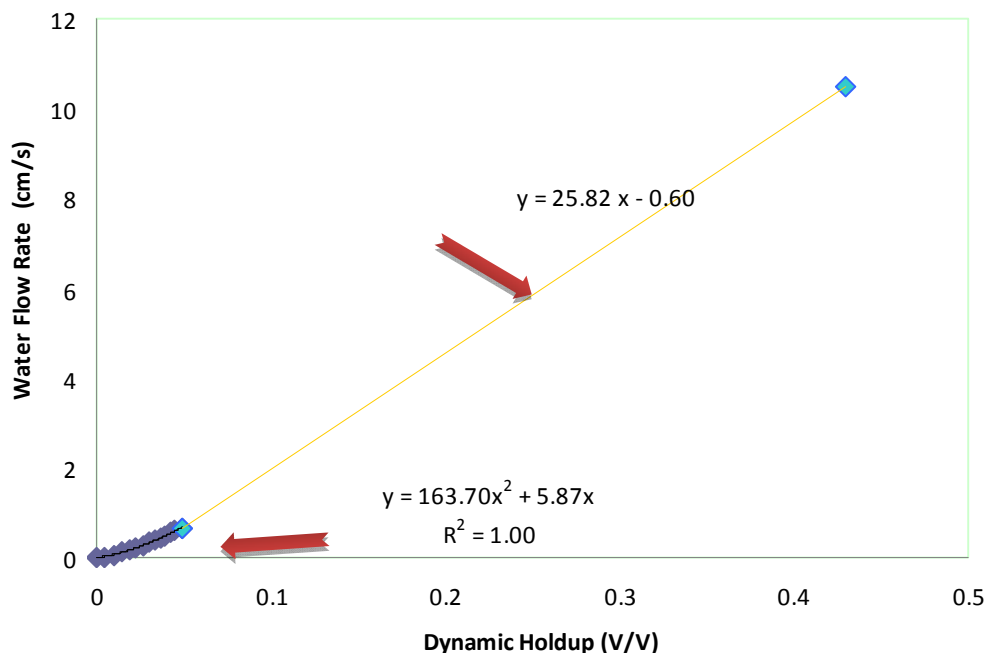
Figure **4-19**: Measured and predicted relationship between water flow velocity and dynamic holdup for 5 mm glass beads.

In summary, a correlation was established between DH and water flow velocity in packed beds, for different sizes of glass beads. Due to the restriction of experiment device, the DH could not be measured directly under high mass transfer rate.

4.2.5 Capillary Fringe Thickness (CFT)

Table **4-6** lists the measurements of CFT for different bead diameters. The mean values of CFT are 2.4 cm (SD=0.084), 1.4 cm (SD=0.114), and 0.6 cm (SD=0.071) for 2, 3, and 5 mm glass beads.

Figure **4-20** illustrates the relationship between average CFT and reciprocal of diameter in packed beds after vertical drainage. The predictions from Lago and Araujo's

model (2001) are also shown in the Figure **4-20** for comparison. The measured values are higher than the predicted values and the dominant reason is likely due to the difference in surface tension between the two situations. Under the circumstance of water drainage, glass beads are wetted and covered with water film after water flows down to a lower elevation, so surface tension, which arises from the forces between molecules of liquid and forces between the liquid and bead surfaces (Massey and Ward-Smith, 2006), keeps liquid molecules from moving down by gravitational force. In contrast, the capillary rise in dry packed bed, the case to which Lago and Araujo's model is applied, is by the dominant forces of capillary effect, and there are no surface tension forces exerted from liquid in upper space. Hence, the capillary rise in dry packed bed is lower than the CFT of pre-wetted packed bed of the same size of glass beads. This difference is more obvious for packed beds with smaller glass beads.
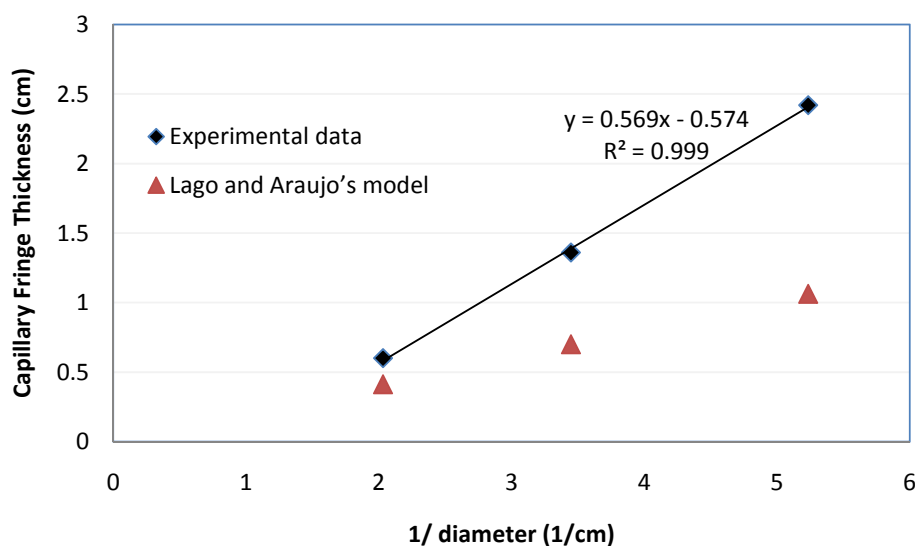
Figure **4-20**: CFT has a linear relationship to inverse of particle diameter. Comparison was made between experimental data and prediction from Lago and Araujo's model (2001).

The trendline in the plot of CFT versus inverse of diameter shows a perfect linear function between H_c and the inverse of particle diameter

$$H_c = \frac{a}{D_p} - b ,$$
                                    4.4

where *a* and *b* are 0.569 (cm^2)and 0.574 (cm), respectively, H_c (cm) is CFT. The coefficient *a* (cm^2) is given as

$$a = k \frac{\sigma}{\rho_l g} *10^4 ,$$
                                    4.5

with σ and ρ_l being surface tension and density of liquid, respectively, g the gravity acceleration, k the constant coefficient (dimensionless) which is named as CF constant. From the equation above, the *k* value can be determined by

$$k = \frac{0.569 *10^{-4} * g\rho_l}{\sigma} = 7.566$$
                                    4.6

where *g* = 9.8 m/s^2, ρ_l = 1000 kg/m^3, and σ = 7.37*10^{-2} N/m (Incropera and DeWitt, 2002).

The mean value of CFT is plotted in Figure **4-21** and is extrapolated to larger particle sizes using Eq. **4.4**. The figure suggests that for particle sizes over 9.5 mm the CF can be neglected.

Table **4-6**: CFT in packed beds from different sizes of glass beads.

Glass Beads Size	2 mm	3 mm	5 mm
	2.5	1.2	0.7
	2.4	1.5	0.5
CFT (cm)	2.5	1.4	0.6
	2.3	1.3	0.6
	2.4	1.4	0.6
Mean (cm)	2.4	1.4	0.6
SD	0.084	0.114	0.071
CoV (100%)	0.35	0.84	1.2
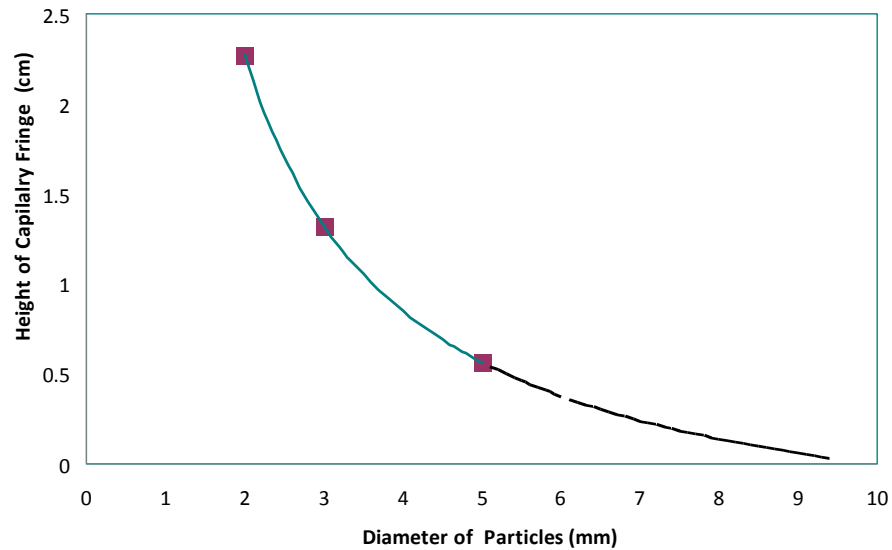
Figure **4-21**: Mean value of CFT for different sizes of particles. Particles sizes greater than 9.5 mm have negligible capillary fringe as extrapolated from measurements for smaller particles.

It is important to note that the CFT was measured at water temperature around 17ºC. Since the CFT is caused by surface tension, the change of water surface tension under high temperature will change the CFT. Assuming CF constant k is a temperature-independent value, then for 2 mm glass beads at temperature 121ºC, coefficient a in Eq. **4.4** will be changed to 0.442 which leads to Hc = 1.7 cm with σ = 5.36 * 10^{-2} N/m and ρ_l = 937 kg/m^3 (from Incroppera and DeWitt, 2002). Hence the CFT decreases 29.2% from 17 ºC to 121ºC. The predicted CFT at higher temperature over 17ºC in packed beds of different sizes of glass beads were illustrated in Figure **4-22**.
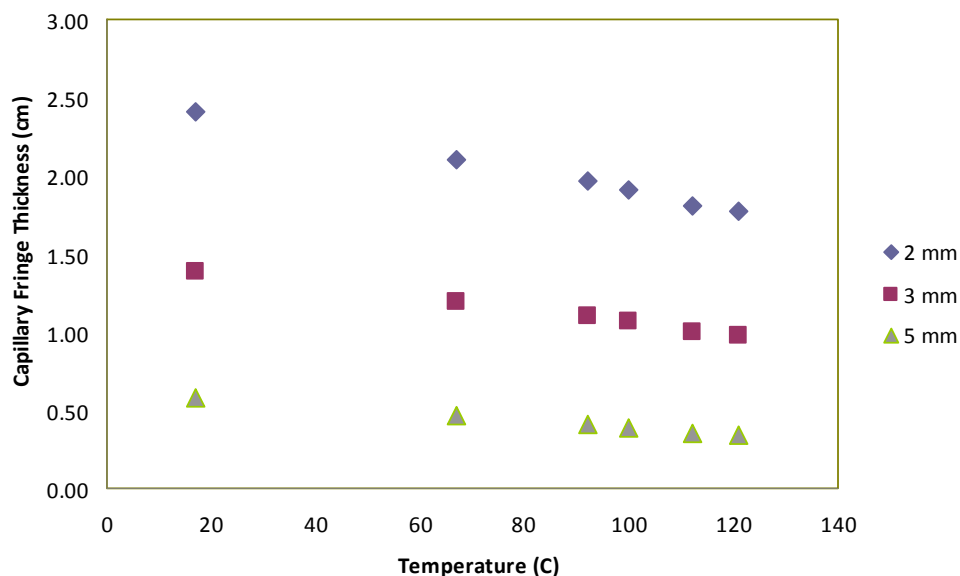
Figure **4-22**: Measured CFT at 17ºC and predicted CFT at higher temperature for different sizes of particles (2 mm, 3 mm, and 5 mm).

4.2.6 Vertical Drainage

For each size of glass beads, a 3 kg of dry weight packed bed was tested in vertical column. The reason that 3 kg of dry weight was selected was that the tube height was 50 cm and the packed bed of 3 kg was 27 cm height, so packed bed depth was approximately half of tube, which left approximately the same saturated water flow time either above or within packed bed. If the bed depth was too large, it was difficult to determine from data when the water level reached the bed surface. On the other hand, if bed depth was too small, the water saturated flow in packed bed occurred over too short a time to accurately measure..

Plotted results are presented in Figures **4-23** to **4-27**. For each, the curve was treated as two sections, linear on the left and higher order on the right. The slope of the

linear section gives the velocity of water draining out of packed bed. Therefore, the slope divided by cross-sectional area of pack bed and density of liquid gives the superficial/convectional velocity ratio of saturated flow. As shown in the figure below, when the water table of saturated flow passes the surface of packed bed, the ratio hardly changes. When the water table reaches the CF, the water flow velocity decreases sharply and then unsaturated flow dominates.
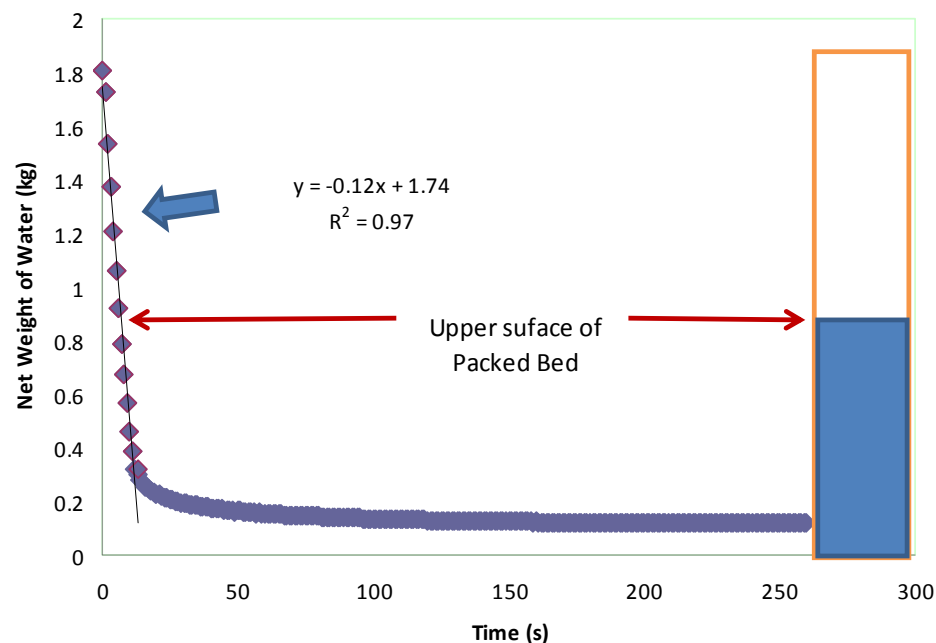
Figure **4-23**: Vertical drainage curve of packed bed from 2 mm glass beads. Red arrows show when the water table reaches to surface of packed bed.

Figure **4-24** and Figure **4-25** show that the vertical drainage curves for 3 kg of 3 mm and 5 mm glass beads, respectively. The difference of the three figures from **4-23** to **4-25** was that the slope of linear function is different, because of the difference of superficial velocities, and the final net weight of water is different, because of the difference of CFT and SH.
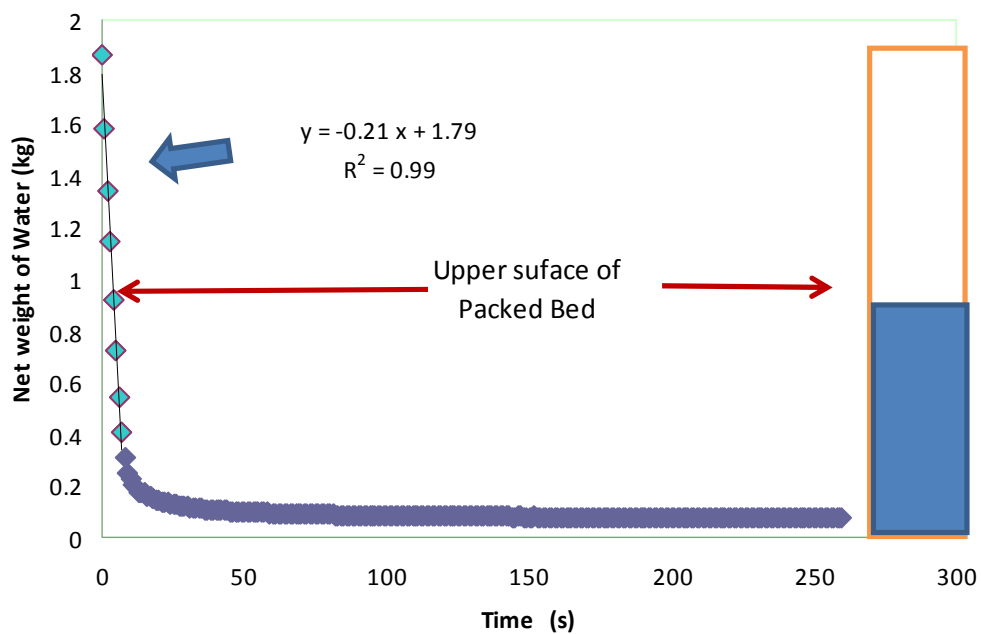
Figure **4-24**: Vertical drainage curve of packed bed from 3 mm glass beads. Red arrows show when the water table reaches to surface of packed bed.
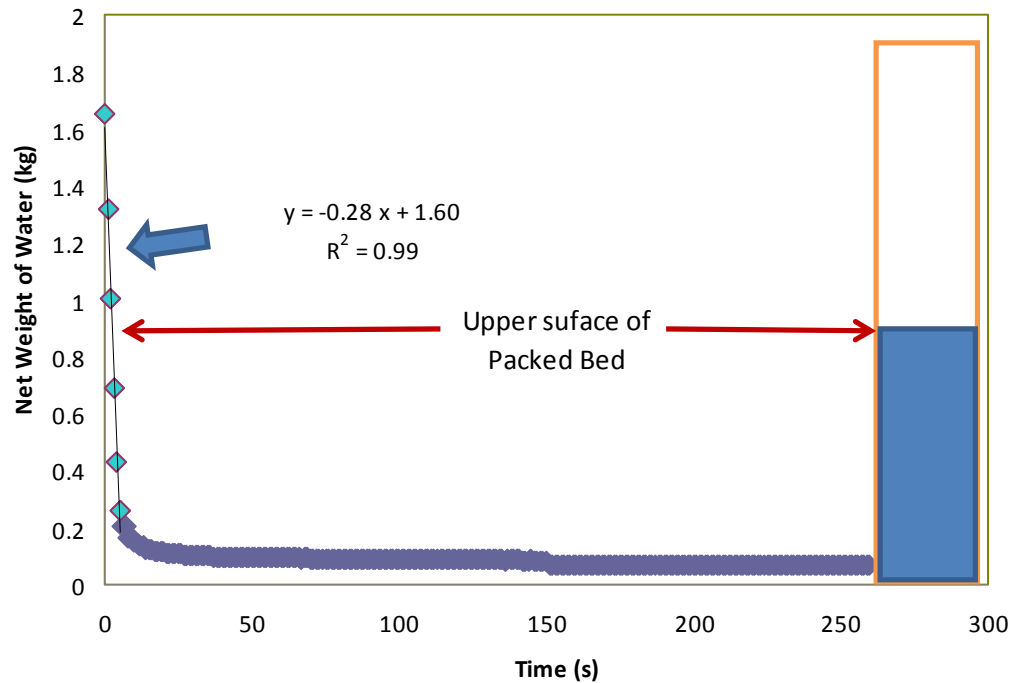
Figure **4-25**: Vertical drainage curve of packed bed from 5 mm glass beads. Red arrows shows when the water table reaches to surface of packed bed.

4.3 Conclusion

In this chapter, the properties of particles and fluid flow in packed bed were determined. From the experimental result, it can be concluded that:

1. For different packed beds with different sizes of uniform glass beads, the porosity is the same.

2. SH gradually increases from top to bottom of packed bed after vertical drainage.

3. CFT increased with the decreasing of glass beads diameter in packed beds. It is expected that CFT will decrease with increasing temperature.

CHAPTER 5

SIMULATOR FOR MEASURING HEAT AND MASS TRANSFER IN SEGMENTED-FLOW ASEPTIC PROCESSING

In this chapter, the PSAP simulator and related devices used in this project are introduced, followed by the experimental setup for measuring the heat and mass flow. The main purpose of this project was to investigate the performance of steam in heating packed beds, therefore, a PSAP simulator was designed and built for experimental investigation.

5.1 Introduction

In PSAP negligible heat and mass transfer occurs between adjacent segment units and all segments are identical (Figure **5-1**), so only one segment needs to be studied. A steam chamber was built to simulate a single segment in PSAP and is described below.
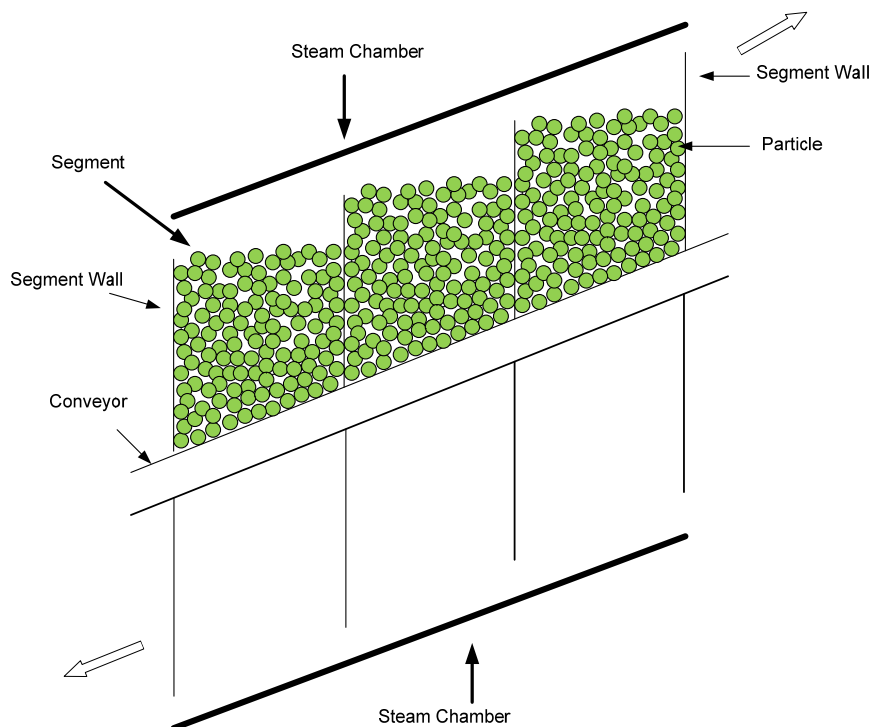
Figure **5-1**: Partial cross-sectional view of steam chamber of PSAP. Segments with particles move from lower left to upper right.

5.2 Steam Chamber

The steam chamber housing was made using a 1.2 m length of 20.3 cm OD (nominal 8-inch) stainless steel sanitary tubing with ID 19 cm. The steam chamber is pictured in Figure **5-2** and sketched in Figure **4-2**. Three ferrules were placed along the tubing length. The bottom ferrule was the water outlet; the middle one was for water level control and steam trap; and the top one was the steam inlet. The steam chamber was filled with water up to middle level and the upper space was filled with pressurized steam. This water-steam system was to simulate the processing of particulate foods in

PSAP where the particulate foods are dropped into water and carried by the conveyor into the steam environment (Figure **2-2**).
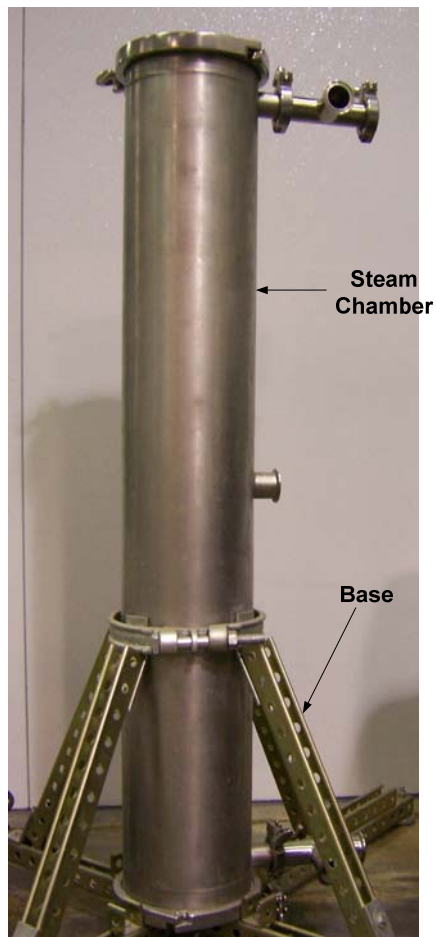
Figure **5-2**: Steam chamber for simulation of PSAP with supporting base.

saturated steam

shaft hole

vent and
pressure meter

7.6cm

20 cm Sanitary Cap
with two 3.8 cm diameter ferrules

120 cm

20 cm

water level
controller

60 cm

drain

8 cm

20x120 cm Flanged Tube
with three 3.8 cm diameter ferrules
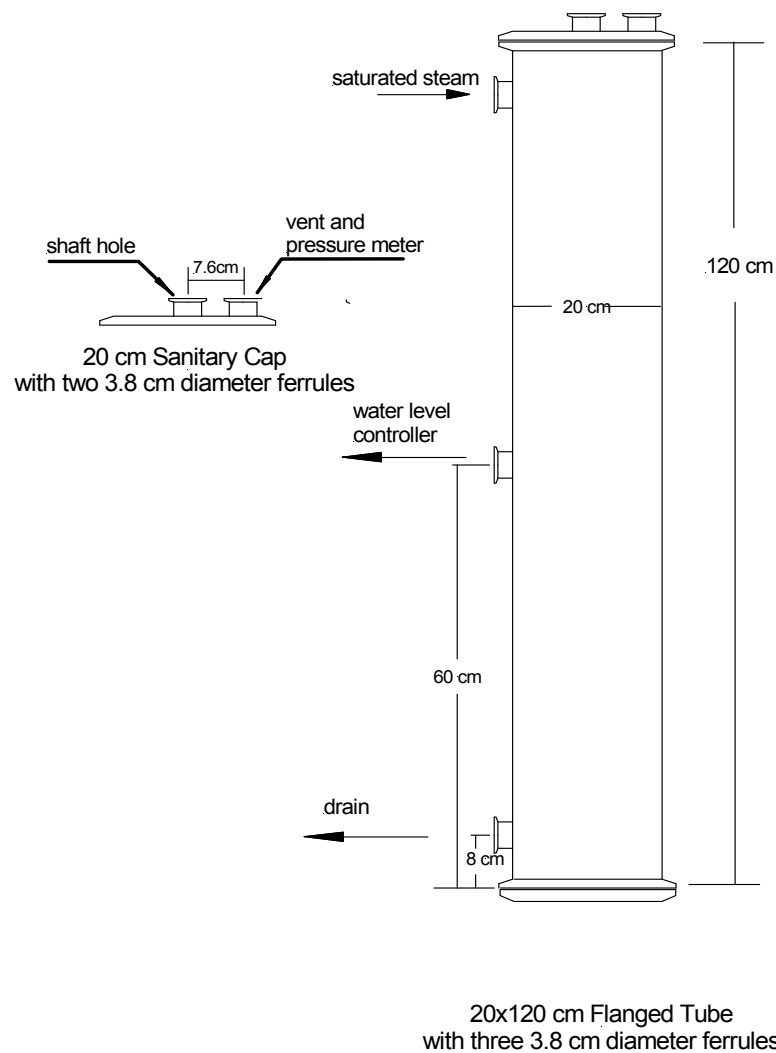
Figure **5-3**: Sketch of steam chamber which was used for the simulation of PSAP.

5.3 Polycarbonate Cylinder

Packed beds were held by polycarbonate cylinder with OD 101 mm, ID 95 mm and height 300 mm (Figure **4-2**).
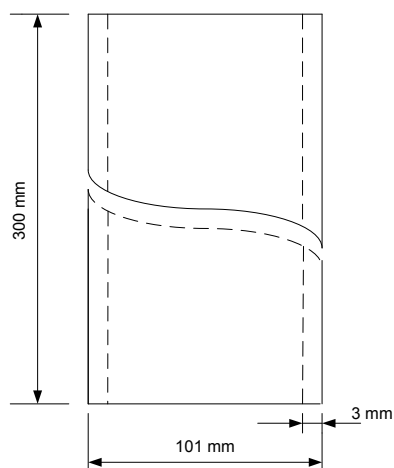
Figure **5-4**: Dimensions of polycarbonate cylinder.

5.4 Ventilation Box

Glass beads were used in this project to simulate particulate foods. A ventilation box was fabricated for drying the beads quickly with forced air flow. As shown in Figure **5-5**, the ventilation box was constructed of wood, leaving three holes on the top and one small hole on the side. Polycarbonate cylinders (OD 20.5 cm, ID 19.8 cm) with sieves (ID 21 cm) at the bottom were set above the three holes on top for holding glass beads. The mesh size in the sieve for different glass beads is presented in Table **4-5**. An electric blower (Model No: 4c440, Dayton Electronic Co., Chicago, IL) was set to the hole on the side to provide air flow into the polycarbonate cylinders.

78

Table **5-1**: Mesh size in sieve for holding and drying glass beads with ventilation box.

Glass Beads Size	2 mm	3 mm	5 mm
Mesh size (US Standard)	18	10	8
Mesh opening (mm)	1.00	2.00	2.38
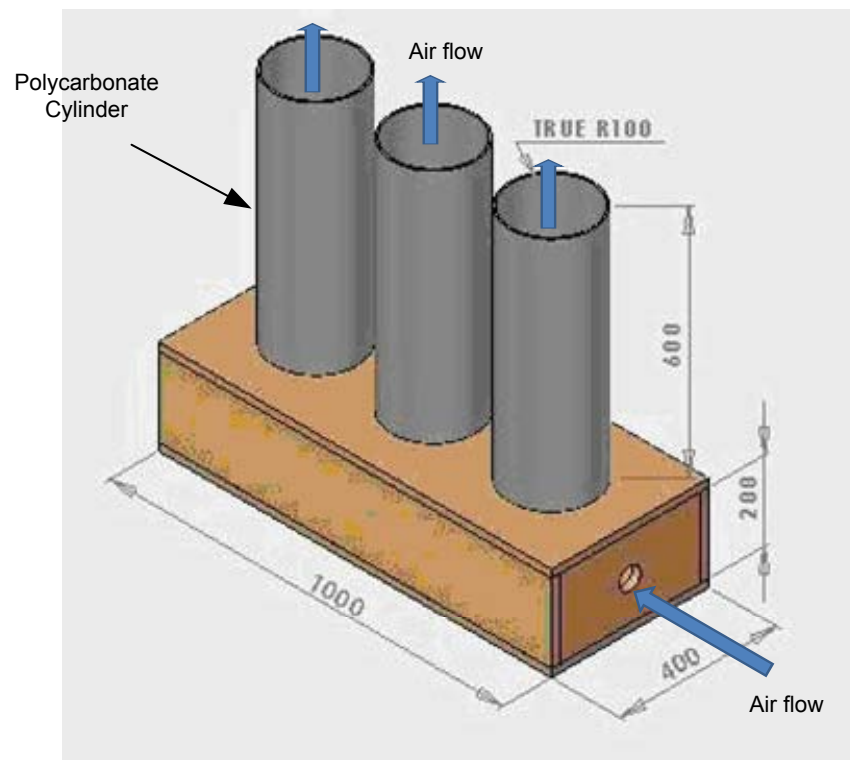
Figure **5-5**: Ventilation box and polycarbonate cylinder for drying glass beads. Unit: mm

5.5 Data Acquisition (DAQ) Device

The purpose of data acquisition is to measure an electrical or physical

phenomenon such as voltage, current, temperature, pressure, or sound. PC-based data

acquisition uses a combination of modular hardware, application software, and a computer to take measurements. DAQ hardware (National Instruments, Austin, TX) acts as the interface between the computer and the outside world. It primarily functions as a device that digitizes incoming analog signals so that the computer can interpret them.

5.5.1 National Instruments USB-6251

The National Instruments USB-6251, shown in Figure **5-6**, was a USB high-speed data acquisition (DAQ) module, which was used to convert the voltage signal measured by thermistors to temperature readings.

Figure **5-6**: NI DAQ 6251 USB device.

5.5.2 National Instruments USB-9162

The National Instruments USB-9162 (Figure **5-7**) was for measuring temperature with themocouples. The USB device had four channels of input from thermocouples, and one USB line to computer for data transfer.

Figure **5-7**: NI USB-9162 device used for thermocouples.

5.5.3 Midi Logger GL450

A data logger (also datalogger or data recorder) is an electronic device that records data over time. The advantage of data loggers is that they can operate independently of a computer. The Graphtec GL450 Midi Logger (Graphtec America Inc., Santa Ana, CA) was a data logger equipped with 10 channels, and expandable to 50 or

even 100 channels. It featured built-in Ethernet and USB 2.0 interfaces, maximum 100 million samples per second or as slow as 1 sample per hour, internal memory and flash memory for data storage, and built-in high input isolation (Figure **5-8**). It was used for recording temperatures measured with thermocouples.

Figure **5-8**: Graphtec Midi Logger type GL450.

5.6 Digital Scale

The Chatillon® DFS digital scale (Ametek Inc, Largo, Fl) shown in Figure **5-9** was used to measure the weight change of packed bed both in vertical drainage under room temperature and heating of packed bed with steam.

Figure **5-9**: Chatillon® Digital Scale for measuring weight change of packed bed.

5.7 Experiment Device Setup for Measuring Heat and Mass Transfer

The experimental setup for measuring temperature change in packed bed is illustrated in Figure **5-10**. A stainless steel hollow shaft with OD 1.59 cm, ID 1.33 cm, and length 95 cm was placed through the cord grip set in the ferrule in the center of the cap of the steam chamber (Figure **5-11**). The shaft moved smoothly up and down through the cord grip, which was used to prevent steam from leaking around the shaft. The polycarbonate cylinder was attached to the bottom of the shaft, and all the thermistor probe cables were routed through the shaft and were connected to the DAQ device.
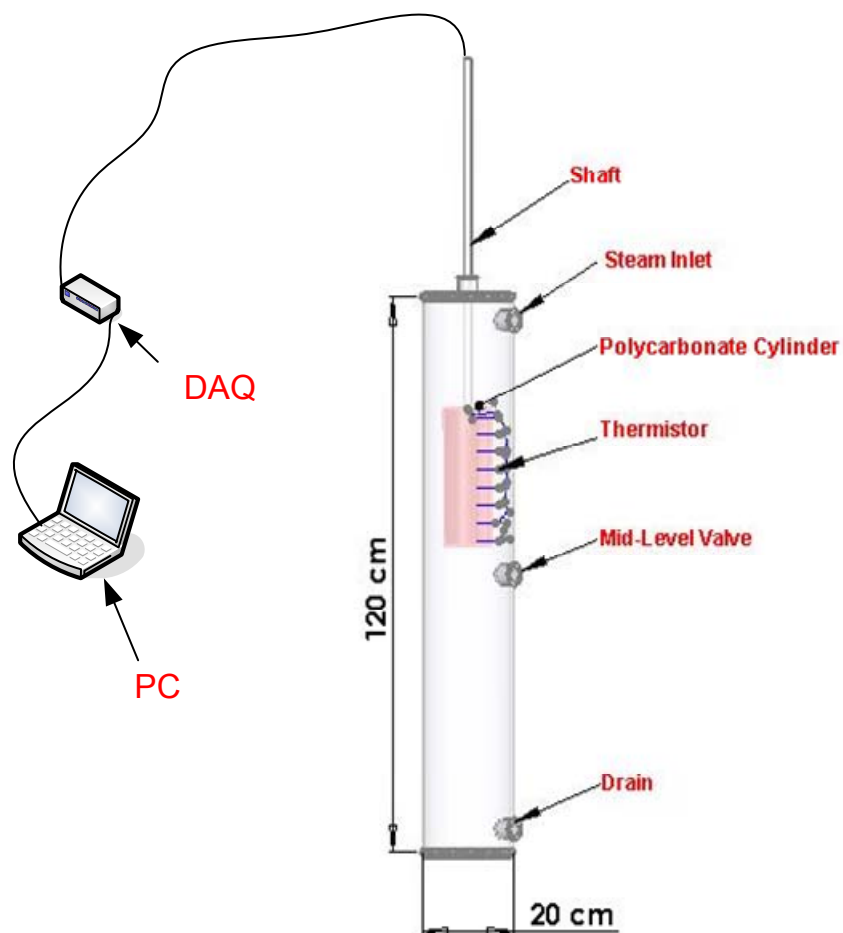
Figure **5-10**: Experimental setup for steam processing the packed bed in steam chamber using thermistors.
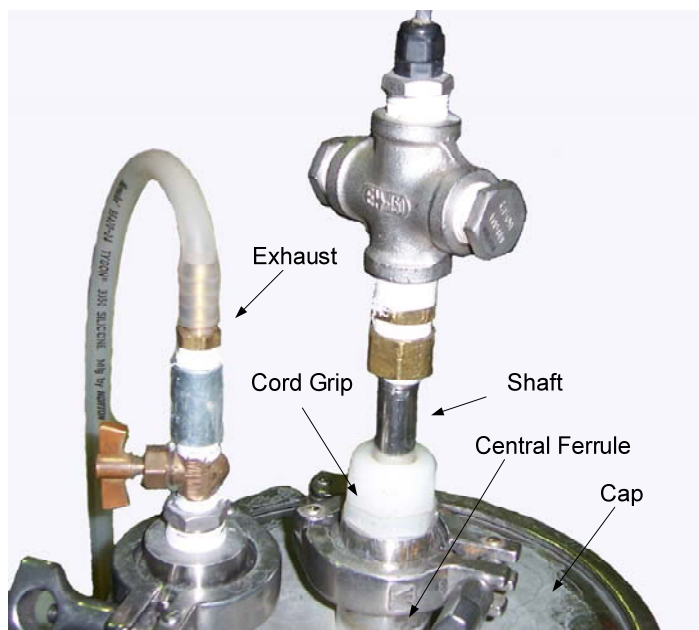
Figure **5-11**: Shaft set through the cap of steam chamber.

To measure both temperature change and mass change in packed bed during
steam processing, the shaft was replaced by a stainless steel wire rope (Figure **5-12**).
The upper end of wire rope was connected to the digital scale (Figure **5-9**) and lower
end was used to hold the polycarbonate cylinder. The whole experimental setup is
shown in Figure **5-13**. Thermocouples were selected because both probe and cable
were small and light so they were easy to handle and hardly interfered with
measurement of weight change during drainage. A wooden stick with diameter 0.6 cm
was placed along the vertical central line of packed bed (seen in Figure **4-10**) to hold the
thermocouple cables. The probes were placed horizontally at different elevations within
and near CF. The data acquisition device was the USB-9162 (Figure **5-7**).
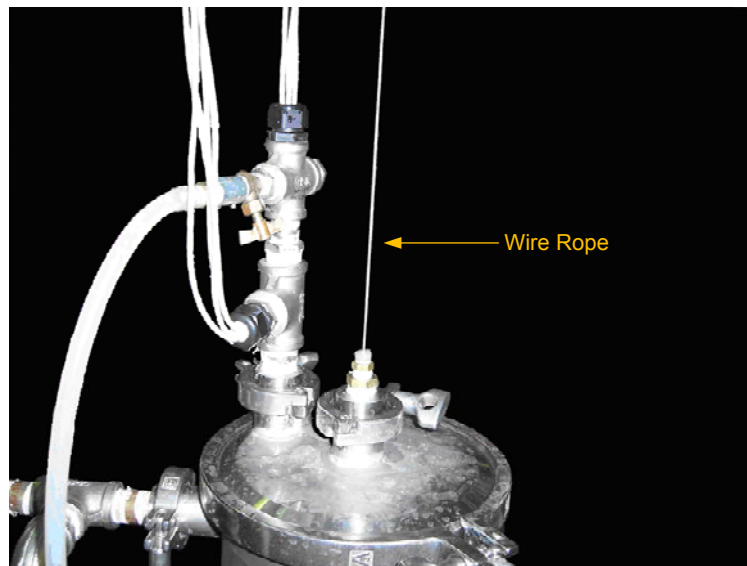
Figure **5-12**: Stainless steel wire rope was used to measure the weight change of packed bed in the steam processing.
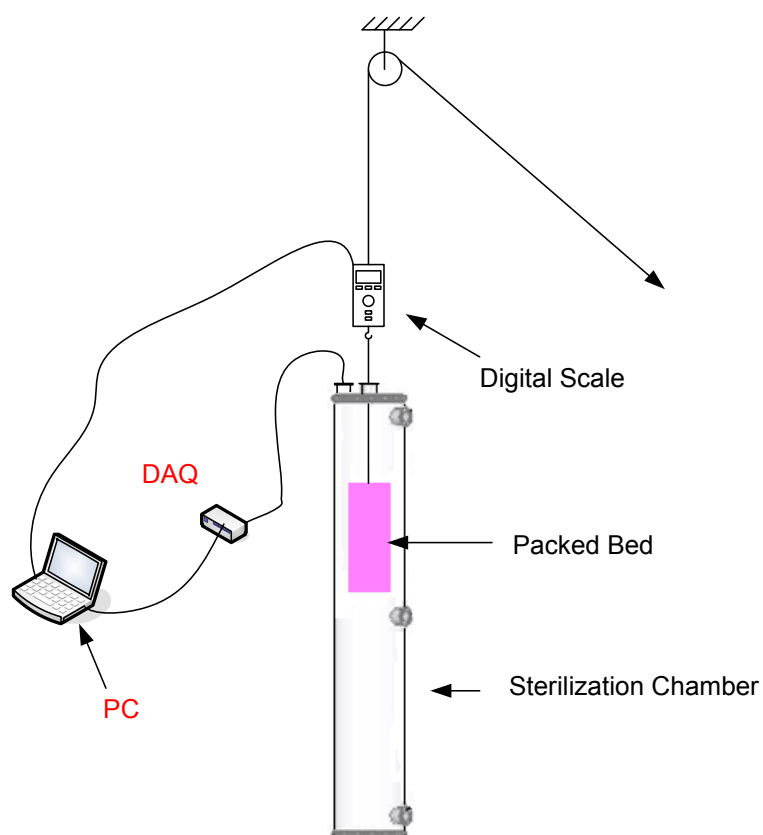
Figure **5-13**: Experimental design for measuring temperature and weight change of packed bed in steam using thermocouples and digital scale.
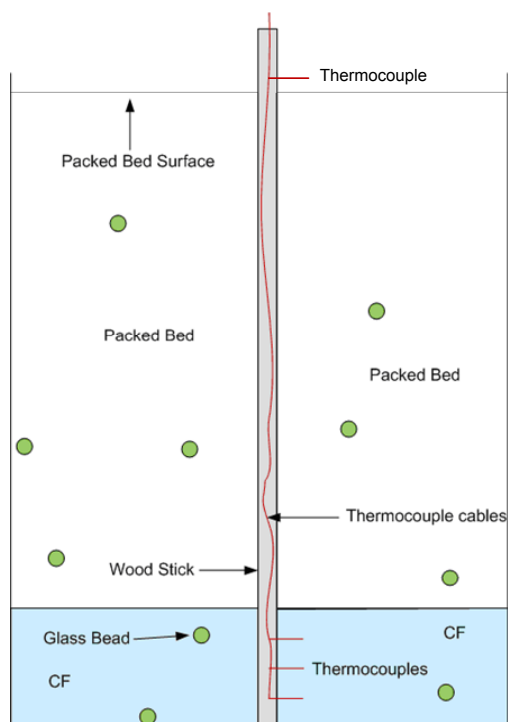
Figure **5-14**: Packed bed instrumented with thermocouples.

As described above, some temperature measurements were made with thermistors while others were made with thermocouples. The advantages and disadvantages of thermistors and thermocouples are summarized in Table **5-2**. To get the general temperature trend along axial direction of packed bed, thermistor probes were selected because data of more than 10 probes could be recorded by a single DAQ. To measure both heat and mass flow, thermocouples were selected because the probes are small and did not interfere with weight measurement.

Thermistors (Logan Enterprises, Inc., West Liberty, OH) were calibrated before use and were found to have an accuracy of 0.2 K. Although not required, calibration was performed on thermocouples before use.

Table **5-2**: Comparison between thermocouples and thermistors.

	Advantage	Disadvantages
Thermocouples	1. Sensitive. React quickly. 2. The cable is light and is easy to handle in experiment. 3. Calibration is not required before use. 4. Small and can be used for measuring two close positions.	1. More noises can be collected together with signal than for thermistors. 2. Not accurate. Error is ±1.5K at room temperature, and ±7K at 121ºC. 3. The USB device (Figure **5-7**) can only accommodate 4 themocouples. 4. The data logger (Figure **5-8**) can handle up to 20 channels of thermocouple, but is not stable for reading the temperature. 5. Thermocouples are much cheaper than thermistors, and are easily made and fixed.
Thermistors	1. Very accurate. The error is within 0.2k after calibration. 2. The USB device (Figure **5-6**) used for thermistors can accommodate up to 16 channels.	1. The probe tip is fragile and is easily broken. 2. The conjugation position of probe shell and cable needs to be sealed to prevent water and steam from entering the shell. 3. Cables are too thick, so are not suitable in measurement of mass change. 4. Expensive. 5. Calibration is required before use.

CHAPTER 6

**NUMERICAL MODEL OF HEAT AND MASS TRANSFER IN PACKED BEDS HEATED
WITH PRESSURIZED STEAM**

In this chapter, a numerical model for simulating heat and mass transfer in a
packed bed from steam to liquid film, and heat transfer inside particles is presented. The
depth of packed bed was divided into two zones, capillary fringe (CF) and the zone
above capillary fringe. It was further assumed that the zone above capillary fringe was
unsaturated after the first few seconds of drainage and was therefore called unsaturated
flow zone (UFZ). Mass and energy balances were both developed in each of the two
zones. The model was developed and run as an Excel spreadsheet (Microsoft® Office
Excel® 2007 SP1 SMO, Microsoft Corporation, Seattle, WA) using a finite difference
method. The model predictions at each elevation inside the bed included liquid holdup
and mass transfer rate, temperature of liquid phase and temperature profile inside
particles.

6.1 Finite Difference Method (FDM)

6.1.1 Introduction

Use of numerical methods for simulating heat and mass transfer for thermal
process calculations continues to increase along with the prevalence and power of
computers (Welt et al., 1997). Numerical methods are favored because, in many cases,
analytical solutions are not available. Development of a reliable thermal process analysis

method requires proper selection of a numerical method, and a sound approach for converting discrete time-temperature data into lethality predictions.

Analytical methods may fail if:

1. The particle differential equation (PDE) is non-linear and can not be linearized without seriously affecting the result.

2. The solution region is complex.

3. The boundary conditions are of mixed types.

4. The boundary conditions are time-dependent.

5. The medium is inhomogeneous or anisotropic.

The finite difference and finite element methods are now two universally used approaches for solving linear and nonlinear differential equations governing engineering problems. Depending on the nature of the problem, each method has its advantages. FDM is simple to formulate, can readily be extended to two or three dimension problems, and is easy to learn and apply. The finite element method (FEM) has the flexibility in dealing with problems involving irregular geometry. However, with the advent of numerical grid generation, the FDM now possesses the geometrical flexibility of the finite element method while maintaining the simplicity of the conventional finite-difference technique.

The FDM was first developed in the 1920s (Thom and Apelt, 1961) under the title "the method of square" to solve nonlinear hydrodynamic equations. The finite-difference techniques are based upon the approximations that permit replacing differential equations by finite difference equations. These finite difference approximations are algebraic in form, and the solutions are related to grid points. Thus, a finite difference solution basically involves three steps:

1. Dividing the solution into grids of points.

2. Approximating the given differential equation by finite-difference equivalence that relates the solutions to grid points.

3. Solving the difference equations subject to the prescribed boundary conditions and/or initial conditions.

6.1.2 Applications of Finite Difference Method (FDM) in Numerical Modeling

The FDM makes it simple to formulate a set of discretized equations from the transport differential equations in a differential manner. The finite-difference (FD) scheme can be easily applied to two or three-dimensional problems (Wang and Sun, 2003). The FDM is normally used for simple geometries such as sphere, slab and cylinder, and has been widely used to solve heat and mass transfer models of many thermal processes such as cooking and frying (Akterian and Fikiin, 1994; Mohamed, 2003), drying (Thorvaldsson and Janestad, 1999; Wang and Brennan, 1995), cooling and freezing (Chau and Gaffney, 1990; Sun and Zhu, 1999), and fluid flow such as vertical drainage (Masciopinto et al., 1994; Pinczewski and Tanzil, 1981; Todsen, 1971).

6.1.3 Modeling with Excel Spreadsheet

Several commercial software applications for modeling of heat and mass transfer and computational fluid dynamics (CFD) exist, such as MATLAB (Mathworks Inc, Natick, MA), Fluent (ANSYS Inc., Canonsburg, PA), ANSYS (ANSYS Inc., Canonsburg, PA), etc. To use these applications properly, the users need to be fully trained. Moreover, such commercial software is expensive. Considering the applicability of the model in this

dissertation, an Excel spreadsheet template was developed for modeling heat and mass transfer and fluid flow which is easy to use and requires little training.

6.2 Mathematical Model

Several models of heat and mass transfer in a packed bed with a phase change have been proposed by investigators (See Literature Review in Chapter **2**). For example, Bergins et al. (2005) presented an analytical model for the description of a one-dimensional condensing flow of steam in a packed bed. The model included an expanded momentum balance and took into consideration both compressibility of the steam and the increase of pressure loss due to the higher condensation rate of initial water filling of the porous structure. However, the authors assumed that condensation only occurred in the condensation front, which is not applicable in this study. Moreover, the research utilized high speed steam, which is different from this project.

6.2.1 Assumptions

In this study, the packed bed was initialized with the beads submerged in water to the top surface of the bed, all at a uniform temperature (Figure **6-1**). The following assumptions were applied:

1. The packed bed of glass beads is isotropic and has a uniform porosity.
2. At time<=0, the liquid (water) phase temperature is equal to the packed bed temperature (solid phase).
3. Only steam (water vapor) is considered as gas specie in the void space of packed beds.

93

4. As illustrated in Figure **6-2**, after saturated flow of vertical drainage the packed bed consists of two zones: Unsaturated flow zone (UFZ) and capillary fringe (CF).

5. Thermophysical and thermodynamic properties of the vapor, liquid, and solid are constant except those specified.

6. The packed bed is horizontally infinite and heat and mass are transferred only vertically.
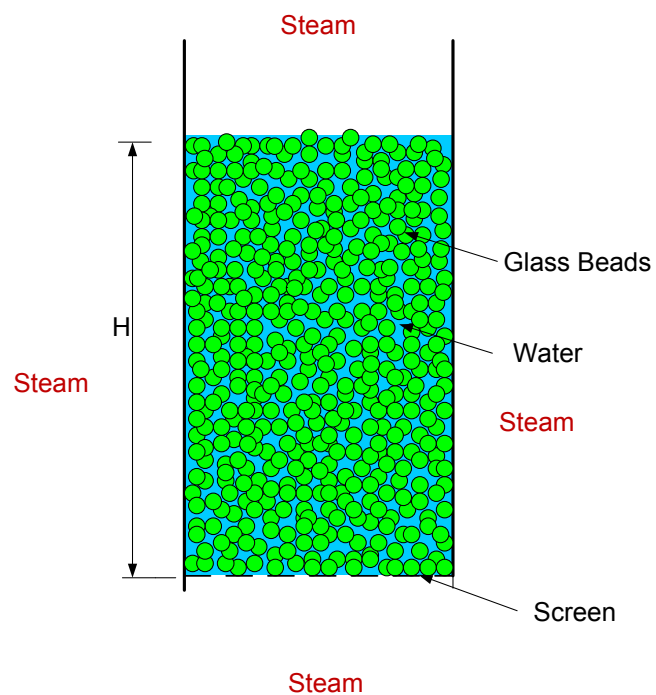
Figure **6-1**: Initial conditions of packed bed, surrounded with saturated steam.
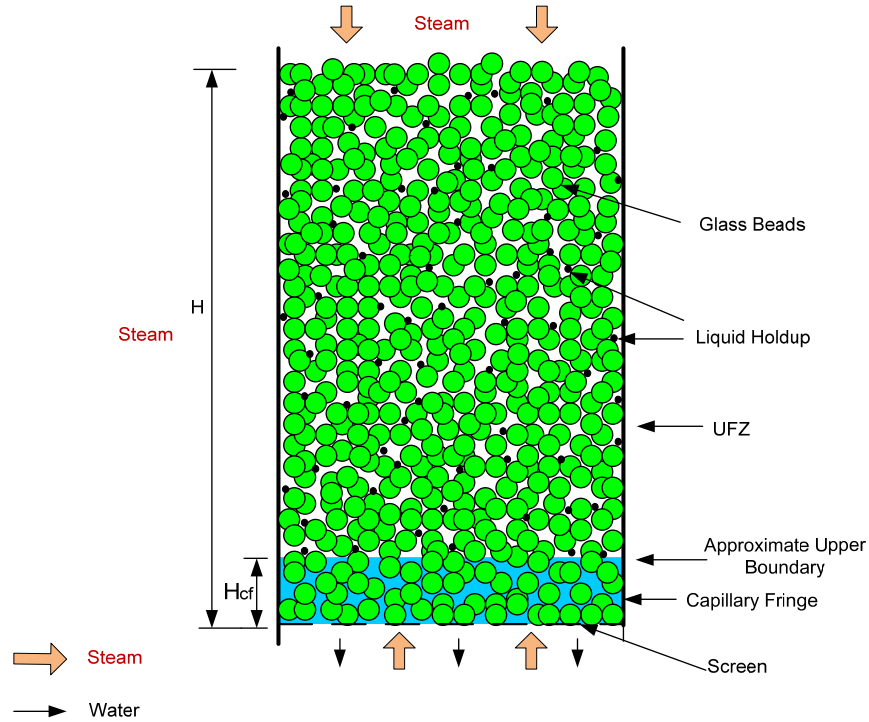
Figure **6-2**: Two zones are formed in packed bed after initial drainage.

Based on these assumptions, the problem was 1-dimensional unsteady heat and mass transfer with isotropic heating at both ends of the packed bed. The overall scheme of this mathematical model was to divide the UFZ and CF into N and M layers, respectively, as shown in Figure **6-3**. Each layer was an element in finite-difference scheme. At each element, the mass balance and energy balance were developed. The total height of packed bed was H, the height of capillary fringe was H_{cf}, and the height of UFZ was H_u. For the consideration of continuum, the height of each element should be at least the double value of glass beads diameter, so Eq. **6.1** needs to be satisfied

$$\frac{H_u}{N} > 2d_p \qquad\qquad \textbf{6.1}$$

where d_p is the particle diameter.
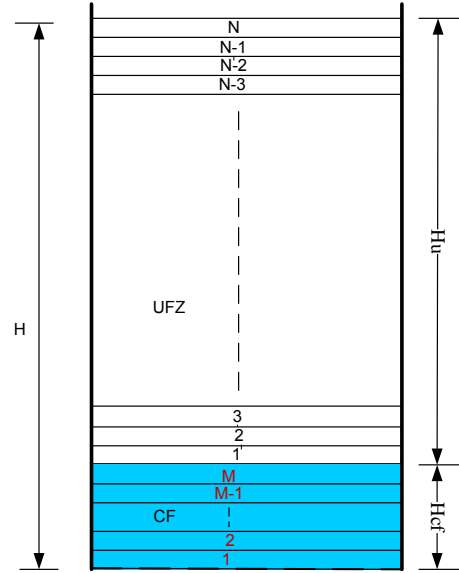
Figure **6-3**: UFZ and CF were divided into layers for the finite difference scheme.

6.2.2 Mass Balance of Liquid

The mass balance over a small volume element of cross-sectional area of packed bed and thickness, *dH*, leads to the governing equation for the liquid phase in UFZ:

$$W_{ini} + W_{in} + W_{cond} - W_{out} = W_{t}$$
6.2

where W_{ini} is the initial liquid volume, W_{in} and W_{out} are the liquid inflow from upper layer and liquid outflow to lower layer, respectively, W_{cond} is the condensate from steam to this element, and W_{t} is the total liquid also the initial liquid at next time step. The finite difference forms of Eq. **6.2** are given as

$$W_{ini,n}^{t} + W_{in,n}^{t} - W_{out,n}^{t} + W_{cond}^{t} = W_{t,n}^{t},$$
$$W_{ini,n}^{t} = W_{t,n}^{t-1},$$
$$W_{in,n}^{t} = W_{out,n+1}^{t},$$
$$W_{out,n}^{t} = W_{in,n-1}^{t},$$

6.3

where n= 1, 2, 3, ……, N, and N is the total number of layers in UFZ and t is the time step.

The liquid mass inflow rate in one layer equals the liquid outflow rate of the upper layer plus the condensate rate in this layer:

$$F_{in,n} = F_{or,n+1} + w_{cond,n},$$

6.4

where w_{cond} is the condensation rate (kg/s), which is equal to

$$w_{cond} = \frac{W_{cond}}{t} = \frac{q_{fg}}{H_{fg}},$$

6.5

with q_{fg} being the condensation heat transfer flux from steam to liquid film, H_{fg} (J/kg) the latent heat of steam.

The water content in each layer, which is also called the total holdup (TH), can be calculated by

$$\beta_{t} = W_{t}/V_{L}$$

6.6

with β_{t} being the total liquid holdup, and V_{L} the volume of each layer in UFZ.

The dynamic holdup β_{dy} is determined by total holdup β_{t} and SH β_{s}

$$\beta_{dy} = \beta_{t} - \beta_{s},$$

6.7

and DH is associated with liquid flow-out rate in each layer. The relationship between DH and liquid outflow velocity ($F_{out,}$ cm/s) was experimentally determined. The

correlations for 2, 3, and 5 mm glass beads are presented in Chapter 4.2.4 and

summarized as follows

$$F_{out} = (k_1 * \beta_{dy}^2 + k_2 * \beta_{dy}) * Ac, \ \beta_{dy} \leq k_5$$
$$F_{out} = (k_3 * \beta_{dy}^2 + k_4 * \beta_{dy}) * Ac, \ \beta_{dy} > k_5$$

6.8

where k_1, k_2, k_3, k_4, k_5 are the coefficients listed in Table **6-1**, Ac is the cross-sectional

area of the packed bed.

Table **6-1**: Coefficients in the equations for mass transfer rate and DH.

Coefficient	2 mm	3 mm	5 mm
K_1	1.464	2.812	3.068
K_2	0.011	0.019	0.037
K_3	0.085	0.114	0.259
K_4	-0.002	-0.000	-0.006
K_5	0.0983	0.0576	0.0486

6.2.3 Energy Balance

6.2.3.1 Energy Balance in Unsaturated Flow Zone (UFZ)

The energy balance over a small volume element of cross-sectional area of

packed bed and thickness *dH* in differential time *dt*, leads to the governing equation for

the liquid phase:

$$Q_{cond} + Q_{in,l} - Q_{out,l} = Q_{st,l} + Q_{st,s}$$

6.9

where Q_{cond} (J) is the heat transferred to the liquid from the steam by condensation, $Q_{in,l}$

(J) is the heat transferred with mass transfer from upper layer, $Q_{out,l}$ (J) is the heat

transferred with water flow to lower layer, $Q_{st,l}$ (J) is the energy stored into liquid film, and

$Q_{st,s}$ (J) is the energy transferred into solid particles.

For given layer in UFZ, the condensation heat transfer rate depends on the heat transfer area, condensation heat transfer coefficient, and temperature difference between steam and contact surface. The following simplifications were applied:

1. The condensation heat transfer coefficient in each layer in UFZ is given as (Popiel and Boguslawski, 1975):

$$h_a = 0.826 * \left[\frac{g\rho_l(\rho_l - \rho_g)k_l^{3}h_{fg}^{'}}{\mu_l(T_a - T_{su})d_p} \right]^{1/4}$$ **6.10**

where,

h_a = condensation coefficient, (W/(m^2·K))

g = gravity acceleration, (m/s^2)

ρ_l = liquid density, (kg/m^3)

ρ_g = steam density, (kg/m^3)

k_l = liquid conductivity, (W/(m·K))

h_{fg}' = modified latent heat of steam, (J/kg)

μ_l = viscosity of liquid, (kg/(m·s))

T_{su} = initial temperature of particles, (K)

d_p = diameter of particles, (m)

h_{fg}' is the modified latent heat of steam (Rohsenow, 1956) in terms of the Jacob number Ja

$$h_{fg}^{'} = h_{fg}(1 + 0.68Ja)$$ **6.11**

2. The local condensation coefficient h_L is proportional to h_a in each layer:

$$h_L = ch_a\varepsilon_L^{p}$$ **6.12**

where c and p are model calibration constants, ε_L is the local porosity and is given as

$$\varepsilon_L = \varepsilon - \beta_t \qquad \text{6.13}$$

with ε being packed bed porosity, β_t the total holdup. So when the packed bed is saturated with water, the local porosity is 0.

3. Each particle in the same layer is covered with the liquid film with the uniform thickness. The sum of mass in the liquid film is equal to the total liquid in the layer.

4. There is no temperature gradient in liquid film.

5. Heat is transferred from the steam to the liquid film is by condensation, while from the liquid film to the solid particles is by convection.

6.2.3.1.1 Energy Inflow by Condensation

The heat transfer by condensation from steam to liquid film is given as

$$Q_{cond} = h_L * S_c * (T_a - T_{lav}) * t_{step} \qquad \text{6.14}$$

with S_c being the condensation heat transfer area (m^2), T_a the ambient steam temperature (K), T_{lav} the average liquid film temperature (K), and t_{step} the time step (s). S_c is expressed as

$$S_c = 4\pi(\frac{d_p}{2} + \delta_{fl})^2 \qquad \text{6.15}$$

where d_p is the particle diameter, δ_{fl} the liquid film thickness.

6.2.3.1.2 Energy Inflow with Heat Transfer

The heat inflow $Q_{in,l}$ is equal to the heat transfer out of upper layer:

$$Q_{in,l,n} = Q_{out,l,n+1} = \rho_l c_{p_l} V_{in,n+1} T_{l,n+1}$$ **6.16**

with ρ_l being the liquid density, c_{p_l} the liquid heat capacity, $V_{in,n-1}$ the liquid inflow

volume per time step, $T_{l,n+1}$ and $T_{l,n}$ the liquid average temperature in layer n+1 and

layer n, respectively.

6.2.3.1.3 Energy Stored in Solid Particles

The energy stored to the solid particles is based on a finite-difference model for a

sphere which was developed by Walker (2006) and used to predict lethality values. The

sphere is considered homogeneous, and divided into concentric shells of equal

thickness of r/X, where r is radius of the sphere, X is the number of shells. The center

shell is the core with outside radius r/X and zero inside radius. Shown in Figure **6-4** are

shells for the finite-difference scheme with X=10. Assuming the sphere is subjected to

uniform convective heating from the ambient fluid or gas, the heat is transferred from

outer media by convection to the sphere, while the heat transferred from the surface of

sphere to the core is by conduction. The average temperature of each shell is calculated

at each time step. The model determines the temperature, average population fraction,

and lethality for each shell.
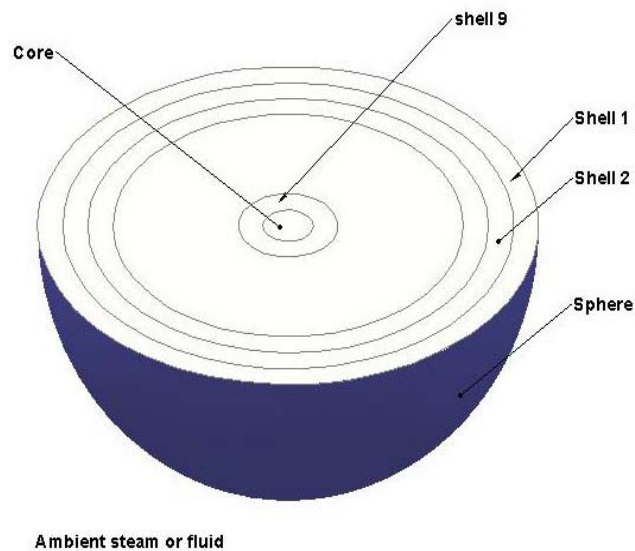
Figure **6-4**: The shells for finite-difference model for heat conduction inside a sphere.

This finite-difference model for heat conduction inside the sphere built the prediction-iteration function to calculate the average temperature in each shell rather than to develop a finite-difference form of the governing equation of heat diffusion in the radial directions in sphere. The model assumed, for each shell unit at each time step, the ambient temperature is equal to the average temperature of outer shell. The temperature difference between outer shell and inner shell is the driving force of heat conduction. The Excel-spreadsheet-based model used an iteration function at each time step. The iteration number per time step depended on how accurate the data needed to be. Too many iterations lead to longer running time, while too few iterations give inaccurate results.

Fourier's law of heat conduction is given as

$$\frac{\Delta Q}{\Delta t} = -kA\frac{\Delta T}{\Delta r}$$

6.17

where $\dfrac{\Delta Q}{\Delta t}$ is the amount of heat transferred in the unit of time, k is the conductivity of

solid, A is the cross-sectional area of heat transfer, and $\dfrac{\Delta T}{\Delta r}$ is the temperature gradient

along the heat transfer direction.

The boundary condition for heat transfer from liquid film to solid particle is given

as

$$-k_s \frac{\partial T_{sh,1}}{\partial r} = h_l (T_{lav} - T_a) \qquad\qquad \textbf{6.18}$$

where k_s is the thermal conductivity of solid particle, T_{lav} the average temperature of

liquid film, T_a the steam temperature, $T_{sh,1}$ the average temperature of shell 1, r the shell

thickness, and h_l the convection coefficient in liquid film.

The heat transferred from shell i (i= 1, 2, 3, …., X) to shell i+1 at each time step

can be written as

$$Q_{insh,i} = k_s A_{sh,i} \frac{\Delta T}{\Delta r} t_{step} \qquad\qquad \textbf{6.19}$$

with $A_{sh,i}$ being the outer surface area of shell i, ΔT the actual temperature difference

between shell i and shell i-1 , Δr the radial thickness of shell $\underline{i}$, and t_{step} the time step.

$\dfrac{\Delta T}{\Delta r}$ is the driving force of heat conduction, and can be obtained from the predicted and

current temperature

$$\frac{\Delta T}{\Delta r} = \frac{T_{presh,i} - T_{cush,i}}{\Delta r} \qquad\qquad \textbf{6.20}$$

where $T_{presh,i}$ and $T_{cush,i}$ are the predicted temperature and current temperature of shell *i* at each iteration, respectively. The Eq. **6.19** can be also written as in regard to mass and heat capacity

$$Q_{sh,i} = m_{sh,i} c_{p_s} \Delta T_{sh,i}$$

6.21

where $m_{sh,i}$ is the mass of shell *i*, c_{p_s} is thermal capacity of the solid particle, and $\Delta T_{sh,i}$ is the increased temperature per iteration.

6.2.3.1.4 Energy Stored in Liquid Phase

The heat stored in liquid film surrounding solid particles has two sources: steam condensation and mass transfer from upper space. Assuming no temperature gradient exists in the liquid film, the temperature increase per time step is given as

$$\Delta T_{fl} = \frac{Q_{st,l}}{m_{fl} c_{p_l}}$$

6.22

where m_{fl} is the mass of liquid film, and c_{p_l} is the thermal capacity of liquid. $Q_{st,l}$ is obtained from Eq. **6.9** which addresses the energy balance.

The temperature increase per time step leads to the average temperature of liquid film for next time step

$$T_{lav}^{t+1} = T_{lav}^t + \Delta T_{lav}$$

6.23

6.2.3.2 Energy Balance in Capillary Fringe (CF)

Heating of the CF by steam is a complex heat transfer phenomenon which involves condensation, conduction, and convection heat transfer, and mass transfer in and out of the capillary fringe (Wu and Walker, 2008). As shown in Figure **6-2** , saturated steam is heating the CF from both the top and bottom after saturated vertical flow. The resulting condensate flows down into the CF and out of the bottom due to the storage limit of the CF. The temperature gradient is toward the center of the CF by the heating on both upper and lower boundaries. Heat is transferred from the fluid into the glass beads by both conduction and convection.

In order to enable a finite-difference solution for heating of the capillary fringe, the following assumptions were made:

(1) The heat transfer in horizontal direction was negligible as it would be for an infinite slab bed;

(2) Heat transfer between adjacent elevations was by both mass transfer and conduction.

(3) Since solid particles were identical and surrounded by fluid, capillary fringe could be treated as isotropic and homogenous slab with uniform mixed density ρ_m, effective thermal conductivity k_{ef}, and effective specific heat capacity $c_{p_{ef}}$.

(4) The heat transfer was by convection from liquid to solid particle in CF.

The heating of a capillary fringe composed of glass beads and water could thus be considered as one-dimensional transient heat conduction and convection in a homogeneous, isotropic body without inner heat generation. Condensation heat transfer took place on top and bottom boundaries and conduction and mass transfer take place inside of the CF.

It is difficult to verbally define an effective thermal conductivity in the capillary fringe of a packed bed since the thermal conductivity is heterogeneous indeed because of random packing and the differences in conductivity between the solid and liquid fractions. However, the effective thermal conductivity can by modeled as an analog of an electric circuit, and the most widely used equation for effective thermal conductivity is Maxwell function (Bird et al., 2002):

$$\frac{k_{ef}}{k_l} = 1 + \frac{3\lambda}{\left(\dfrac{k_s + k_l}{k_s - k_l}\right) - \lambda}$$ 6.24

where k_s and k_l are thermal conductivity of solid particle and liquid, respectively; λ is the volume fraction of solid particles. Mixed density ρ_m and effective specific heat $c_{p_{ef}}$ can be obtained from local volume average properties (Izadifar et al., 2006):

$$\rho_m = (1 - \varepsilon)\rho_s + \varepsilon\rho_l$$ 6.25

$$c_{p_{ef}} = \frac{\rho_s c_{p_s}(1 - \varepsilon) + \rho_l c_{p_l}\varepsilon}{\rho_m}$$ 6.26

where ε is the porosity of packed bed; ρ_s and ρ_l are the densities of solid particles and fluid, respectively.

At the two boundaries of CF, convection heat transfer occurs:

$$-k_{ef}\left.\frac{\partial T_{cf_0}}{\partial x}\right|_{x=0} = h_{CF,up}(T_{cf_0} - T_a)$$ 6.27

$$-k_{ef}\left.\frac{\partial T_{cf_L}}{\partial x}\right|_{x=L} = h_{CF,low}(T_{cf_L} - T_a)$$ 6.28

Where $h_{cf,up}$ and $h_{cf,low}$ are condensation coefficients at upper and lower boundaries of CF, respectively, T_{cf_0} and T_{cf_L} are temperatures at the upper and lower boundaries of CF,

respectively, x is the coordinate vertically upwards, and *L* is the total height of CF which equals H_{CF}.

The model for predicting the temperature change at different elevations was developed with the finite difference method. The capillary fringe was divided into 10 horizontal layers and an energy balance was completed at each time step of each layer. An iteration function was used at each time step to enable the continuous calculation.

For a given elemental layer, the energy balance is given as

$$E_{incon,m} + E_{inma,m} - E_{outcon,m} - E_{outma,m} = E_{st,m} ,$$ **6.29**

$$E_{incon,m} = E_{outcon,m-1}$$ **6.30**

$$E_{inma,m} = E_{outma,m+1} ,$$ **6.31**

where E_{incon} and E_{inma} are the energy inflow by conduction and mass transfer, respectively; E_{outcon} is the heat outflow by conduction, and subscript m, $m-1$, $m+1$ denote the layer numbers.

As shown in Figure **6-5**, conduction heat transfer is from two boundaries to center of CF, so in a certain layer, the average temperature is lower than both conjoint layers. Since heat transfer conditions are not symmetric from the center line of CF, the slowest-heated layer may vary.
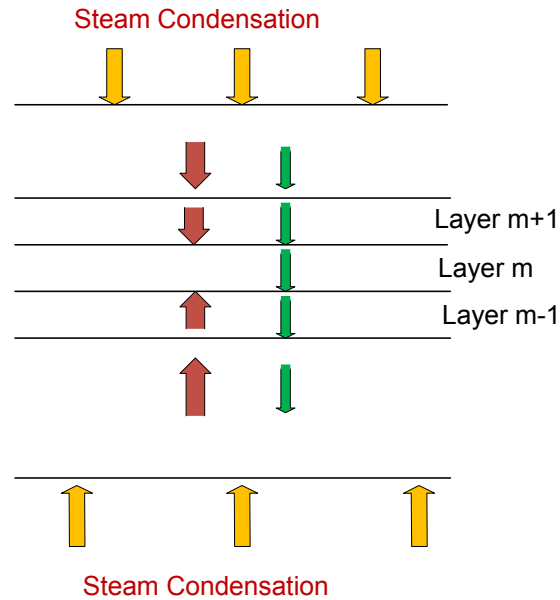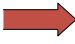
Figure **6-5**: Heat transfer direction in capillary fringe.

Note: condensation heat transfer
 conduction heat transfer
 heat transfer with mass flow

The energy inflow by conduction is given as

$$E_{incon} = k_{ef} A_c \frac{\Delta T}{\Delta x} t_{step} ,$$ **6.32**

where k_{ef} is the effective thermal conductivity of CF, A_c is the cross-sectional area of the packed bed, $\Delta T / \Delta x$ is the temperature gradient between conjoint layers, and t_{step} is the time step.

The energy outflow by conduction is equal to the energy inflow by conduction at the next layer, i.e.

$$E_{outcon,m} = E_{incon,m-1}$$ **6.33**

The energy inflow to layer *m* in CF with mass transfer is given as

$$E_{inma,m} = c_{p_l} V_{in} \rho_l T_{CF,m+1}$$ **6.34**

with c_{p_l} being heat capacity of fluid, V_{in} mass inflow volume, and $T_{CF,m+1}$ the average

temperature of layer m+1.

At the top and bottom boundaries, conduction heat transfer is zero,

$$E_{incond,m=0} = 0$$ **6.35**

$$E_{outcond,m=10} = 0 .$$ **6.36**

In given layer, the temperature change per iteration is

$$\Delta T_{cf} = \frac{E_{st}}{m_{cf} c_{p_{ef}}}$$ **6.37**

where m_{cf} is the total mass in layer m.

The temperature change leads to the calculated temperature

$$T_{cf,m}^{j+1} = T_{cf,m}^{j} + \Delta T_{cf}$$ **6.38**

where *j* is the time step.

With iteration per time step, the average temperature of each layer can be

obtained. The model also contains the calculation of heat conduction inside solid

particles in capillary fringe which is similar to the model described above for UFZ.

6.3 Excel Spreadsheet Program of Finite-Difference Model

6.3.1 Run and Stop Function

Iteration is the repeated recalculation of a worksheet until a specific numeric condition is met. Excel cannot automatically calculate a formula that refers to the cell — either directly or indirectly — that contains the formula. This is called a circular reference. If a formula refers back to one of its own cells, one must determine how many times the formula should recalculate. Circular references can iterate indefinitely. However, one can control the maximum number of iterations and the amount of acceptable change. The iteration function is shown in Table **6-2** and the flow diagram for run and stop of Excel program is show in Figure **6-6**.

Table **6-2**: Iteration function in finite-difference model of Excel spreadsheet using five iterations per time step.

Variable Name	Symbol	Value	Unit	Formula
Initialize Iterations	INIT	False or true		Input false or true
Iteration count per time step	ITER	0 to 5		=IF(INIT,0, IF(ITER=5,0,ITER+1)))
Elapsed time	Time	0.00	s	=IF(INIT,0,IF(ITER,Time,Time+t step))
Time step	tstep	0.005	s	

In an Excel spreadsheet, number 0 stands for logical value "FALSE" and all other numbers stand for logical value "TRUE", in any logical function. To initialize the FD model, input "True" or any number except "0" for the variable INIT. To run the FD model, input "False" or number "0" in the same cell. When the "stop condition" is reached, the program stops running. For example, if the grogram needs to be stopped when elapsed time is over 400, the stop function is written as

$$IF(Time>400,1,IF(ITER=5,0,ITER+1)). \qquad \textbf{6.39}$$
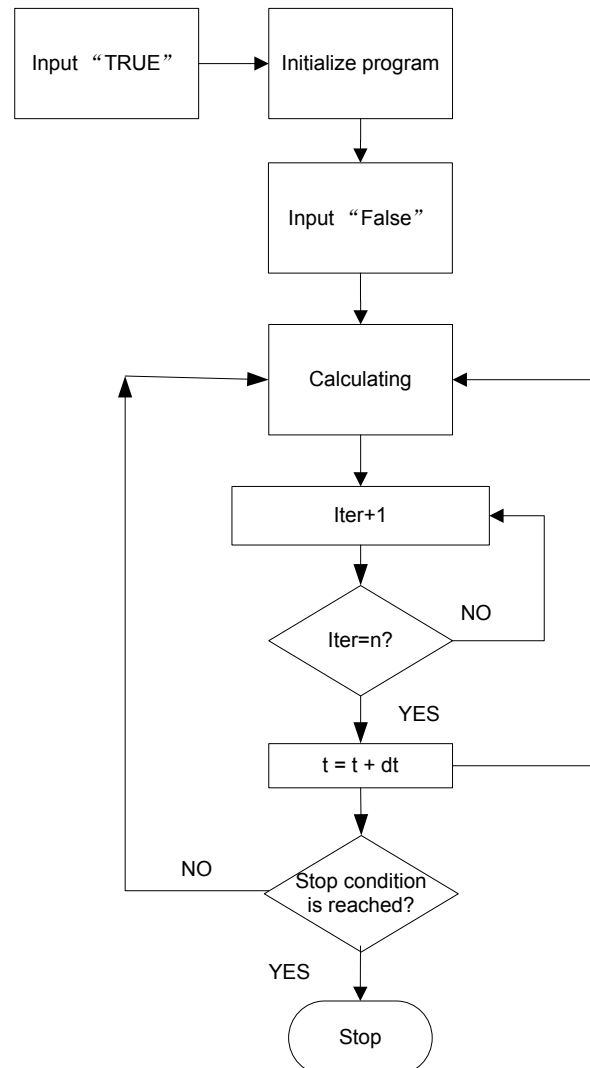
Figure **6-6**: Flow diagram showing the RUN and STOP function in Excel program.

Notes: t is time, dt is time step, Iter is iteration number. n=5 in this research.

6.3.2 Constant Parameters

The constant parameters specify the properties of the packed bed and the thermophysical and thermodynamic properties of its solid, liquid and steam components (Table **6-3**). All the constant parameters are highlighted in blue within the spreadsheet. The model parameters for UFZ and CF are shown in Table **E-1** Table **E-2**, respectively.

Table **6-3**: Constant parameters in Excel spreadsheet program.

Variable Name	Symbol	Value	Unit	Notes
Cylinder inside diameter	Dc	0.095	m	
Specific density of glass beads	Rhoc	2877	kg/m^3	at 25ºC
Bulk density of glass beads	Rhobu	1554	kg/m^3	at 25ºC
Conductivity of solid	ks	1.06	W/m·K	
Specific heat of solid	Cps	846	J/kg·K	
gravity acceleration	g	9.8	m/s^2	
viscosity of liquid	mu	279E-6	N·s/m^2	
water density	rhol	957.8	kg/m^3	
Specific heat capacity of liquid	Cpl	4217	J/kg·	at 100ºC
Conductivity of liquid	kl	0.687	W/m·K	at 100ºC
Surface tension of liquid	sigma	5.89E-2	N/m	at 100ºC

CHAPTER 7

EXPERIMENTAL INVESTIGATION OF HEATING OF PACKED BEDS WITH ISOTROPIC SATURATED STEAM

In this chapter, experiments designed to investigate the water flow and temperature change in packed beds of glass beads in pressurized-steam are described. The results were later used to verify the numerical model for simulating the packed beds.

7.1 Experiment Procedure

The thermistors were horizontally inserted into the packed bed as shown in Figure **7-1**. The elevation between each probe was 3.8 cm, and the bottom probe was 1.9 cm depth from bottom. Probes were numbered from 1 to 8 from bottom. Depending on weight of glass beads used, the upper probes were exposed only to steam.
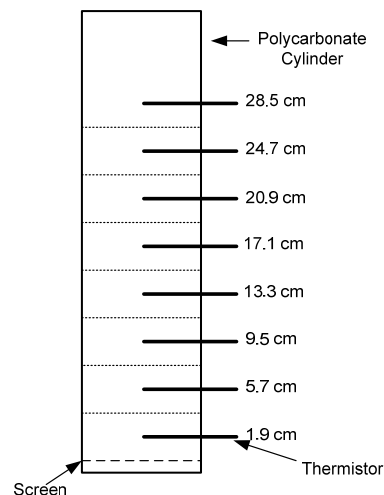
Figure **7-1**: Position of thermistor probes through the wall of polycarbonate cylinder. Dimensions shown are from the screen. The dashed lines represent the possible surface of bed for different experiments.

The general experimental procedure to investigate the heating of packed bed with saturated steam was as follows:

1. Fill cylinder with selected size and weight of glass beads and place in the experimental device as shown in Figure **5-13**.

2. Lower the polycarbonate cylinder to bottom of chamber.

3. Close drainage outlet, open mid-level valve and fill the chamber with clean tap water up to middle level.

4. Close water inlet (bottom valve), open steam valve to fill the upper space of chamber with saturated steam, allowing steam and air to vent out from the mid-level valve. Venting required approximately 15- 20 seconds.

5. Close mid-level valve to allow steam to pressurize and heat the upper part of chamber to steady state conditions at approximately 121˚C. This required approximately 15 seconds.

6. Move the shaft upward to raise the packed bed into the pressurized steam environment. Steam starts to heat the packed bed.

7. Observe and record probe temperatures using LabView program (Figure **7-2**).

After each trial, the beads and experimental device were cooled to below 17˚C by running tap water through the system. Experiments were conducted in a lab environment with room temperature 25±3ºC.

Figure **7-2**: Control panel of LabView program for collecting temperature data using thermistor probes.

7.2 Experiment Results and Observations

To minimize differences between trials caused by slightly different initial and steam temperatures, temperatures were converted to non-dimensional accomplished temperature fraction (ATF)

$$ATF = \frac{T - T_i}{T_a - T_i}.$$ **7.1**

Similarly, unaccomplished temperature fraction (UTF) is defined as

$$UTF = \frac{T_a - T}{T_a - T_i}.$$ **7.2**

The variation in the initial temperature of packed bed was partially due to the tap water temperature, which changed with use and seasonally. The steam used in this experiment came from the general steam supply of the Agricultural Engineering Building (University Park, PA), which was shared with other users and utilities. Therefore the steam supply was not constant, leading to steam pressure fluctuations which were mostly but not fully eliminated by the steam pressure regulator.

7.2.1 General Trend in Steam Penetration

Different bed depths of 5 mm and 3 mm glass beads were tested first to obtain the general trend of temperature history in packed beds under steam processing. Steam pressure was set at 2.05×10^5 Pa absolute pressure (121ºC). Time zero was when the water table falls to upper surface of bed.

The results for 5 mm and 3 mm glass beads, respectively, with 8, 15, and 23 cm bed depths, are shown in Figure **7-3** and Figure **7-4**, respectively**.** It is clear that the different elevations in the packed beds were heated in top to bottom order. The delay time for each curve reflects the movement of the steam heating front.

It was noted that the delay time for the bottom probe, as shown in Figure **7-3** to Figure **7-4**, is obviously larger than those of other curves. Since the distance between each temperature probe is constant (3.8 cm), the steam penetration speed, which is related to the water drainage speed, is decreasing when the water table level approaches bottom of packed bed. This effect is different from CF because lowest probe was above CF (CFT= 1.0-1.4 cm for 3 mm glass beads, and CFT= 0.4-0.6 cm for 5 mm glass beads).
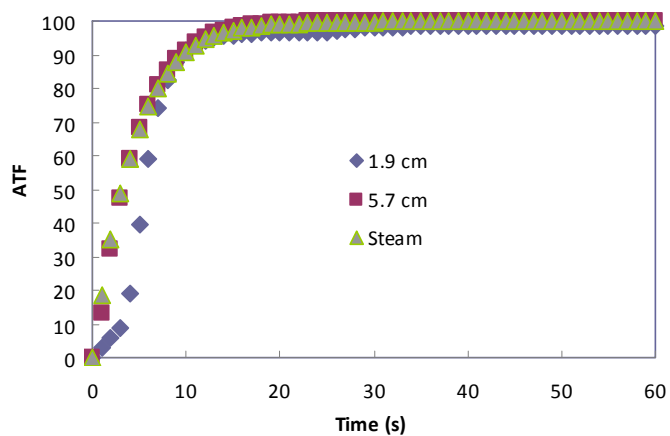
(a)
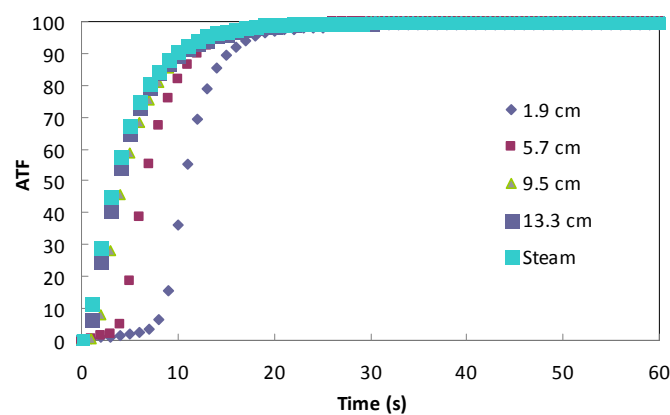
(b)
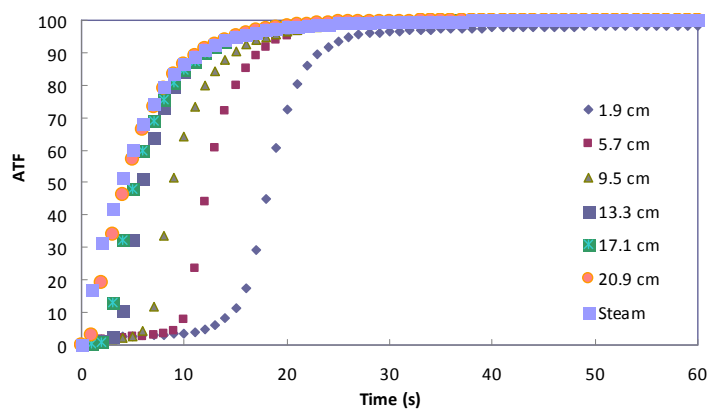
(c)

Figure **7-3**: Steam penetration experiment results for 8, 15, and 22 cm bed depths of 5 mm glass beads.
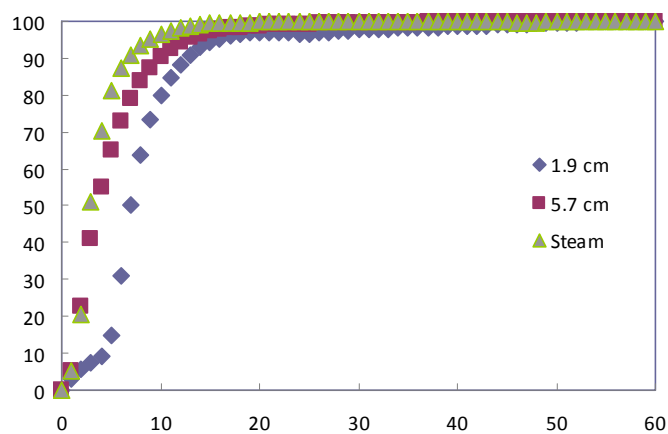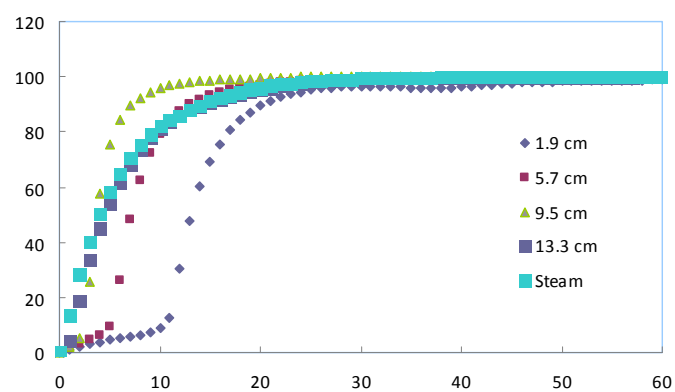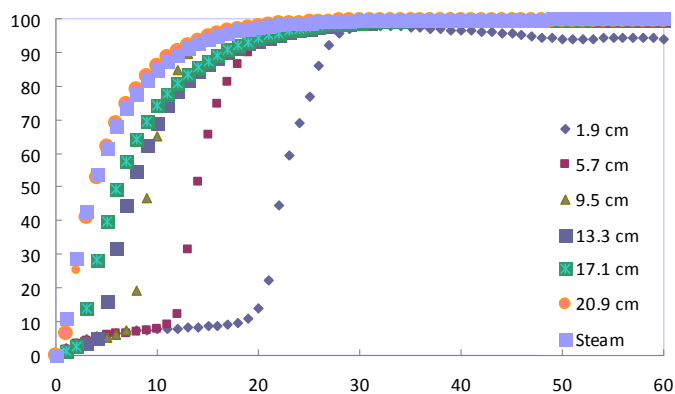
Figure **7-4**: Steam penetration experiment result for 8, 15, and 23 cm bed depths of 3 mm glass beads.

7.2.2 Measuring Temperature History of Capillary Fringe (CF)

The positions of the thermistor probes were changed to allow the bottom probe to stay in CF of 2 mm glass beads. Due to the limitation of device, the minimum depth of bottom probe was set to 1 cm depth from bottom, which was out of the range of CF of 5 mm glass beads which is 0.4-0.6 cm. The results are shown in Figures **7-5** to **7-7** and only data from the first 400 s were plotted.
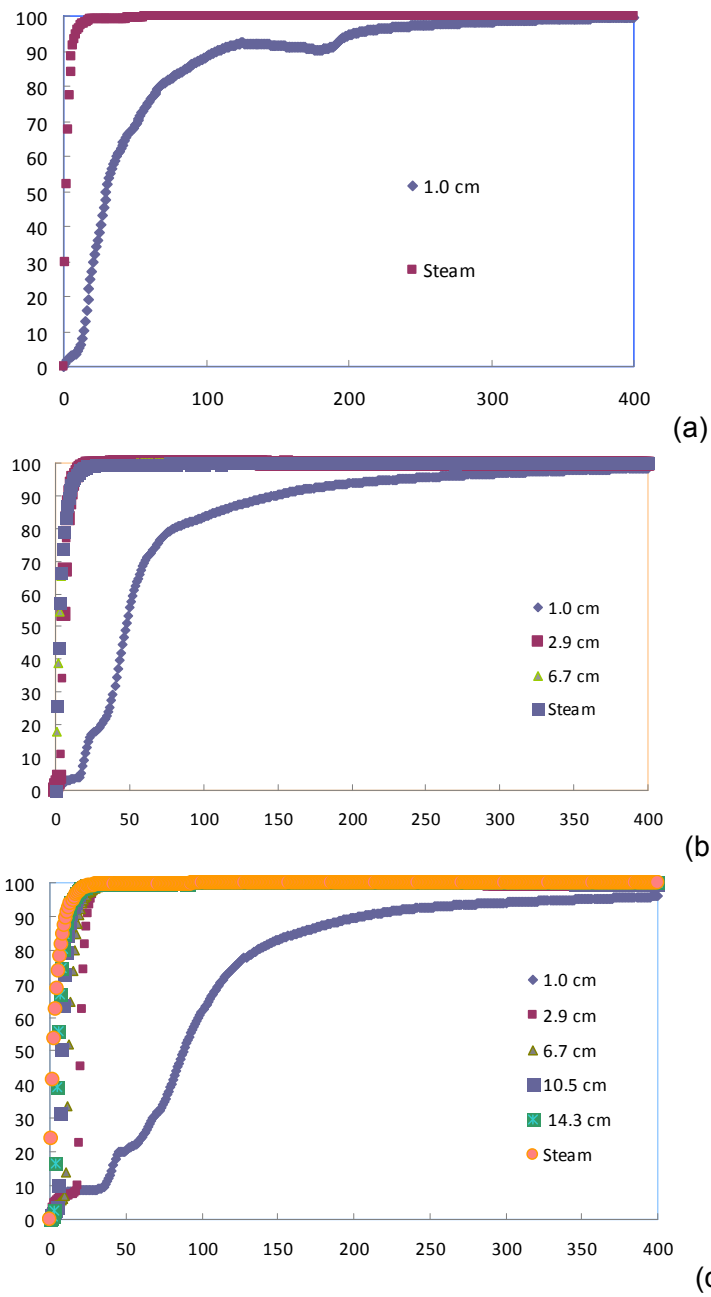
Figure **7-5**: Steam penetration experimental result for bed depths of 2, 11 and 18 cm of 2 mm glass beads. (a) 2 cm. (b) 10 cm. (c) 18 cm.
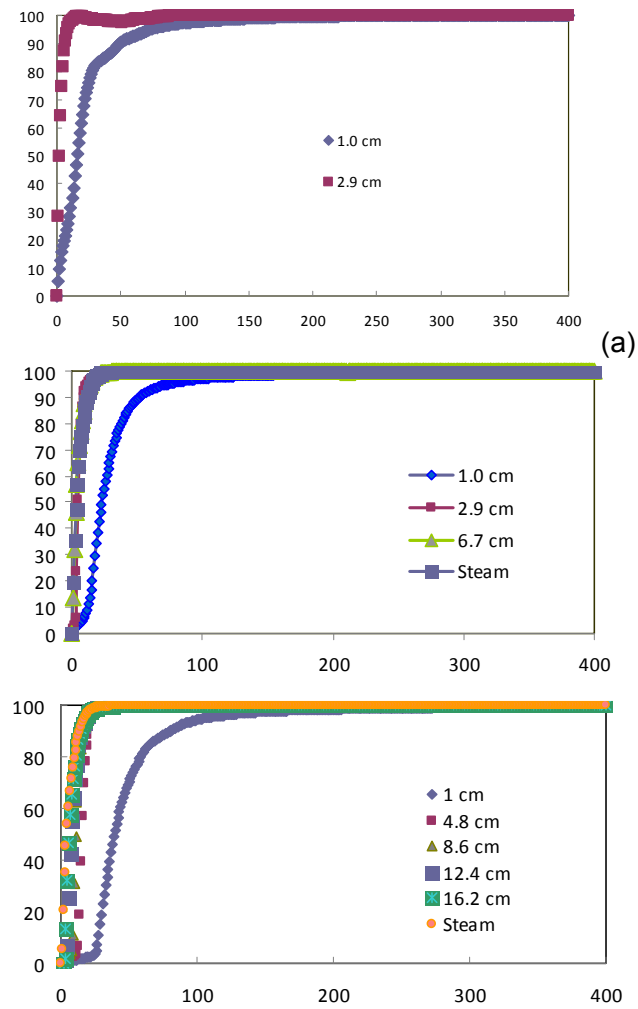
Figure **7-6**: Steam penetration experimental result for bed depths of 2, 11, and 18 cm of 3 mm glass beads. (a) 2 cm. (b)10 cm. (c) 18 cm.
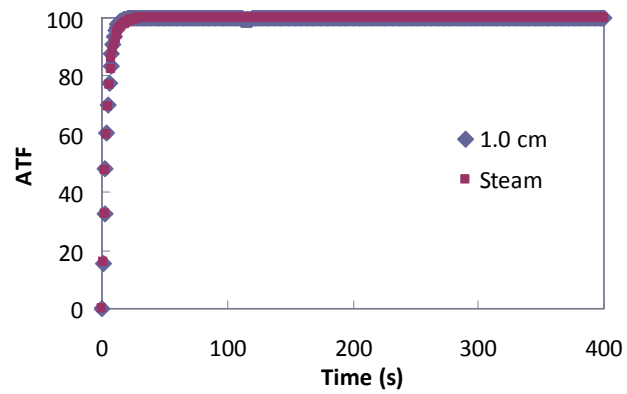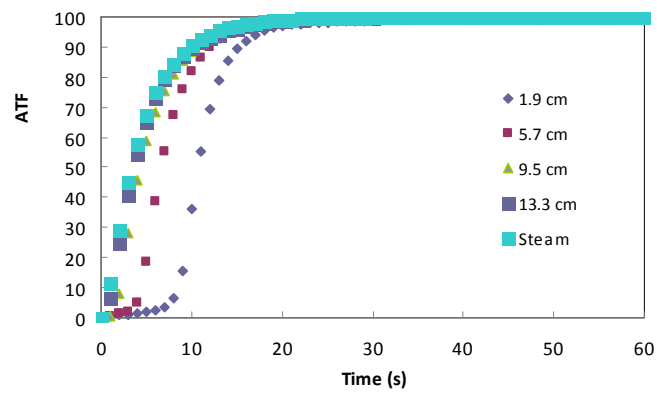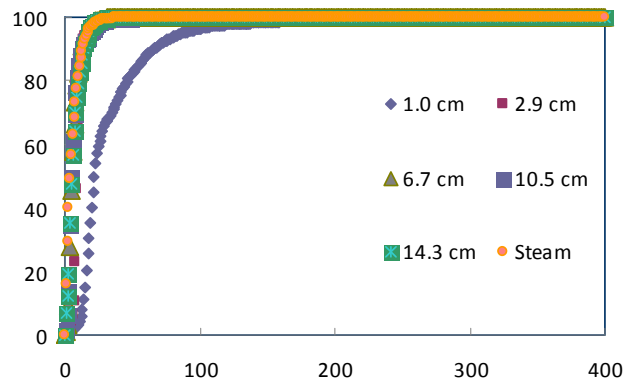
Figure **7-7**: Steam penetration experimental result for bed depths of 2, 11, and 18 cm of 5 mm glass beads. (a) 2 cm. (b)10 cm. (c) 18 cm.

From Figure **7-5** to Figure **7-7**, it can be seen that the bottom probe was heated slower in deeper packed bed. To clearly see the trend, we can compare the ATF of bottom probe (1.0 cm depth) with different bed depths for the same size of glass beads. The maximum ATF (%) of bottom probe illustrated in Figure **7-8** is 97 for each depth of packed bed from 2 mm glass beads. It is shown that the bottom probe was heated with greater delay by adding more glass beads to packed bed, which is caused by the longer time needed for vertical drainage and steam penetration. The time taken to reach ATF=97% was approximately 100 s for 2.0 cm, 310 s for 11 cm, and 470 s for 18 cm. Similar curves can be obtained for 3 mm and 5 mm glass beads, and are shown in **Appendix C** in Figure **C-1** and Figure **C-2**, respectively.
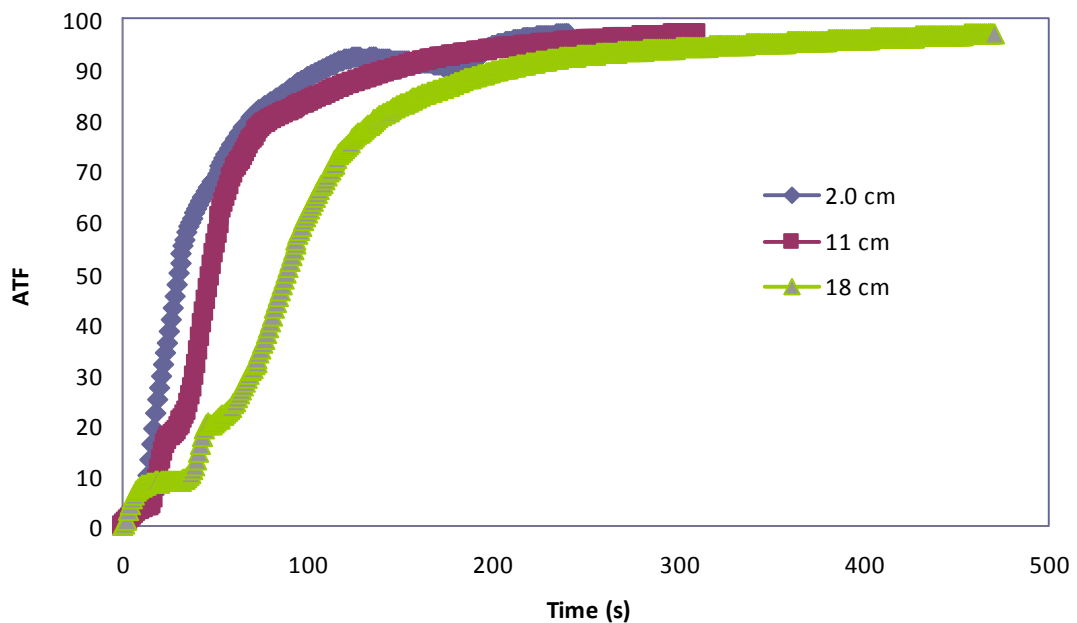
Figure **7-8**: ATF of the bottom probe (1.0 cm depth) for 2 mm glass beads. Curves end at where ATF=97%.

Figure **7-9** shows the effect of bead size on heating at the 1 cm level, all with a

bead depth of 18 cm. The 2 mm beads were the slowest heating while the 5mm beads

were the fastest and the reason is that the probe in packed bed of 2 mm glass beads

stayed in the center of CF, while the 1 cm depth for 3 mm and 5 mm, were placed on the

edge and in the UFZ, respectively.
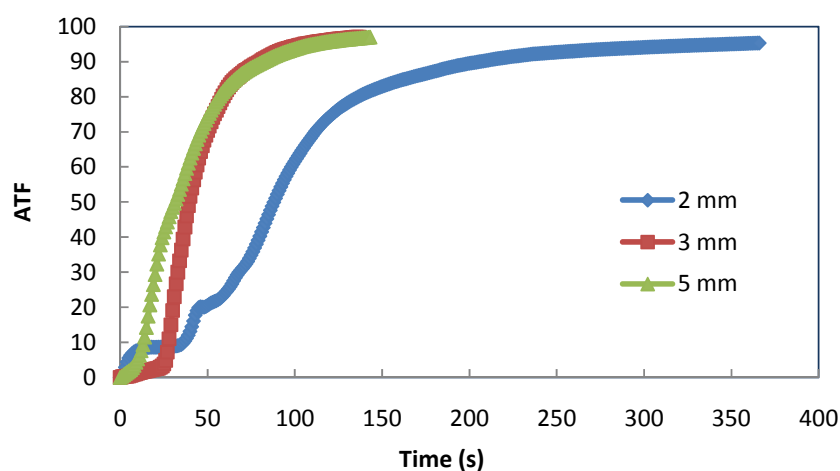
Figure **7-9**: Temperature fraction at elevation of 1 cm depth using 2 mm, 3 mm, and 5
mm glass beads (18 cm bed depth). Curves were ended at ATF=97%.

7.2.3 Thermocouples plus Digital Scale for Measuring Temperature and Weight Change

From the results above, it can be seen that the CF is heated more slowly than

other portions of the packed beds. However, the temperature history right above and

within the CF needed more investigation. Therefore, simultaneous measurements of

weight and temperature were performed for 2, 3 and 5 mm glass beads. For 3 and 5 mm

glass beads, probes were placed right in the middle of CF and at positions above CF.

The representative results are shown in **Appendix C** from Figure **C-8** to Figure **C-9**. For

2 mm glass beads, experiments were performed to measure the temperature distribution in and immediately above CF to determine the "coldest" point. The CFT for 2mm beads is about 1.8-2.4 cm, so CF is thicker than that of 3 and 5 mm glass beads.

7.2.3.1 Investigation at Capillary Fringe for 2 mm Glass Beads

The experimental setup is shown in Figure **5-10** and both temperature and weight of packed bed were measured as a function of time.

Thermocouple probes were located at 0.7, 1.2 and 1.7 cm from the bottom. The fourth probe was placed 1 cm above the surface of bed. As earlier, steam pressure was set at 2.05×10^5 Pa absolute pressure (121ºC). Three replications were performed.

Additional trials were conducted with the bottom probes changed to 2.2, 2.7, and 3.2 cm from bottom, with the top probe was in the same position. These changes were made in order to test the temperature trend on the edge of CF. Three replications were performed.

Representative results of 18 cm bed depth of 2 mm glass beads are presented in Figure **7-10** and Figure **7-11** with probes positions changed. Data from -50 to 800 s were plotted, with time zero being when the water level falls to bed surface.

From Figure **7-10** and Figure **7-11** it can be seen clearly that the sharp increase of steam temperature and sharp decrease in weight of packed bed occurred at the same time. Basically there was little temperature difference between the positions of 0.7 cm and 1.2 cm, while the 1.7 cm position heated more slowly.

The summarized temperature result for elevations from 0.7 cm to 3.2 cm (from bottom) in steam processing in 18 cm depth of 2 mm glass beads is illustrated in Figure **7-12**. It shows that except at the beginning of processing (the first 100 s), the

temperature at positions of 1.7 cm and 2.2 cm were lower than those of 0.7 cm and 1.2 cm, but the difference was not much. Also it shows obviously that the UFZ was heated much faster than CF.
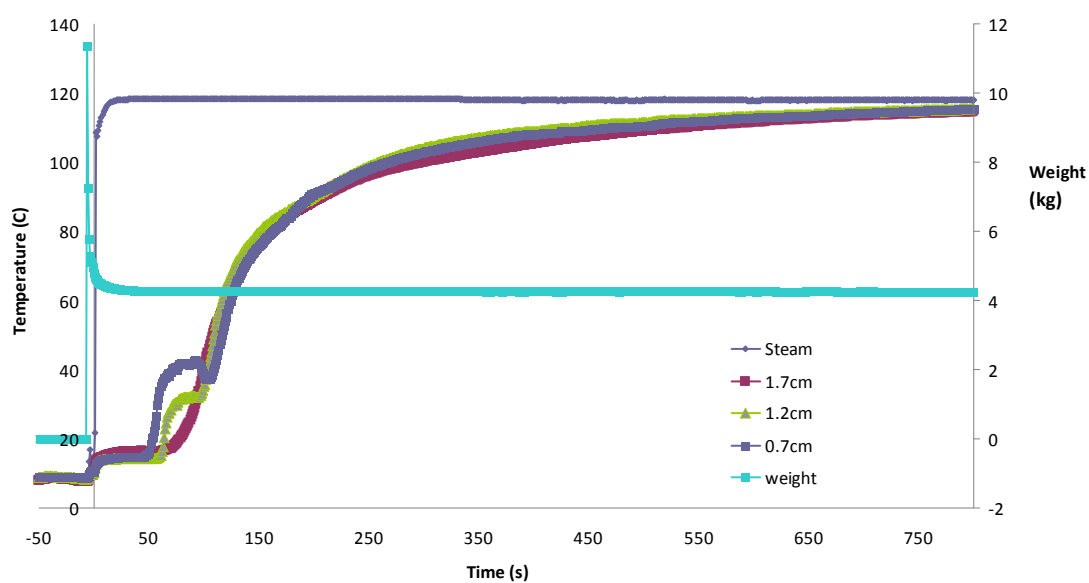
Figure **7-10**: Representative result for simultaneous measurement of temperature and weight in 18 cm high packed bed. Glass Beads size: 2 mm and all measurements except "weight" are temperature.
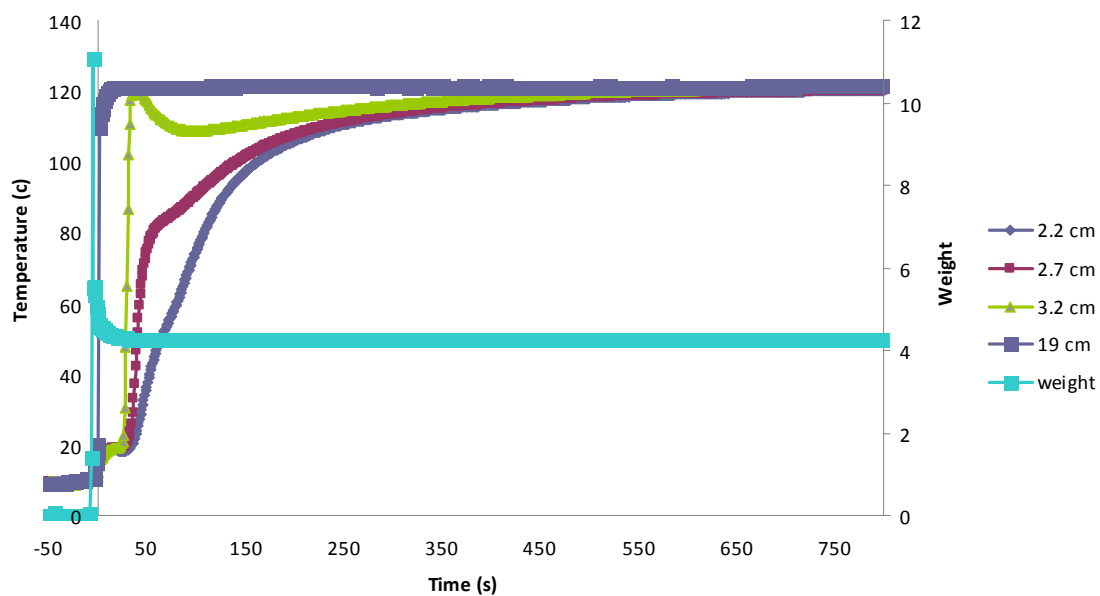
Figure **7-11**: Simultaneous measurement of temperature and weight in 18 cm depth packed bed. Glass Beads size: 2 mm and all measurements except "weight" are temperature.
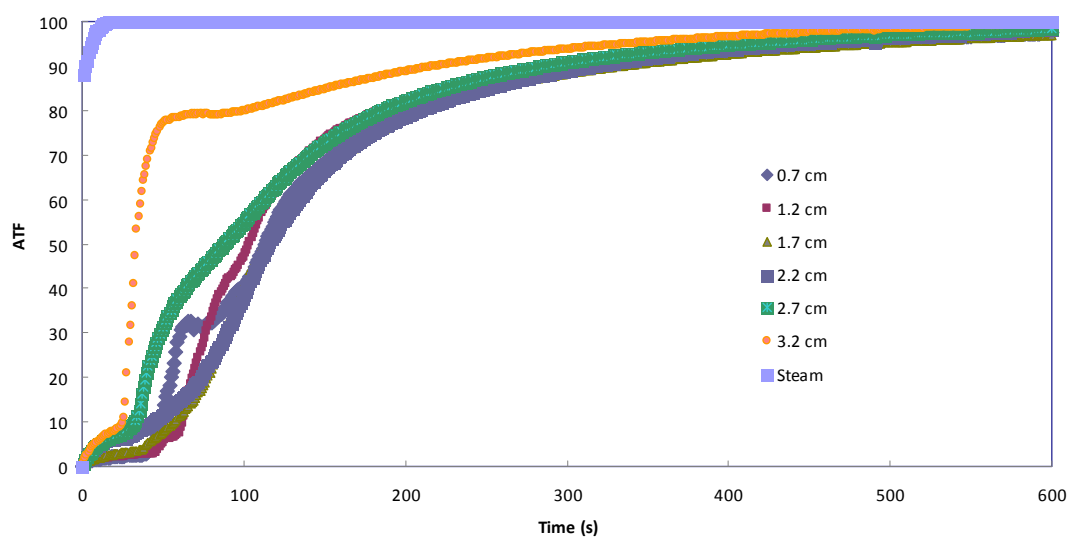
Figure **7-12**: Summarized temperature histories inside and right above CF of packed bed for 2 mm glass beads. CFT is 1.8 cm (calculated for 121ºC) to 2.4 cm (20ºC).

7.2.3.2 Experiments with Different Depths and Sizes of Glass Beads

The selected depths for each size of glass beads were 10 and 18 cm. For 2 mm and 3 mm glass beads, the thermocouple probes were positioned as shown in Figure **7-13**. For 5 mm glass beads it is shown in Figure **7-14**.
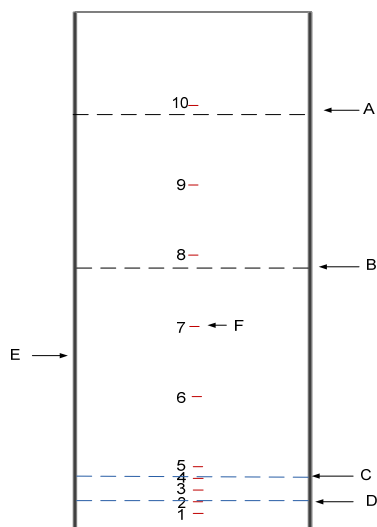
Figure **7-13**: Positions of thermocouple probes for measuring temperature in packed bed of 2 and 3 mm glass beads. (Notes: A, Upper surface of 18 cm high packed bed. B, Upper surface of 11 cm high packed bed. C, Upper edge of CF of 2 mm glass beads. D, Upper edge of CF of 3 mm glass beads. E, Polycarbonate cylinder. F, thermocouple probe. Thermocouple positions: 1). 0.7 cm. 2). 1.2 cm. 3). 1.7 cm. 4). 2.2 cm. 5). 2.7 cm. 6). 5.7 cm. 7). 8.7 cm. 8). 11.7 cm. 9). 14.7 cm. 10). 19 cm.
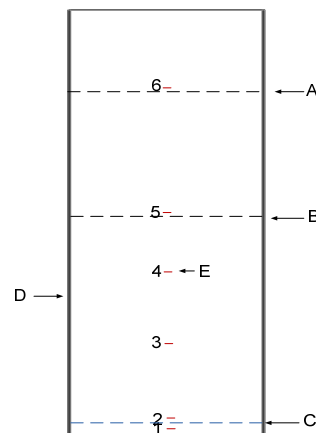
Figure **7-14**: Positions of thermocouple probes for measuring temperature in packed bed of 5 mm glass beads. (Notes: A, Upper surface of 18 cm high packed bed. B, Upper surface of 11 cm high kg packed bed. C, Upper edge of CF. D, Polycarbonate cylinder. E, thermocouple probe. Thermocouple positions: 1). 0.3 cm. 2). 0.8 cm. 3). 5.3 cm. 4). 8.3. 5). 11.3 cm. 6). 18.7 cm.

As shown in Figure **7-15**, the temperature history has the same pattern as in Figure **7-12** (which was for a nearly identical experiment), except that the elevation of 2.7 cm in Figure **7-15** was heated faster than that shown in Figure **7-12**. This may have been caused by a slight change of probe position. Generally, the CF (below 2.4 cm) and the region right above CF (2.4 cm to 2.7 cm) are heated slower than the upper space.
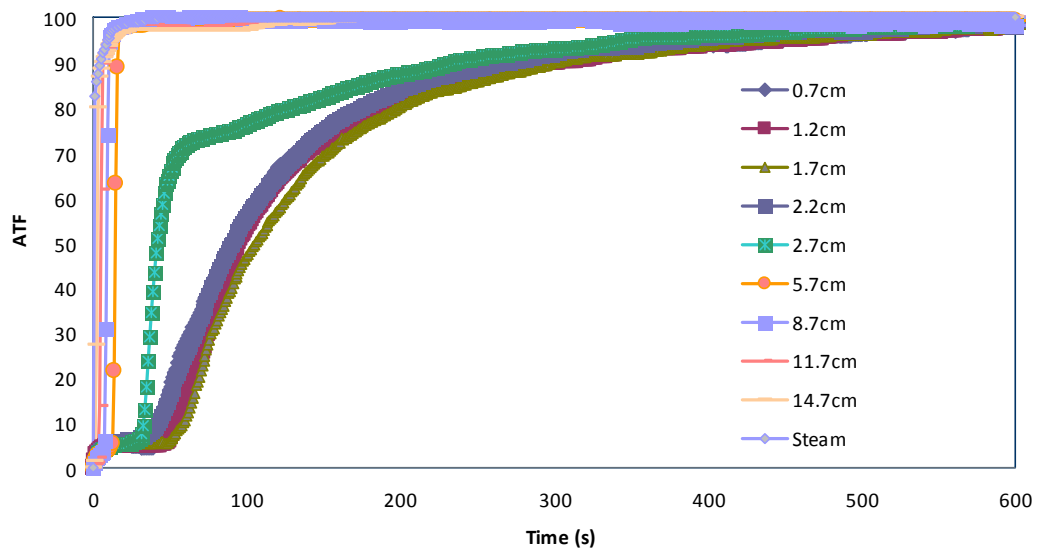
Figure **7-15**: Temperature history at different positions from bottom to top of 2 kg packed bed (18 cm depth) of 2 mm glass beads. Data ended where the last curve reached to ATF=97%.

The rest of experiment results for temperature history in packed bed depth of 11 cm from 2 mm, 18 cm from 3 mm, 11cm from 3 mm, 18 cm from 5 mm, and 11 cm from 5 mm glass beads are shown in **Appendix C** from Figure **C-4** to Figure **C-7**. For comparison, the same scale was set for X and Y axis in each curve.

7.3 Summary

For 2 and 3 mm glass beads the region which is heated most slowly is within CF. For 5 mm glass beads the CF is thin and so no measurements were attempted in that region. The lowest temperature measured was at the lowest elevation measured, 1.0 cm above bottom of bed and slightly above CF.

There are several reasons to explain why the bed does not heat from bottom as fast as it heats from top:

A.   Steam pressure gradient existed inside the steam chamber. When the packed was drawn from water, the steam pressure near the interface of water and steam was not as high as on the top of steam chamber.

B.   The water draining from bottom of packed beds prevented the steam from heating the bottom of packed beds.

C.   The capillary fringe, however, was the major reason to prevent the bottom of packed bed from heating. Because the capillary fringe is a saturated zone filled with water and particles it prevents the steam from entering that region.

CHAPTER 8

MODEL VALIDATION AND DISCUSSION

Experimental results presented in **Chapter 7** were used to validate the model for predicting the heat and mass transfer in packed bed which was presented in **Chapter 6**. The validation included both mass and heat transfer with different depths and sizes of glass beads in steam processing.

Model validation is possibly the most important step in the model building sequence. Validation of a model can be nothing more than quoting the R^2 statistic from the fit (which measures the fraction of the total variability in the response that is accounted for by the model). Unfortunately, a high R^2 (coefficient of determination) value does not guarantee that the model fits the data well. The accuracy of a model depends on many factors: the application range of the model, the complexity of the system, the error distribution, etc. In this research, the model is evaluated by four parameters: slope, interception, and R-square of best fit line for observation vs. prediction, and root mean square error (RMSE). In theory, the best model should indicate that slope is 1, interception is 0 (origin), R^2 is 1, and RMSE=0, in which case the plot of observation vs. prediction is a 45° straight line. However, that usually can not happen in realistic modeling.

8.1 Model Validation for Heat Transfer

Modeling validation was completed as follows. For modeling heat transfer in packed beds of different sizes of glass beads, two bed depths were selected for model

verification: 18 cm and 11 cm. For each bed depth, the comparison includes graph of data of observation and prediction versus time, plot of observation versus prediction (ATF<=97%), and root mean square error (RMSE). RMSE is a generally used reference for evaluating model performance, and is given as (Gaile and Willmott, 1984)

$$RMSE = \left[\frac{\sum_{i=1}^{N} (P_i - O_i)^2}{N} \right]^{0.5}$$

8.1

where P_i and O_i are predicted and observed values at case i, respectively and N is the number of cases. A smaller RMSE indicates a better performing model.

For all the results presented in **Section 8.1.1** to **8.1.6**, the modeled output is considered to be the optimum, and the optimum coefficient constant c and power p in Eq. **6.12** for the finite-difference model are 0.364 and 3, respectively. A further discussion on constant c and power p are presented in **Section 8.4 Model Calibration**.

8.1.1 2 mm Glass Beads – 18 cm Bed Depth

The selected temperature histories of 18 cm bed depth for 2 mm glass beads were at 1.0 cm (midpoint of CF), 2.9 cm (region right above upper boundary of CF), and 6.7 cm (middle of unsaturated zone) from bottom. The experiment temperatures presented here were measured by thermistors and earlier presented in Figure **7-5**.

The comparison between predicted and observed ATF at the three locations are shown in Figure **8-1** to **8-3**. The predicted data at elevation of 1.0 and 2.9 cm show good agreement with the observation (Figure **8-1** and Figure **8-2**) while the predicted data at elevation of 6.7 cm do not match the observation very well (Figure **8-3**).
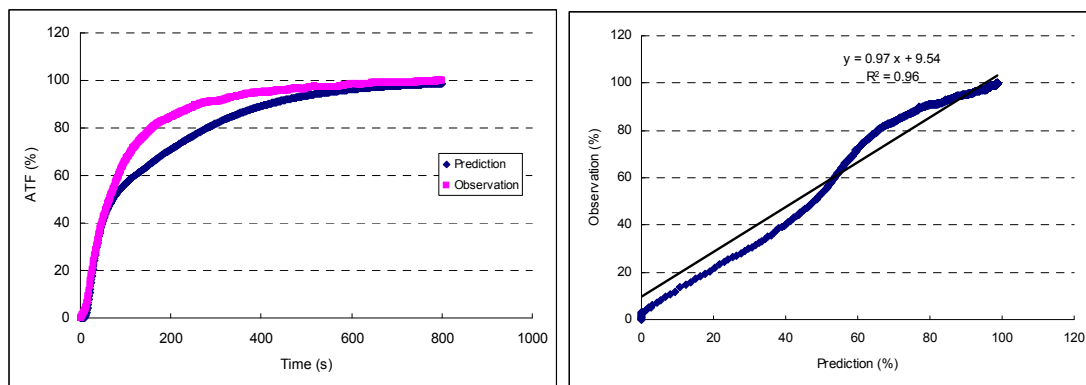
Figure **8-1**: Comparison between measured and predicted ATF at 1.0 cm from bottom (vertical center of CF) in 18 cm depth of packed bed from 2 mm glass beads. RMSE=8.98%.
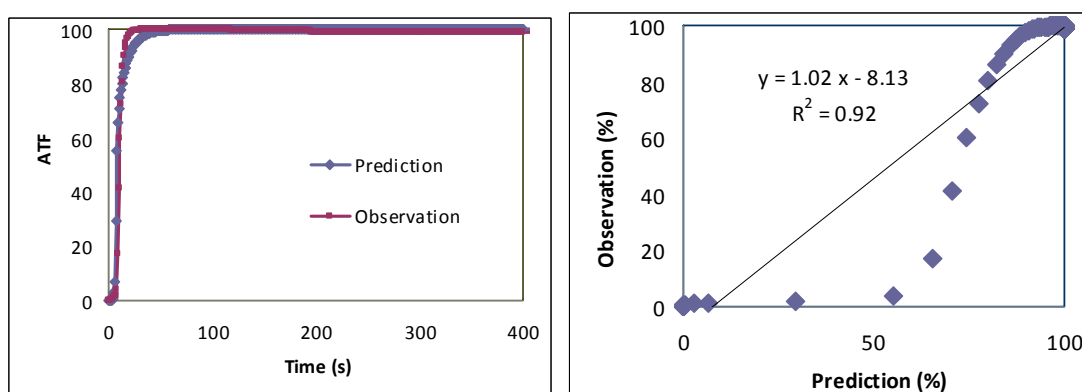
Figure **8-2**: Comparison between measured and predicted ATF at 2.9 cm from bottom (vertical center of CF) in 18 cm depth of packed bed of 2 mm glass beads. RMSE= 12.4%.
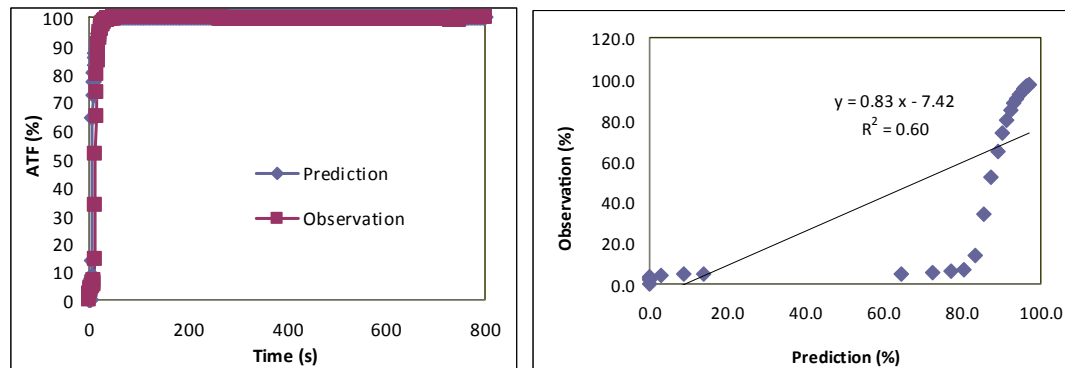
Figure **8-3**: Measured and predicted ATF at 6.7 cm from bottom in 18 cm depth of packed bed of 2 mm glass beads. RMSE=33.0%.

In Figure **8-2,** from the plot of observation vs. prediction one can see that most of the error comes from where ATF< 80%, which is the beginning of heating process. The trendline slope of observation versus prediction is 1.02, R-square is 0.92 and RMSE is 12.4 %, indicating a good match of output of model with observation. The elevation of 2.9 cm is in layer 2 of UFZ in finite-difference model. If predicted data in layer 3 (3.6 cm to 4.4 cm) instead of layer 2 (2.8 cm to 3.6 cm) is selected for validation, better fit between observation and prediction is obtained as shown in Figure **8-4**. The RMSE decreases to 7.9% from 12.4%, and R-square increases to 0.99 from 0.92.

Although there are no standards for a model to be stated as "good", in this research when slope is between 1.1 to 0.9, intercept is between -10 to 10%, $R^2 > 0.9$, and RMSE<10%, the model is treated as a good or excellent model. However, this is not the absolute standard. For example, in Figure **8-3** the slope and interception are 0.83 and -7.42, respectively, with R-square 0.80 and RMSE 33%. However, most of the error is derived from the first 50 seconds as shown in the left graph. So the modeled result is still acceptable.
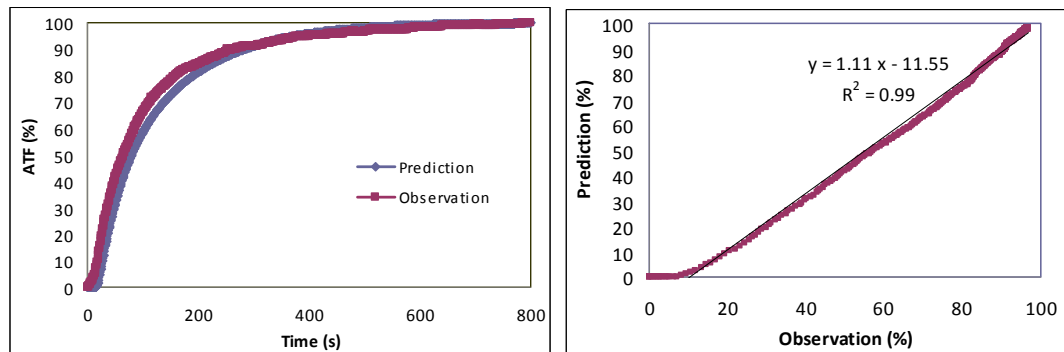
Figure **8-4**: Comparison between measured and predicted ATF in 18 cm depth of packed bed of 2 mm glass beads. Predicted data was taken from Layer 3 (3.6 to 4.4 cm) by finite-difference model. Observed data was taken from elevation 2.9 cm. RMSE=7.9%.

8.1.2 2 mm Glass Beads – 11 cm Bed Depth

The selected elevations for 11 cm bed depth with 2 mm glass beads were 1.0, 2.9, and 6.7 cm. The experimental data was measured by thermistors and presented in Figure **7-5.**

The comparison between predicted and observed ATF at the three locations are shown in Figures **8-5** to **8-7**. All the predicted data at the three elevations show good agreements with the observations, except at the elevation of 6.7 cm, similar to that seen for the 18 cm bed depth.
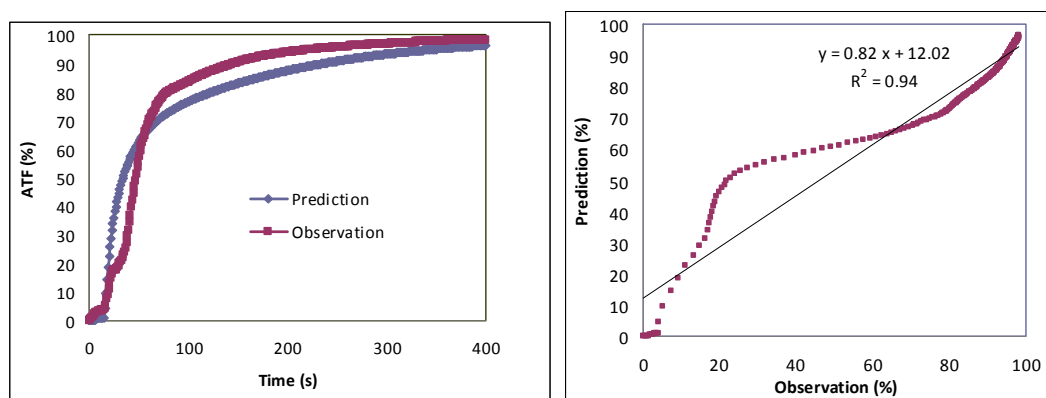
Figure **8-5**: Comparison between measured and predicted ATF at elevation 1.0 cm from bottom (vertical center of CF) of 11 cm depth of packed bed from 2 mm glass beads. RMSE=7.70%.
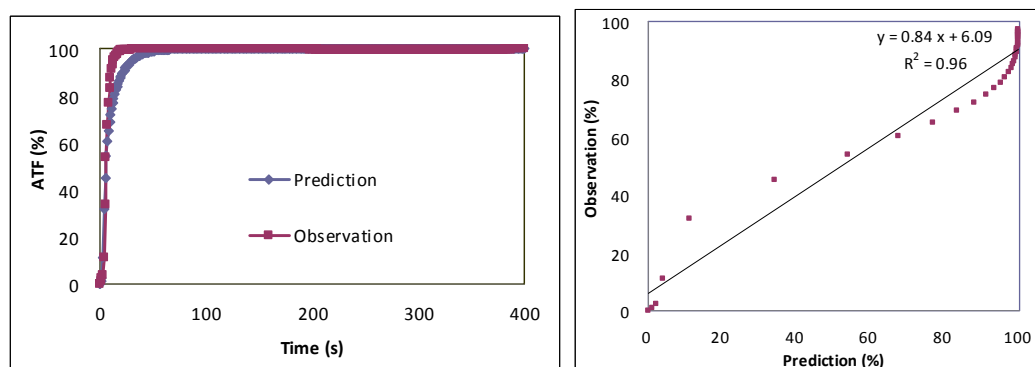
Figure **8-6**: Comparison between measured and predicted ATF at elevation 2.9 cm from bottom in 11 cm depth of packed bed from 2 mm glass beads. RMSE= 10.3%.
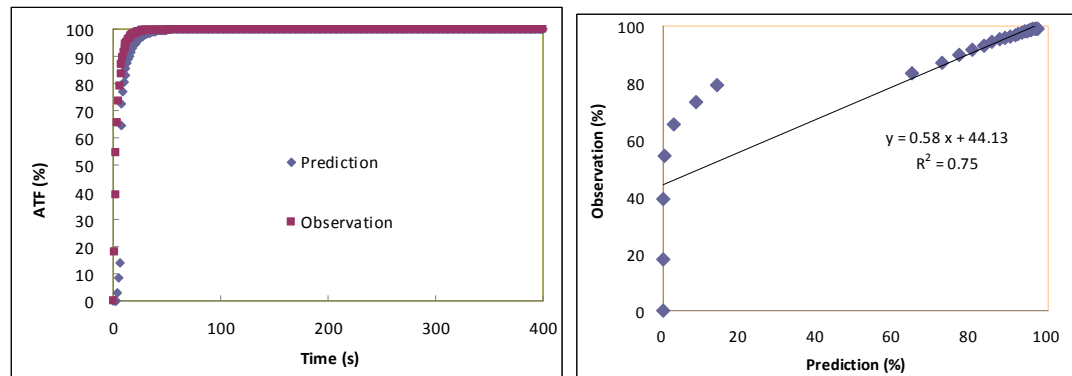
Figure **8-7**: Comparison between measured and predicted ATF at elevation 6.7 cm from bottom in 11 cm depth of packed bed from 2 mm glass beads. RMSE **=** 26.7%.

8.1.3 3 mm Glass Beads – 18 cm Bed Depth

The selected elevations for model validation in 18 cm depth of packed bed with 3 mm glass beads were 0.7 cm, 2.9 cm, and 6.7 cm. The experimental data were collected by thermocouples and was presented in Figure **7-6**. The experimental and modeled data to 300 seconds were compared.

As illustrated in Figure **8-8** to Figure **8-10**, the modeling data have good agreement with the experimental data, especially at center of CF, which is approximately the coldest spot in the bed and therefore most important for thermal processing of foods. At elevation of 1.7 cm and 11.7 cm, mostly the error came from the beginning of curves. At the high end of ATF the prediction shows much better agreement with observation, which is more important than at the beginning of processing.
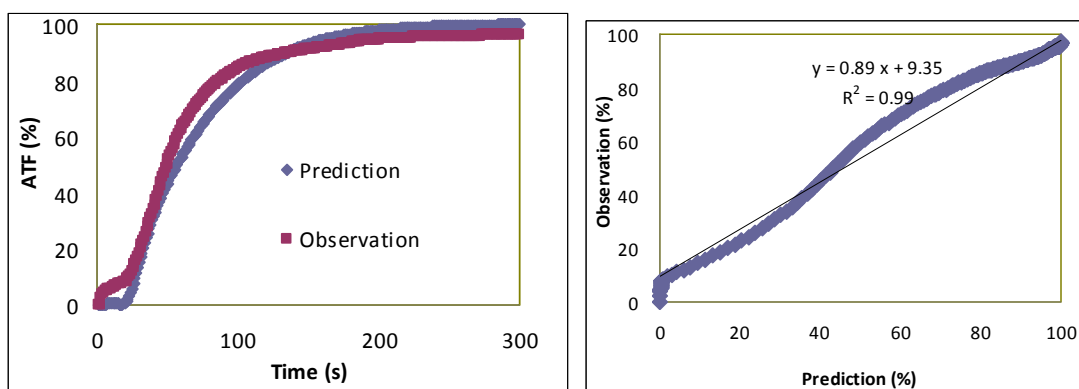
Figure **8-8**: Comparison between measured and predicted ATF at elevation 0.7 cm (Center of CF) from bottom in 18 cm depth of packed bed of 3 mm glass beads. RMSE= 4.7%.
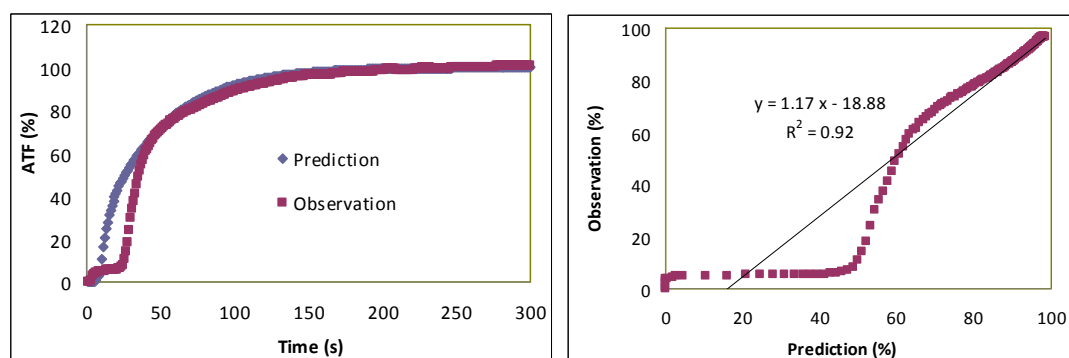
Figure **8-9**: Comparison between measured and predicted ATF at elevation 1.7 cm (above CF) from bottom in 18 cm depth of packed bed of 3 mm glass beads. RMSE =11.6%.
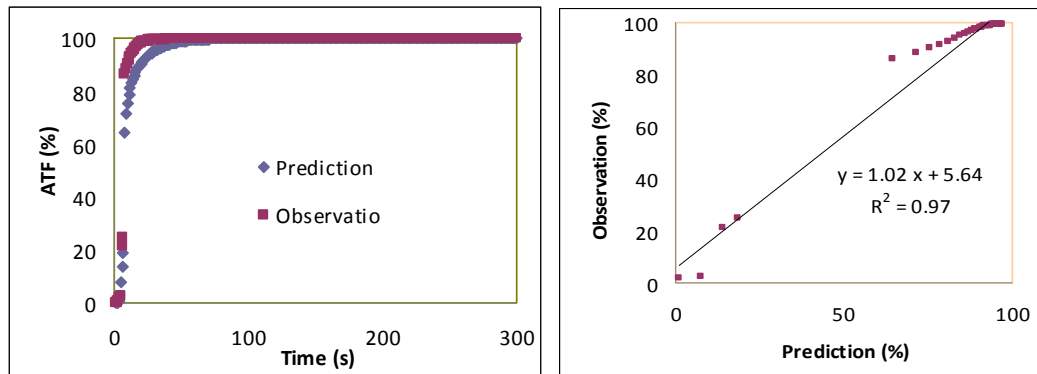
Figure **8-10**: Comparison between measured and predicted ATF at elevation 11.7 cm from bottom in 18 cm depth of packed bed of 3 mm glass beads. RMSE=8.4%.

8.1.4 3 mm Glass Beads – 11 cm Bed Depth

The selected elevations for model validation in 11 cm depth of packed bed of 3 mm glass beads were 0.7, 1.7, and 5.7 cm. The experimental data were collected by thermocouples and are presented in Figure **7-6.**

As illustrated in Figures **8-11** to **8-13**, the modeled data have good agreement with the experimental data, especially at center of CF. At the elevation of 1.7 cm and 5.7 cm, it can be seen from the plots of observation vs. prediction that mostly the error came from the beginning of the data.
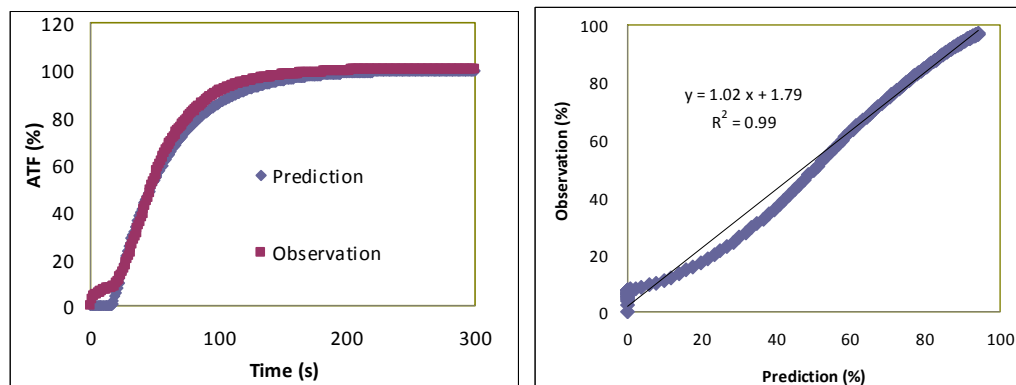
Figure **8-11**: Comparison between measured and predicted ATF at elevation 0.7 cm (Center of CF) from bottom in 11 cm depth of packed bed from 3 mm glass beads. RMSE = 4.3%.
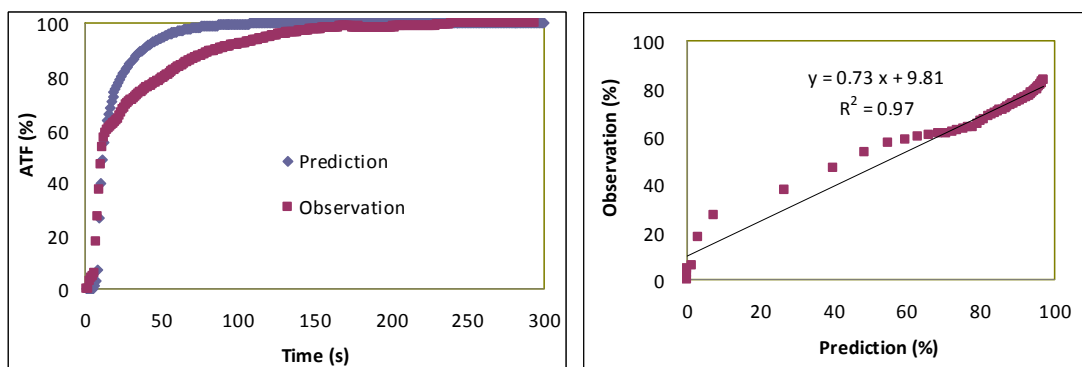
Figure **8-12**: Comparison between measured and predicted ATF at elevation 1.7 cm (above CF) from bottom in 11 cm depth of packed bed of 3 mm glass beads. RMSE=10.6%.
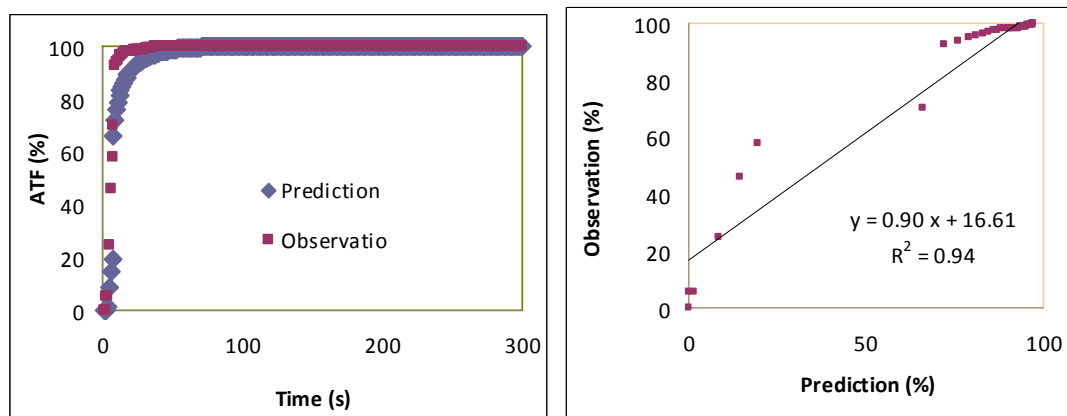
Figure **8-13**: Comparison between measured and predicted ATF at elevation 5.7 cm (above CF) from bottom in 11 cm depth of packed bed of 3 mm glass beads. RMSE=9.4%.

8.1.5 5 mm Glass Beads – 18 cm Bed Depth

Three elevations, 0.3 cm (center of CF), 0.8 cm, and 5.3 cm were used to compare the ATF between modeled and experimental data in 18 cm depth of packed bed of 5 mm glass beads. The experimental data were collected by thermocouples. The first 200 seconds of experimental and modeled data were compared.

The modeled data, as shown in Figure **8-14** to Figure **8-16** for different elevations, have acceptable to good agreement with experimental data. Most of the errors are from the beginning of processing. However, at lower elevations the predicted data do not show the same good agreement as those for smaller glass beads, as can be seen in Figure **8-14** to Figure **8-15**. The reason may be because packed bed with 5 mm glass beads has very shallow CF, and around the CF the heat and mass transfer is too complicated for the model to accurately predict.
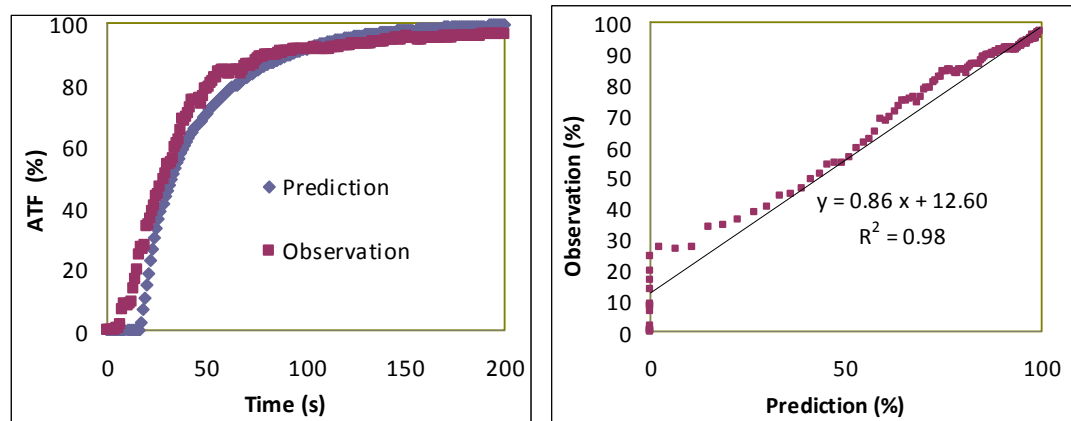
Figure **8-14**: Comparison between measured and predicted ATF at elevation 0.3 cm (Center of CF) from bottom in 18 cm depth of packed bed of 5 mm glass beads. RMSE= 6.04%.
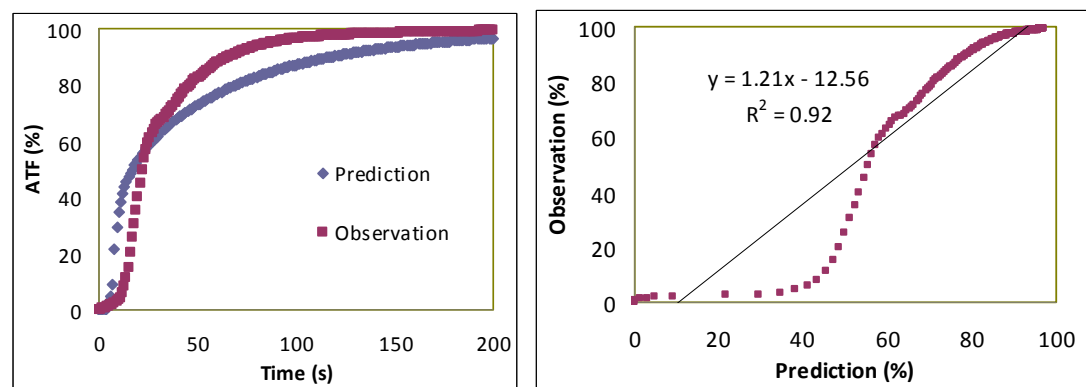
Figure **8-15**: Comparison between measured and predicted ATF at elevation 0.8 cm from bottom in 18 cm depth of packed bed of 5 mm glass beads. RMSE=9.8%.
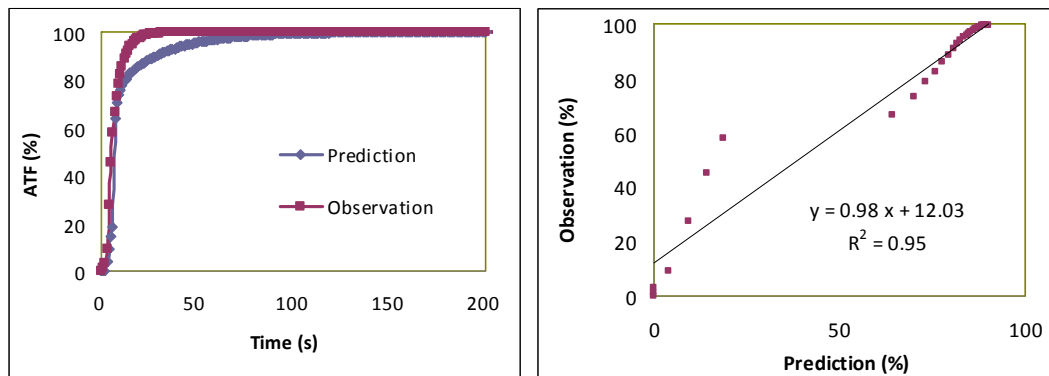
Figure **8-16**: Comparison between measured and predicted ATF at elevation 5.3 cm from bottom in 18 cm depth of packed bed with 5 mm glass beads. RMSE=13.3%.

8.1.6 5 mm Glass Beads – 11 cm Bed Depth

Three elevations, 0.3 cm (center of CF), 0.8 cm, and 5.3 cm were used to compare the ATF between modeled data and experimental data in 18 cm depth of packed bed. The experimental data were collected by thermocouples and was presented in Figure **7-7**. The first 110 seconds of experimental and modeled data were compared.

The comparison illustrated in Figures **8-17** to **8-19** shows good agreement between the prediction and observation. However, the error is generally larger compared to the results for smaller beads.
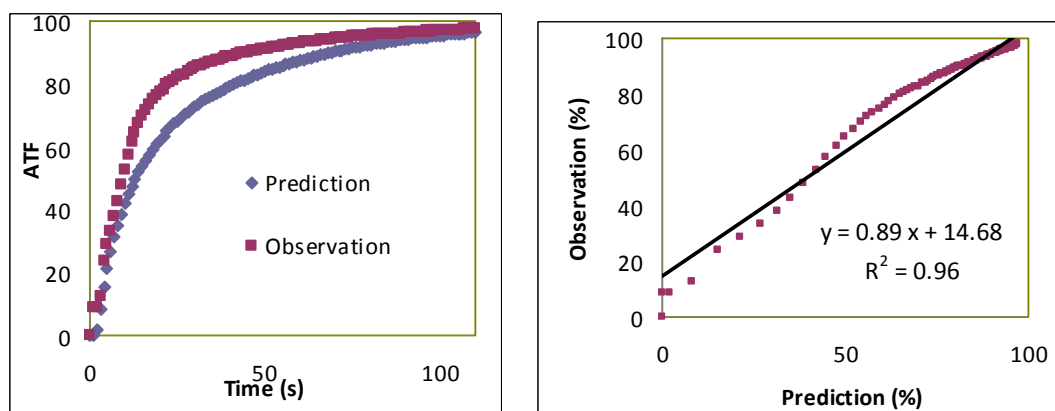
Figure **8-17**: Comparison between measured and predicted ATF at elevation 0.3 cm (Center of CF) from bottom in 11 cm depth of packed bed of 5 mm glass beads. RMSE=8.0%.
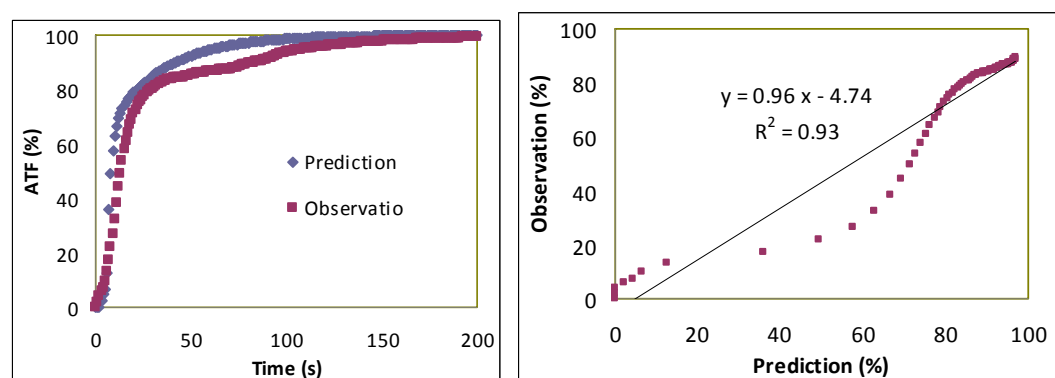
Figure **8-18**: Comparison between measured and predicted ATF at elevation 0.8 cm (Center of CF) from bottom in 11 cm depth of packed bed of 5 mm glass beads. RMSE=10.7%.
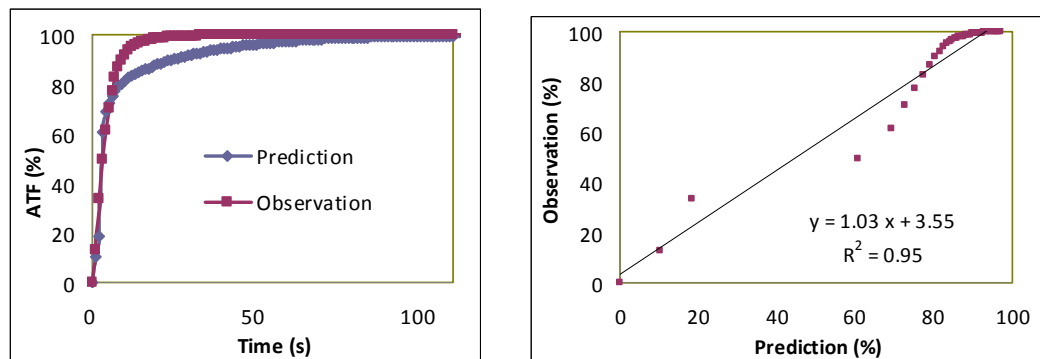
Figure **8-19**: Comparison between measured and predicted ATF at elevation 5.3 cm (Center of CF) from bottom in 11 cm depth of packed bed of 5 mm glass beads. RMSE=7.8%.

8.1.7 Summary on Modeling of Heat Transfer

The heat transfer in packed bed with different sizes and amount of glass beads can be well predicted by the finite-difference model which was presented in **Chapter 6** based on the comparison between predictions and observations shown above. The model works better for more weight than less weight of packed bed, and better within CF than at higher elevations in UFZ.

For example, in Figure **8-3**, a poor relationship between prediction and observation is shown: trendline slope is 0.83, R-square is 0.60 and RMSE is 33.0%. The following reasons may explain the error between the prediction and observation:

1. The plot between prediction versus observation is from the data of the first 26 s (ATF<=97), which is a short time compared to 500 s when the temperature in CF is heated to ATF=97.

2. It is difficult to synchronize the starting time for experiment with the model. One or two second delay or advancing of the experiment starting time when the packed bed surface was exposed to steam

environment can lead to large error at the beginning due to the rapid

increase of temperature.

3.   The mass transfer equation between DH and mass transfer speed is

measured under smaller water flux. The DH under high water flux was

estimated, which can create larger error for the processing at the

beginning.

4.   The predicted variable SH, which was measured with 3 mm glass

beads, may have a large error when applied to larger and smaller glass

beads. The change of particle diameter leads to the change of capillary

pressure and therefore static holdup.

8.2 Model Validation for Mass Transfer in Drainage

The finite-difference model can predict the cumulative mass transfer through the

packed bed and the net weight of water retained in the column. Experiments were

performed to verify the mass transfer aspects of the model. The experimental setup was

shown in Figure **5-13** and Figure **4-4** for with- and without-steam experiments,

respectively.

8.2.1 Bed Depth of 27 cm

The mass transfer through 27 cm (3 kg) depth of packed bed was first

investigated using different glass beads and no steam. The representative result of

cumulative mass transfer of predicted and observed data for 2 mm glass beads are

shown in Figure **8-20**, followed by comparison between observation and prediction in

Figure **8-21**. The comparison of mass transfer in packed bed from 3 mm and 5 mm glass beads, are presented in Figure **D-1** and Figure **D-2**, respectively**.** The thermophysical properties were set at 17ºC.

As shown in Figure **8-21** there is good agreement between observed and predicted data for water flow. The major error may come from the assumed linear relationship between DH and water flow speed, as shown in Figure **4-17** to Figure **4-19** at high water flux.
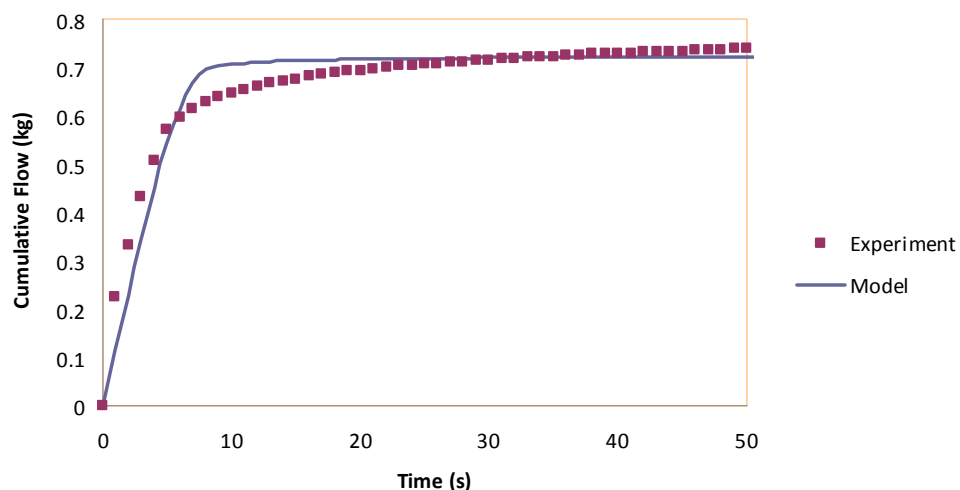
Figure **8-20**: Comparison between predicted and observed data for cumulative water flow out 27 cm depth packed bed of 2 mm glass beads with no steam.
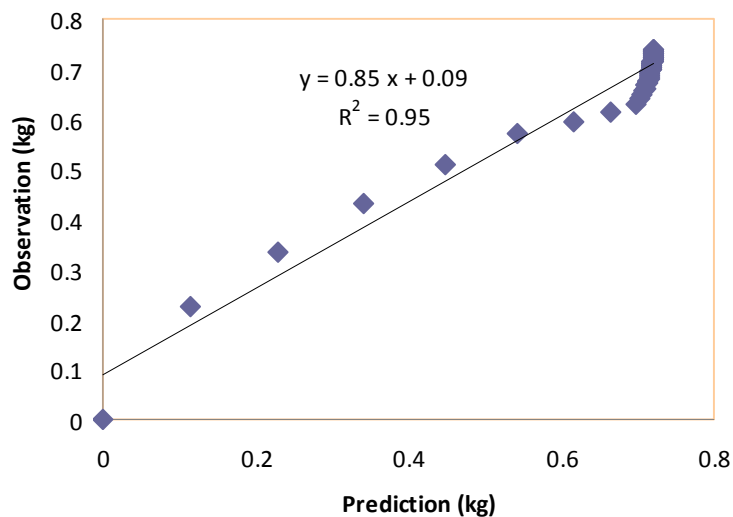
Figure **8-21**: Model validation for cumulative water flow out 27 cm depth packed bed of 2 mm glass beads with no steam. RMSE=0.04 kg.

The representative comparison of liquid drainage velocity at bottom of 27 cm depth of packed bed from 2 mm glass beads in the fist 50 s between experimental and modeled data are shown in Figure **8-22** and Figure **8-23**. The comparison for 3 mm and 5 mm glass beads are illustrated in Figure **D-3** and Figure **D-4**, respectively, and other conditions are the same. The result shows that with no steam applied the finite-difference model provides good prediction of mass flow velocity in drainage.
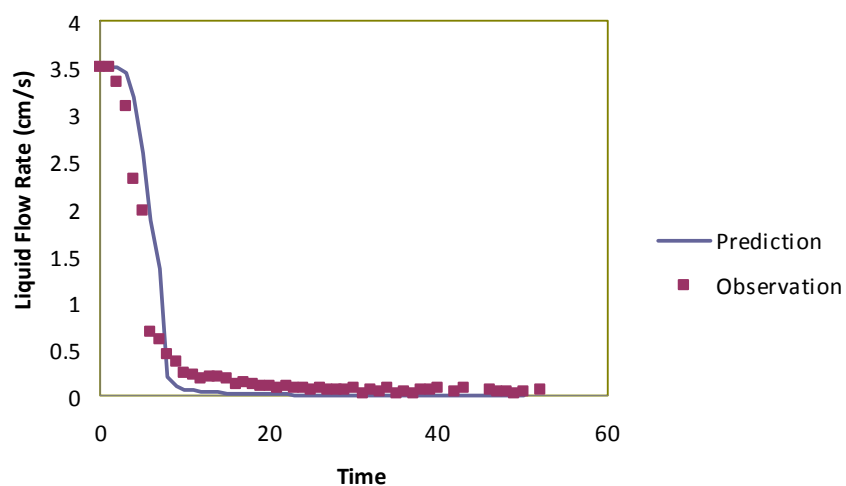
Figure **8-22**: Comparison between predicted and observed data for water velocity at bottom of 27 cm depth packed bed of 2 mm glass beads with no steam.
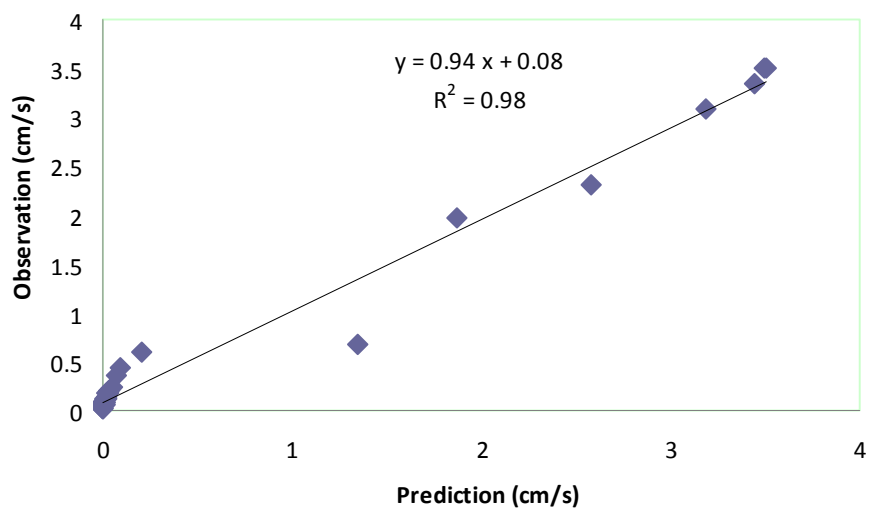
Figure **8-23**: Model validation for water velocity at bottom of 27 cm depth packed bed of 2 mm glass beads with no steam. RMSE=0.16 cm/s.

8.2.2 Bed Depth of 18 cm with Steam Processing

The mass transfer through 18 cm (2 kg) depth of packed bed was investigated in steam heating environment. The experimental setup for simultaneous measurement of temperature and weight change was illustrated in Figure **5-10**. A representative result for cumulative mass transfer of predicted and observed data for 2 mm glass beads are shown in Figure **8-24**, followed by comparison between observation and prediction in Figure **8-25**. Figure **8-26** and Figure **8-27** show the model validation for water flow velocity in 18 cm depth of packed bed of 2 mm glass beads under steam processing. Similar comparisons for 3 mm and 5 mm glass beads are presented in Figure **D-5** Figure **D-6**, respectively. The thermophysical properties of liquid were set at 100ºC.

For cumulative mass transfer, the predictions and observations do not show good agreement. For example, for 2 mm glass beads, the predicted cumulative flow is faster than observed. The trendline equation between observation and prediction with slope 0.67 and R-square 0.83 in Figure **8-25** shows that the finite-difference model does not predict the mass transfer very well in steam environment, compared to the results shown earlier for the mass transfer in packed bed without steam.

The following reasons may explain the difference between observation and prediction for mass transfer in packed bed under steam processing:

1. The correlation between DH and water flow rate was measured under room temperature but not in steam environment.

2. The predicted correlation between DH and water flow rate for high water flux was developed based on room temperature rather than for steam environment.

3.   Under steam processing, thermophysical properties of water are
        variable with temperature change. More important, the temperature at
        different elevation of packed bed is different.
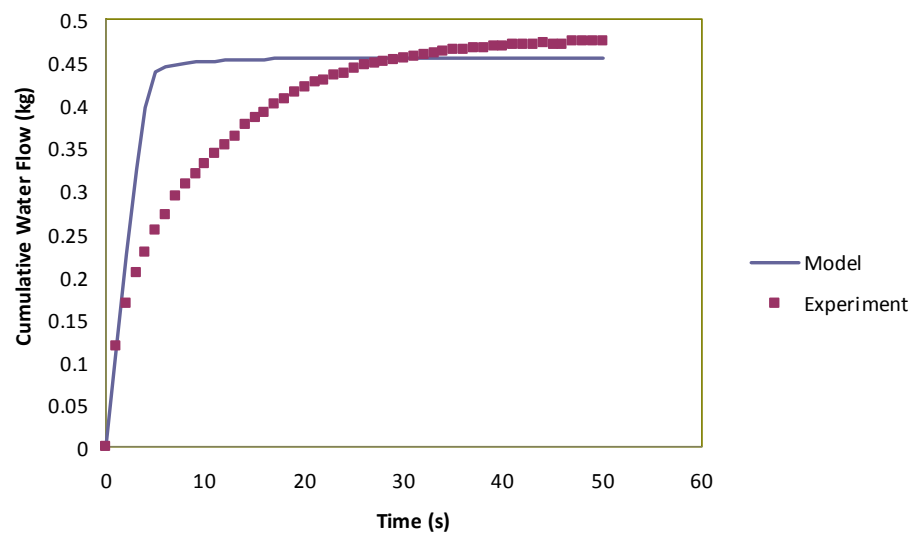
Figure **8-24**: Comparison between predicted and observed data for cumulative water
flow out 18 cm depth packed bed of 2 mm glass beads.
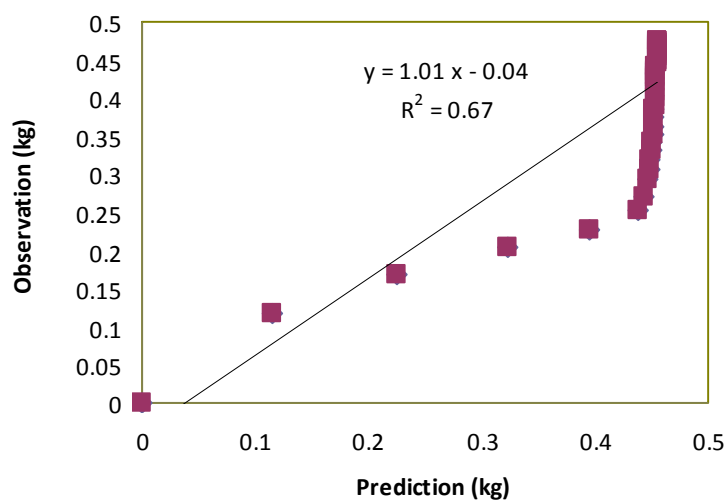
Figure **8-25**: Model validation for predicted and observed data for cumulative water flow out 18 cm depth packed bed of 2 mm glass beads. MSRE=0.08 kg.
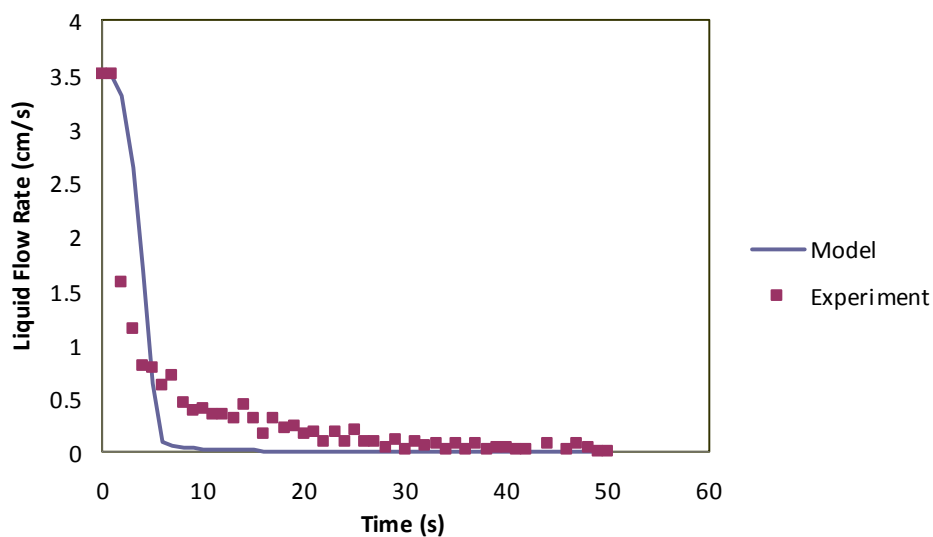
Figure **8-26**: Comparison between predicted and observed data for velocity of water flow out of 18 cm depth packed bed of 2 mm glass beads.
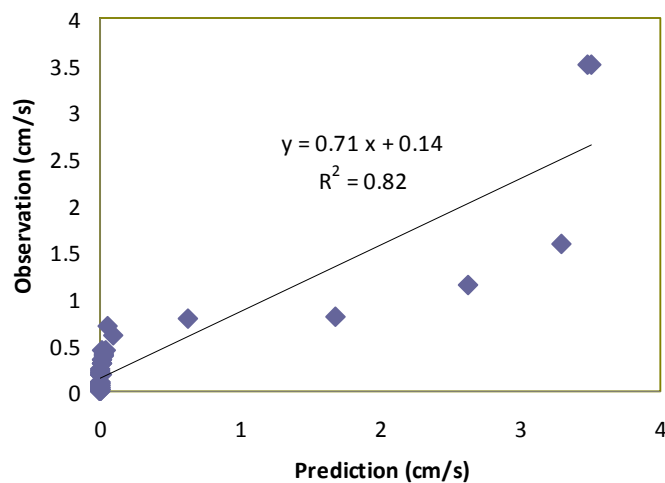
Figure **8-27**: Model validation for velocity of water flow out of 18 cm depth packed bed of 2 mm glass beads. RMSE= 0.29 cm/s.

8.2.3 Residual Water in Packed Beds

The weight of residual water in packed bed after 50 s is summarized in Table **8-1**. The results for 27 cm bed depth were obtained without steam while results for 18 cm were for steam processing. The results show good agreement and that more residual water is retained in packed beds from smaller particles.

Table **8-1**: Residual water (kg) after 50 s vertical drainage in packed beds.

Bed Depth		2 mm	3 mm	5 mm
27 cm	Obs*	0.156	0.126	0.095
	Pre**	0.160	0.123	0.105
18 cm	Obs	0.126	0.121	0.083
	Pre	0.133	0.101	0.083

* Observation
** Prediction

8.3 Water Content as a Function of Bed Depth

The model validation results presented in Sections **8.1** and **8.2** suggest a well developed finite-difference model which can predict heat and mass transfer very well in packed beds. The water content at different elevations during drainage of packed bed can also be predicted by the finite-difference model.

The model results for water content changing with time at different elevations in packed beds are shown in Figures **8-28** to **8-30**. The total liquid holdup (V/V) decreases sharply almost immediately, and for larger glass beads the total liquid holdup decreases faster than for smaller glass beads. This result is consistent with the observations in drainage experiments.
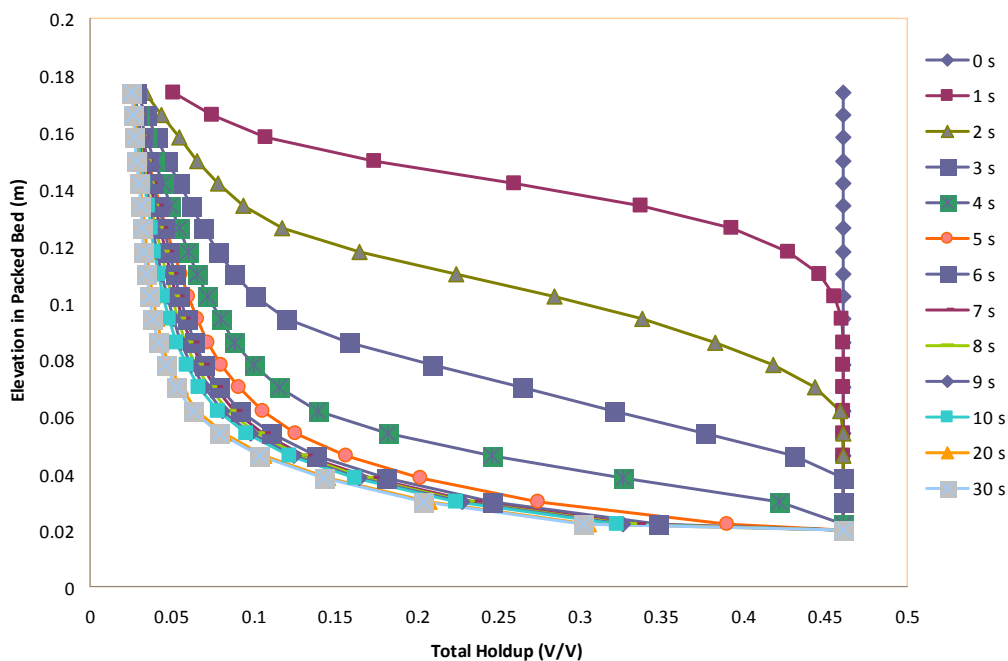
Figure **8-28**: Total liquid holdup changing with time at different elevations in 18 cm depth packed bed of 2 mm glass beads.
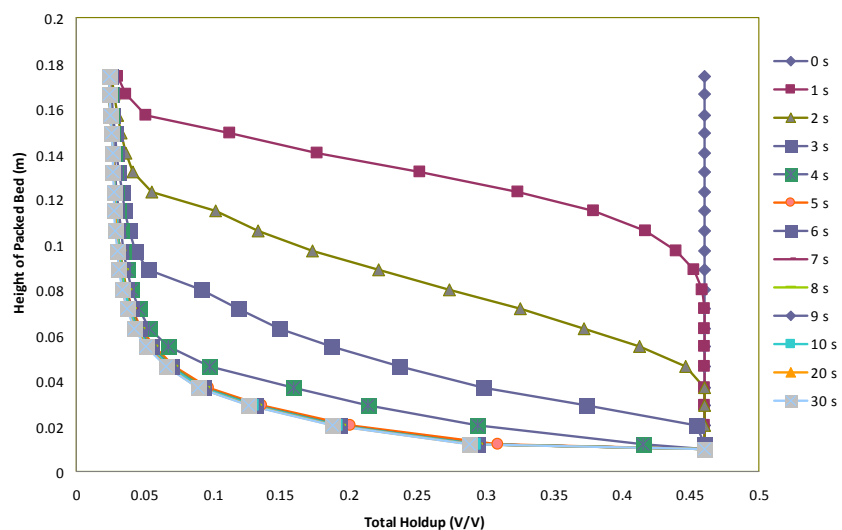
Figure **8-29**: Total liquid holdup changing with time at different elevations in 18 cm depth packed bed of 3 mm glass beads.
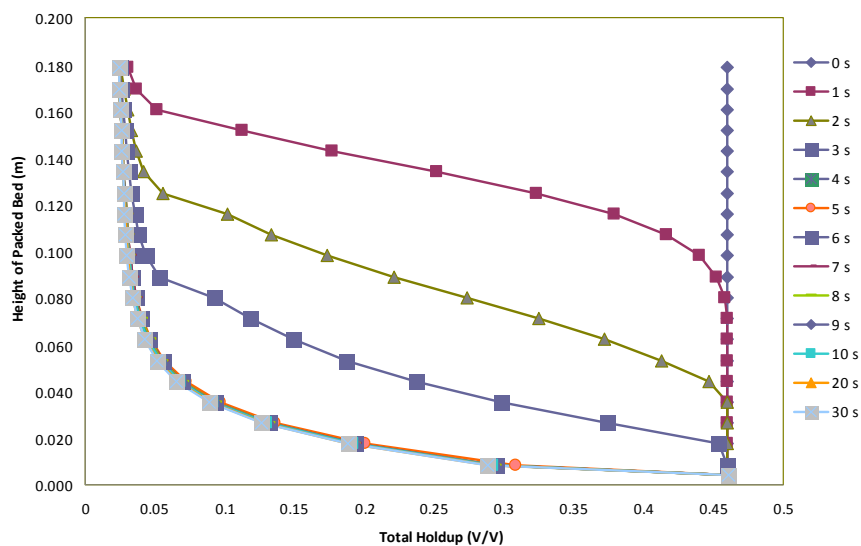
Figure **8-30**: Total liquid holdup changing with time at different elevations in 18 cm depth packed bed from 5 mm glass beads.

8.4 Model Calibration

Model calibration is the process of modifying the input parameters to a model until the output from the model matches observed set of data (EMSI, 2009). In the numerical model, the local condensation coefficient is given as by combining Eq. **6.10** and Eq. **6.12**

$$h_L = 0.825c \left[\frac{g\rho_l(\rho_l - \rho_g)k_l^3 h_{fg}'}{\mu_l(T_a - T_{su})D_p} \right]^{1/4} \varepsilon_L^{\,p}. \qquad \textbf{8.2}$$

For the model output addressed above, the constant *c* and power *p* are 0.364 and 3 and are considered as the optimum values. Before calibration, the value of c was 1, and was taken from the literature as described in Section **2.4.2**. The value of p was initially set as 1. Only *c* and *p* were calibrated by the model.

8.4.1 Parameter *c*

Firstly, power *p* was kept at the original value. Then different values of parameter *c* were tested. For 18 cm bed depth, the middle point of CF was heated unreasonably slowly if c=1, therefore the result is not shown here. Figure **8-1** shows much better predicted data when c was changed to 0.364. For calibration c was changed from 0.364 to 0.121, as shown in Figure **8-31**. Compared to Figure **8-1**, R-square of trendline dropped by 3.1% from 0.96 to 0.93, and RMSE increased by 140% from 8.9 to 21.4, indicating larger error was obtained by changing parameter *c* from 0.36 to 0.121.
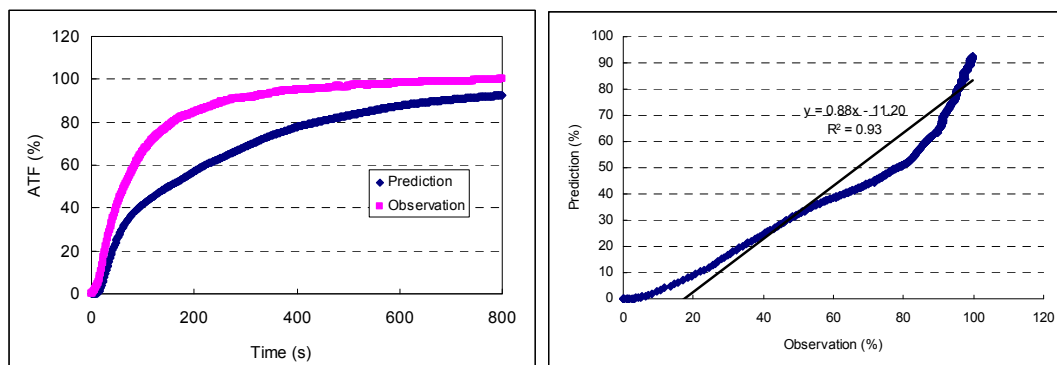
Figure **8-31**: Results before model calibration at center point of CF for 18 cm bed depth of 2 mm glass beads. Parameter c is 0.121. RMSE=21.4%.

From Figure **8-31** we can see that the predicted data increase slower than observed data, therefore, a larger *c* value was tried at 0.61. As shown in Figure **8-32** for the temperature comparison at middle point of CF, the R-square was increased to 0.98 from 0.96 and RMSE dropped to 4.75 from 8.9. However, the slope of trendline decreased to 0.93 from 0.96, compared to the result shown in Figure **8-**1. Therefore, with parameter c increased from 0.364 to 0.61, the modeled output does not show obvious improvement.
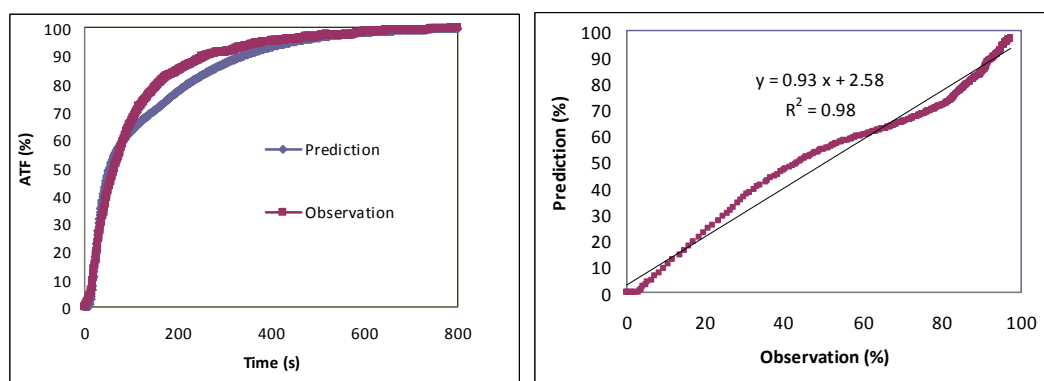
Figure **8-32**: Results for a trial model calibration at center point of CF for 18 cm bed depth of 2 mm glass beads. Parameter c is 0.61. RMSE=4.75%.

At elevation of 2.9 cm, a better result was obtained after parameter c was set to 0.61 as shown in Figure **8-33**, compared to the result shown in Figure **8-2**. The trendline slope was almost the same, 1.08 versus 1.02. R-square increased slightly by 5.4% from 0.92 to 0.97, and RMSE decreased by 27.7%.
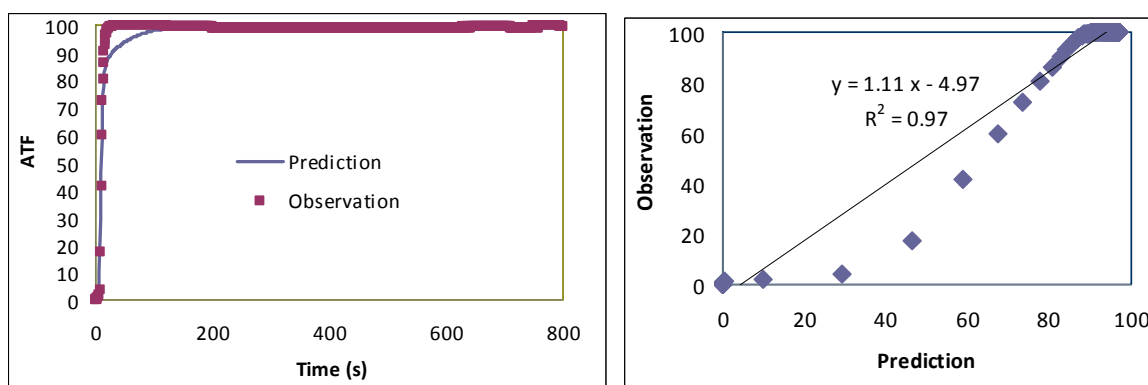
Figure **8-33**: Results for a trial model calibration at 2.9 cm elevation for 18 cm bed depth of 2 mm glass beads. Parameter c is 0.61. RMSE=8.96%.

However, at higher elevations such as 6.7 cm, c=0.61 gave worse result as shown in Figure **8-34**, compared to the result shown in Figure **8-3**. The trendline equation shows that slope decreased to 0.73 to 0.83, R-square decreased to 0.54 from 0.60, and RMSE increased to 36.9% to 33.0%.
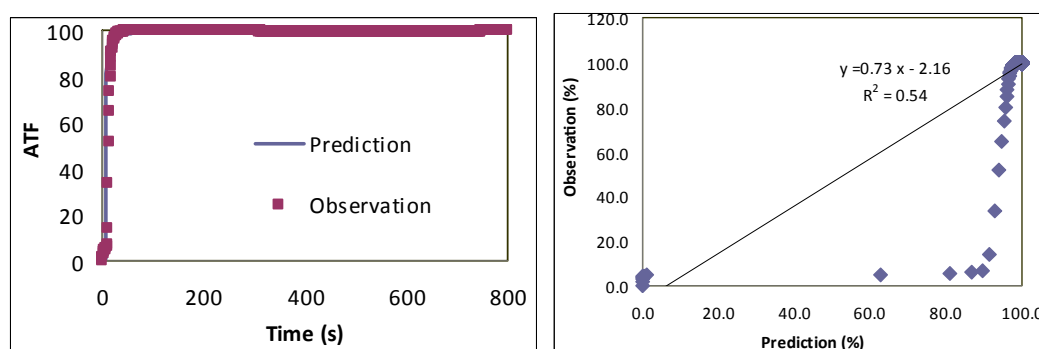
Figure **8-34**: Results for a trial model calibration at 6.7 cm elevation for 18 cm bed depth of 2 mm glass beads. Parameter c is 0.61. RMSE= 36.9%.

8.4.2 Power *p*

Power *p* was changed from 3 at 4 to check the effect on model output by keeping parameter *c* unchanged at 0.364. For 18 cm depth of packed bed, the middle point of CF was heated slower if power *p* was changed from 3 to 4, as shown in Figure **8-35**. Compared to Figure **8-1**, R-square of trendline was dropped slightly from 0.96 to 0.95, slope was decreased by 11.3% from 097 to 0.86, and RMSE was increased from 8.98% to 19.6%, indicating worse output were obtained if power p was set at 4. If power *p* was changed to 2, a worse result was also obtained as shown in Figure **8-36**, compared to Figure **8-1**.
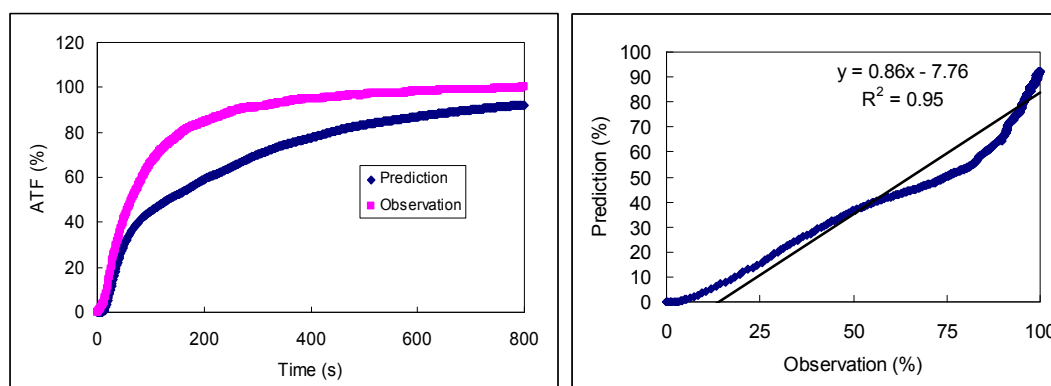
Figure **8-35**: Results for a trial model calibration at center of CF for 18 cm bed depth of 2 mm glass beads. Power *p* is 4. RMSE=19.6%.
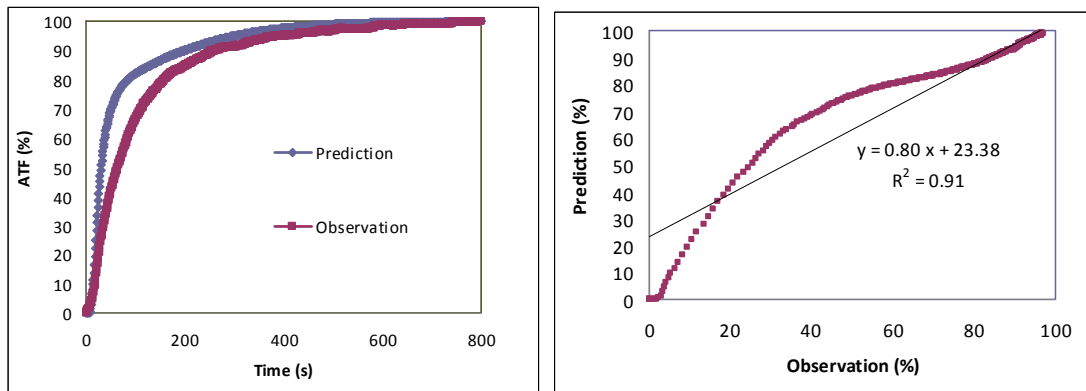
Figure **8-36**: Results for a trial model calibration at center of CF for 18 cm bed depth of 2 mm glass beads. Power *p* is 2. RMSE=10.58%.

8.5 Bed Depth Effect

8.5.1 Observation vs. Prediction

Both observations and predictions show that with increased bed depth, it takes longer time to heat the packed bed to certain temperature. This can be seen clearly by plotting the bed depth versus the heating time.

As shown in Figure **8-37**, the time taken to reach ATF=90% in CF increases with the increase of bed depth. Meanwhile, for the same depth of packed bed, it takes longer time to heat the CF to ATF=90 for smaller glass beads. For example, with 3 mm glass beads, the time taken to reach ATF=90 in CF for bed depth 2 cm, 11 cm, and 18 cm are 50, 98 and 135 s, respectively. These trends are clear from both the predicted and measured data in Figure **8-37,** further proving that that the FD model works well to predict the heating history of the packed bed and CF.
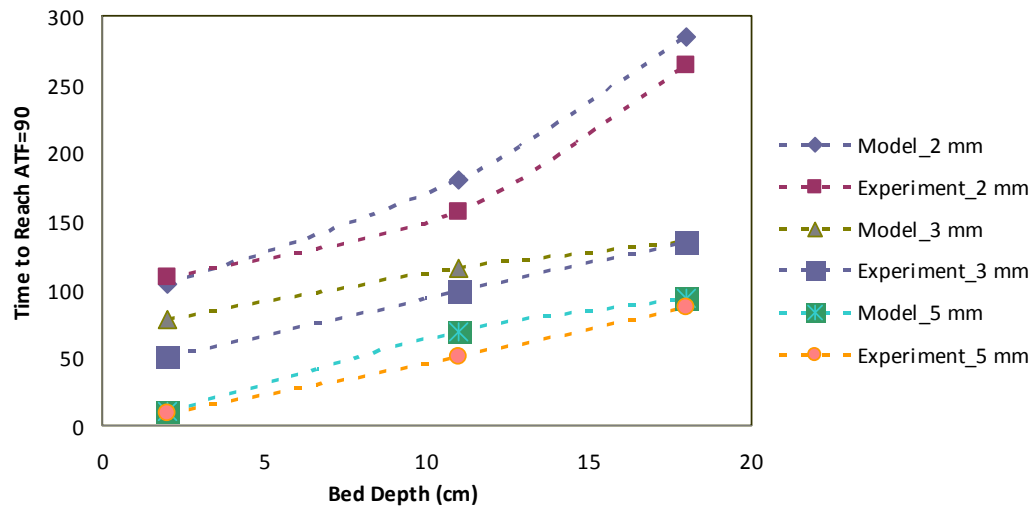
Figure **8-37**: Bed depth summary when CF temperature is heated to ATF=90.

8.5.2 Suggested Bed Depth

Obviously the CF is heated more slowly than the other portions of the packed bed in isobaric steam heating. With smaller particles, such as 2 mm glass beads, it takes much longer time to heat the CF. Increasing bed depth also increases the time to heat the CF but particle size is much more important than bed depth. However, even assuming that these trends are accurately predicted by the model, and that accurate properties data are available for real foods, it is still not a trivial problem to predict the optimal bed depth for a thermal sterilization process. Lethality, quality degradation, and economic components are missing from the model and adding these components is beyond the scope of the current project. Generalizations about optimum bed depth are the limit to what the current research can provide. Following is an example. Supposing

the processing steam and particle properties are similar to those used in the

experiments described herein, then:

1). For 2 mm glass beads it takes at least 3.3 minutes (200 s) to heat the center

of CF to ATF>=90% when the bed depth is 2 cm as shown in Figure **7-5** (a), which

means the CF needs to be processed 3.3 minutes longer to reach the same lethality of

the top of the bed. If 3.3 minutes is a short period compared to the required processing

time at the top of the bed, then this bed depth would be acceptable. However, the

processing time for the top of the bed is likely to be about 5 minutes, which means the

top of the bed would be over processed 3.3 minutes—and be of poor quality—by the

time the bottom of the bed becomes sterile. Under these circumstances the optimum

bed depth for 2 mm particles would be considerably less than 2 cm.

2). For 5 mm glass beads at 2 cm depth, Figure **7-7** shows that it takes 0.3

minutes (20 s) to heat the top and bottom to ATF=90%. So a 2 cm bed depth for 5 mm

glass beads would be no problem (probably it's too shallow). If the bed depth is

increased to 11 cm, the time difference increases to 1.7 minutes (100 s), and that is still

a relatively short time too, compared to the top processing time of 5 minutes. However, if

bed depth increases to 18 cm, the time difference increases to 2.5 minutes (150 s) and

that is becoming a relatively long time compared to 5 minutes. Because deeper bed

depths mean lower capital and operating costs, the optimal bed depth would likely be

around 11 cm.

3). For even larger particles, say 10 mm, the CF is expected to be negligible. Still,

it will take some time for the steam fronts to move through the bed. Figure **7-3** shows

that for 5 mm particles, the steam front travels through the 22 cm bed in about 15 s. This

is a short time compared to 5 minutes and for larger particles the travel time will be even

less because the pore sizes are larger and the condensation rate will be less due to

lower specific surface area. Clearly, 22 cm bed depth would be fine for 10 mm particles and the economic optimum bed depth would probably be much deeper. Other bed depth factors, such as particle damage due to compaction, could become the limiting factor rather than heating rate for some foods.

8.6 Conclusion

The FD model developed in **Chapter 6** is capable of predcting the heat and mass transfer in packed beds with different depths of particle sizes. The predicted temperature history has good agreement with the observed data. With regards to the mass transfer, although the model is subjective to the limitation of experimental apparatus, the predicted data still shows an acceptable correlation with the observed data. Model calibration showed that optimum output from modeling were obtained when parameter *c* and power *p* were set at 0.364 and 3, respectively. It is notable that reasonable results were obtained from the model after calibration using only two constants. This suggests that the model is fundamentally sound.

CHAPTER 9

SUMMARY AND CONCLUSIONS

The overall objective of this research was to develop a numerical model to predict the heat and mass transfer in packed beds subject to heating with isobaric steam in a segmented-flow aseptic processing system. Glass beads in packed beds were used to simulate the food particles in each segment of the system.

The characteristics of the packed bed, including particle diameter, particle density, bulk density, packed bed porosity, static liquid holdup, dynamic liquid holdup, capillary fringe thickness, and vertical drainage were investigated first. A pressurized-steam segmented-flow aseptic processing simulator was designed and built for experimental investigation on the temperature and weight change during steam heating of packed beds. Different bed depths using 2, 3, and 5 mm glass beads were tested.

A finite difference model was developed to predict the heat and mass flow in packed beds, and was solved using an Excel spreadsheet. The iteration function in the spreadsheet enabled the program to keep running until the target condition was reached.

The model validation shows that the finite difference model is capable of predicting the heat and mass flow in packed beds with different depths and particle sizes. The predicted temperature fraction at lower elevations (inside capillary fringe) had good agreement with the observed data, with slope of predicted vs. observed between 0.9 to 1.1, interception between –10% to 10%, R^2 above 0.9 and RMSE less than 10%. At higher elevations (half bed depth and above), the model shows acceptable prediction with the observed data, with R^2 above 0.60. The reason for the larger errors seems clear; the model does not account for the steam pressure gradient through the bed, which

means the bed heats slower than the model predicts unless the gradients are negligible. This was a conscious omission because the gradients were expected to be and are negligible except during the first few seconds that it takes the steam front to traverse the bed. The capillary fringe causes a much greater delay in heating, compared to the time for steam front passage, which means that errors due to the omission of the pressure gradient are inconsequential from a practical perspective. On the other hand, omitting the pressure gradient function allowed for a relatively simple model which executed quickly and gave good insight about the slowest heating zone which is the capillary fringe. For mass flow without steam, the predicted data for cumulative mass flow and water flow velocity showed good correlations with the observed data, with slope 0.85 and 0.94, interception 0.09 and 0.08, R^2 0.95 and 0.98, RMSE 0.04 and 0.16, for cumulative mass flow and mass flow velocity, respectively. However, under steam pressure, the modeled data did not show good agreement with observed data (e.g. R^2 was 0.67 for cumulative flow). Again, the reason for the error seems to be theomission of the steam pressure gradient from the model. The bulk of the drainage occurs during the first few seconds and the steam gradient greatly reduces the pressure gradient for draining water from the bed, thus slowing down and delaying the drainage. All this happens during the first few seconds which means it is inconsequential to the practical application of the model.

The following key conclusions were drawn based on experimental observation and model validation:

9.1 Characteristics of Packed Beds

1). The average measured diameters of the 3 sizes of glass beads were 1.91 mm, 2.90 mm, and 4.92 mm. The packed bed porosity was 0.46 for each size of glass beads.

2). For elevations above 10 cm from capillary fringe, the static holdup was almost constant. The average values of SH above the capillary fringe were 0.29 for different sizes of glass beads. Between upper boundary of capillary fringe and elevation of 10 cm (from capillary fringe), static holdup decreased sharply.

3). At low water flow rates, a second order polynomial equation was given to explain the relationship between dynamic holdup and water flow rate. While with higher flow rates, a straight line was satisfactory.

4). At room temperature, the mean values of capillary fringe thickness were 2.4, 1.4 and 0.6 cm for 2, 3, and 5 mm glass beads. Due to the change in surface tension, capillary fringe thickness decreases with higher liquid temperature. The predicted capillary thicknesses at 121ºC were 1.8, 1.0 and 0.3 cm for 2, 3, and 5 cm glass beads, respectively.

9.2 Numerical Model for Heat and Mass Flow in Packed Bed

The overall numerical model was composed of 4 sub-models: mass flow in drainage, heating of liquid film in the unsaturated flow zone, heating of capillary fringe, and heat transfer inside glass beads. The overall scheme of this mathematical model was to divide the unsaturated flow zone and capillary fringe into N and M layers, respectively, and mass and energy balances were developed in each layer.

9.3 Experimental Investigation on Heat and Mass Flow in Packed Beds

1). The general trend of heating of packed bed shows that the packed beds were heated from top to bottom in order except the capillary fringe was heated from both top and bottom.

2). Capillary fringe was heated slowest because the water in capillary fringe prevents steam from penetrating the packed bed.

3). The capillary fringe was heated faster with the increase of particle diameter for same depth of packed bed because the capillary fringe thickness decreased with larger particles.

9.4 Model Validation

1). Good agreement between observation and prediction was obtained for temperature history for various elevations in packed beds and for different glass bead diameters.

A. At elevation of 1 cm (capillary fringe) in 18 cm bed depth of 2 mm glass beads, model validation showed that the root mean square error (RMSE) was 8.98%, R-square was 0.96 and slope of trendline of observation versus prediction was 0.97.

B. At elevation of 2.9 cm (region right above capillary fringe) in 18 cm bed depth of 2 mm glass beads, model validation showed that RMSE was 12.4%, R-square was 0.92 and slope of trendline of observation versus prediction was 1.02.

C. At elevation of 1 cm (capillary fringe) in 11 cm bed depth of 2 mm glass beads, model validation showed that RMSE was 7.70%, R-square was 0.94 and slope of trendline of observation versus prediction was 0.83.

D. At elevation of 2.9 cm (region right above capillary fringe) in 11 cm bed depth of 2 mm glass beads, model validation showed that RMSE was 10.3%, R-square was 0.96 and slope of trendline of observation versus prediction was 0.84.

E. At elevation of 0.7 cm (capillary fringe) in 18 cm bed depth of 3 mm glass beads, model validation showed that RMSE was 4.7, R-square was 0.99 and slope of trendline of observation versus prediction was 0.89.

F. At elevation of 1.7 cm (region right above capillary fringe) in 18 cm bed depth of 3 mm glass beads, model validation showed that RMSE was 11.6, R-square was 0.92 and slope of trendline of observation versus prediction was 1.17.

G. At elevation of 0.7 cm (capillary fringe) in 11 cm bed depth of 3 mm glass beads, model validation showed that the root mean square error (RMSE) was 4.3, R-square was 0.99 and slope of trendline of observation versus prediction was 1.02.

H. At elevation of 1.7 cm (region right above capillary fringe) in 11 cm bed depth of 3 mm glass beads, model validation showed that the root mean square error (RMSE) was 10.6, R-square was 0.97 and slope of trendline of observation versus prediction was 0.73.

I. At elevation of 0.3 cm (capillary fringe) in 18 cm bed depth of 5 mm glass beads, model validation showed that RMSE was 6.04, R-square was 0.98 and slope of trendline of observation versus prediction was 0.86.

J. At elevation of 0.8 cm (region right above capillary fringe) in 18 cm bed depth of 5 mm glass beads, model validation showed that RMSE was 9.8, R-square was 0.91 and slope of trendline of observation versus prediction was 1.14.

K. At elevation of 0.3 cm (capillary fringe) in 11 cm bed depth of 5 mm glass beads, model validation showed that RMSE was 8.0, R-square was 0.96 and slope of trendline of observation versus prediction was 0.89.

L. At elevation of 0.8 cm (region right above capillary fringe) in 11 cm bed depth of 5 mm glass beads, model validation showed that RMSE was 10.7, R-square was 0.93 and slope of trendline of observation versus prediction was 1.07.

M. The most difficult temperature prediction, also the worst, in this research, was the elevation right above CF. One reason was that the dynamic holdup and static holdup in the zone right above CF were difficult to predict precisely. Another reason was the beginning time of heat processing was hard to synchronize with experimental data. At higher elevations for certain particle size the temperature prediction was also not good, for example, at elevation of 11 cm bed depth with 2 mm glass beads. The main reason is the pressure gradient that occurred at the beginning of processing, but was not included in the model. Another reason was the beginning time of heat processing was hard to synchronize with experimental data. A one second starting time difference could lead to much larger error.

2). Good agreement between observation and prediction was obtained for mass flow in packed bed without steam heating.

A. For cumulative mass flow in 27 cm bed depth with 2 mm glass beads, the RMSE, R-square and slope of trendline of observation versus prediction were 0.04, 0.95, and 0.85, respectively.

B. For cumulative mass flow in 27 cm bed depth with 3 mm glass beads, the RMSE, R-square and slope of trendline of observation versus prediction were 0.4, 0.96, and 0.98, respectively.

C. For cumulative mass flow in 27 cm bed depth with 5 mm glass beads, the RMSE, R-square and slope of trendline of observation versus prediction were 0.34, 0.98, and 0.90, respectively.

3). In steam processing of packed beds, the prediction of mass flow did not show good agreement with observation due to the limitation of drainage measurement.

A. For cumulative mass flow in 18 cm bed depth with 2 mm glass beads, the RMSE, R-square and slope of trendline of observation versus prediction were 0.08, 0.67, and 1.00, respectively.

B. For cumulative mass flow in 18 cm bed depth with 3 mm glass beads, the RMSE, R-square and slope of trendline of observation versus prediction were 0.45, 0.65, and 1.07, respectively.

C. For cumulative mass flow in 18 cm bed depth with 5 mm glass beads, the RMSE, R-square and slope of trendline of observation versus prediction were 0.05, 0.78, and 1.02, respectively.

D. Better drainage measurement and modeling prediction for packed beds in steam processing are expected.

4). The optimum values for parameter c and power p in the finite-difference model were 0.364 and 3, respectively, as shown in model calibration.

9.5 Bed Depth

A summarization of the heating time versus bed depth showed that the predicted and observed data have the same trend and are close to each other, which doubly confirms that the finite difference model works well. Finding the optimum bed depth is beyond the scope of this research project and for aseptic processing would involve the addition of lethality, food quality, and economic components to the model. From the trends seen in this research it seems reasonable that for 2 mm particle the opimium bed depth would be much less than 3 cm, for 5 mm particles it would be around 11 cm while for 10 mm particles bed depth would likely not be a limiting factor.

9.6 Summary

The major contribrition of this research was to provide an effective model to simulate the heat and mass transfer in a packed bed when subjected to the heating of isobaric steam to be used as a tool for helping to determne the optimum depth of packed bed in various processing situations. The limitation of this model, however, suggests that when the numerical model is applied to the industrial production, necessary adjustment will be needed for different scenarios since the model was developed based on properties of glass beads. For industrial application, the parameters of the packeds beds need to be revised, and in some cases the deformation of the particles will need to be taken into consideration.

CHAPTER 10

RECOMMENDATIONS FOR FUTURE WORK

his research project resulted in a validated finite-difference model capable of predicting the heat and mass flow in packed beds with different depths and different sizes of glass beads under steam processing. The limitations of this research included: (1) spherical solid particles (glass beads) were used for modeling and experimental investigation instead of the real food particles; (2) correlation between dynamic holdup and water flow was experimentally determined under low water flux, and no data were obtained for higher water flux due to the limitation of experimental devices; (3) the finite-difference model assumes the heat and mass transfer is one dimensional, but radial heat and mass transfer may also occur; (4) friction loss of steam flow was not considered.

Therefore, the contributions, as well as the limitations, of this research suggest the following possibilities for future work:

(1) Find a better solution to determine the correlation between DH and water flow rate at relatively high water flux under both steam and atmospheric pressure.

(2) Improve the mass flow components in finite-difference model.

(3) Investigate the performance of packed beds of particulate foods, such as soy beans, chickpeas, green peas, etc, in steam processing.

(4) Adjust the finite-difference model developed in this dissertation so that it can be applicable in different particulate foods.

(5) Apply the finite-difference model developed in this dissertation for larger range of glass beads, with diameter smaller than 2 mm and larger than 5 mm.

(6) Apply the finite-difference model developed in this dissertation for irregular shape or other shapes of solid particles, rather than spherical particles.

(7) Experimentally determine and validate equations for the local condensation coefficient.

(8) Validate the model of heat transfer in solid particles presented in this dissertation by experiments.

Consider the momentum balance into the finite-difference model.

REFERENCES

Abdelrahim, K. A., H. S. Ramaswamy, and M. Marcotte. 1997. Residence time distributions of meat and carrot cubes in the holding tube of an aseptic processing system. *Food Science and Technology* 30(1): 9-22.

Akterian, S.G., K.A. Fikiin. 1994. Numerical simulation of unsteady heat conduction in arbitrary shaped canned foods during sterilization processes. *Journal of Food Engineering* 21(3): 343-354.

Alhamdan, A., and S. Sastry. 1997. Residence time distribution of food and simulated particles in a holding tube. *J. of Food Eng.* 34: 271-292.

Anderson, N. M. 2006. Continuous steam sterilization segmented flow aseptic processing of particles food. PhD diss. University Park, PA.: Pennsylvania State University, Department of Agricultural and Biological Engineering.

Anderson, N. M., and P. N. Walker. 2005. Continuous steam sterilization segmented-flow aseptic processing of particle foods. ASAE Paper No. 056041. St. Joseph, MI.: ASAE.

Bates, R.L. and J.A. Jackson. 1980. *Glossary of Geology.* 2nd ed. Falls Church, VA.: American Geological Institute.

Beasley, D.E., and J.A. Clark. 1984. Transient response of a packed bed for thermal energy storage. *Int. J. Heat Mass Transfer* 27(9):1659-1669.

Bergins, C., S. Crone, and K. Strauss. 2005. Multiphase flow in porous media with phase change. Part II: analytical solutions and experimental verification for constant pressure steam injection. *Transport in porous media* 60: 275-300.

Bird, R. B., W. E. Stewart, and E. N. Lightfood. 2002. *Transport Phenomena.* 2nd edition. New York, N.Y.: John Wiley and Sons.

C8057. 2009. Research Methods in Psychology: Analysis of Covariance (ANCOVA). Available at http://www.statisticshell.com/ancova.pdf. Accessed 22 April 2009.

Califano, A.N., and N.E. Zaritzky. 1993. A numerical method for simulating heat transfer in heterogeneous and irregular shaped foodstuffs. *Journal of Food Process Engineering* 16(3): 159-171.

Carslaw, H.S., and J.C. Jaeger. 1959. *Conduction of Heat in Solids.* 2nd ed. Oxford, England: Clarendon Press.

Chau, K.V., and J.J. Gaffney. 1990. A finite-difference model for heat and mass transfer in products with internal heat generation and transpiration. *Journal of Food Science* 55(2): 484-487.

Chen, H., B.P. Marks, and R.Y. Murphy. 1999. Modeling coupled heat and mass transfer convection cooking of chicken patties. *Journal of Food Engineering* 42(3): 139-146.

Crone, S., C. Bergins, and K. Strauss. 2002. Multiphase flow in homogenous porous media with phase change. part I: numerical modeling. *Transport in Porous Media* 49: 291-312.

DiCarlo, D.A. 2003. Drainage in finite-sized unsaturated zones. *Advances in Water Resources* 26: 1257-1266.

Dhir, V.K. 1975. Quasi-steady laminar film condensation of steam on copper spheres. *ASME Journal of Heat Transfer* 1: 347-351.

Dhir, V.K., and J.H. Lienhard. 1971. Laminar film condensation on plane and axisymmetric bodies in nonuniform gravity. *Journal of Heat Transfer* 93(1): 97-100.

Dincer, I. 1994. Unsteady heat-transfer analysis of spherical fruit to air flow. *Energy* 19(1): 117-123.

Dockal, J.A. 2009. Grain Morphology: Roundness, Surface Features, and Sphericity of Grains. Available at http://people.uncw.edu/dockal/gly312/grains/grains.htm. Accessed 4 April 2009.

Elgin, J.C., and F.B. Weiss. 1939. Liquid holdup and flooding in packed towers. *Industrial Engineering Chemistry* 31:435-445.

EMSI. 2009. Model Calibration. South Jordan, UT.: EMSI. Available at http://www.ems-i.com/gmshelp/Model_Calibration/Model_Calibration.htm. Accessed in 1st June 2009.

Erdogdu, F., M.O. Balaban, and K.V. Chau. 2003. Modeling of heat conduction in elliptical cross-section (oval-shapes) using numerical finite difference models. Transport Phenomena in Food Processing. Boca Raton, Fl.: CRC Press.

Ergun, S. 1952. Fluid flow through packed columns. *Chemical Engineering Progress* 48 (2): 89-94.

Faghri, A., and Y. Zhang. 2006. *Transport Phenomena in Multiphase Systems*. Sa Diego, CA.: Elsevier Inc.

Fujioka, Y., and T. Kitamura. 1964. Approximate solution of a vertical drainage problem. *Journal of Geophysical Research* 69(24): 5249-5255.

Gaile, G.L., and C.J. Willmott. 1984. *Spatial Statistics and Models*. Hingham, MA.: Kluwer Boston Academic Publishers.

Ghani, A.G. A., M.M. Farid, X.D. Chen, and P. Richards. 1999. Numerical simulation of natural convection heating of canned food by computational fluid dynamics. *Journal of Food Engineering* 41: 55-64.

Haverkamp, R., M. Vauclin, J. Touma, P.J. Wierenga, and G. Vachaud. 1977. *Soil Science Society of American Journal* 41: 285-294.

Hilden, J.L., and K.P. Trumble. 2003. Numerical analysis of capillarity in packed spheres: planar hexagonal-packed spheres. *Journal of Colloid and Interface Science* 27(2): 463-474.

Holman, J. P. 1997. *Heat Transfer.* 8th ed. United States: McGraw-Hill, Inc.

Holub, R.A., M.P. Dudukovic, and P.A. Ramachandran. 1993. Pressure drop, liquid holdup, and flow regime transition in trickle flow. *AIChE Journal* 39(2): 302-321.

Hu, H. 2005. Mixed convection turbulent film condensation on a sphere. *Applied Mathematics and Computation* 170: 1194-1208.

Hu, H., and A.M. Jacobi. 1992. Vapor shear and pressure gradient effects during filmwise condensation from a flowing vapor onto a sphere. *Experimental Thermal and Fluid Sciences* 5: 548-555.

Huan, Z., S. He, and Y. Ma. 2003. Numerical simulation and analysis for quick-frozen food processing. *Journal of Food Engineering* 60: 267-273.

Ikediala, J.N., L.R. Correia, G.A. Fenton, and A.N. Ben. 1996. Finite element modeling of heat transfer in meat patties during single-sided pan-frying. *Journal of Food Science* 61: 796-802.

Incropera, F. P., and D. P. DeWitt. 2002. *Fundamentals of Heat and Mass Transfer.* 5th ed. Hoboken, NJ.: John Wiley and Son, Inc.

Lzadifar, M., O-D. Baik, and C. J. Simonson. 2006. Modeling of the packed bed drying of paddy rice using the local volume averaging (LVA) approach. *Food Research International* 39: 712-720.

Jacobi, A.M. 1992. Filmwise condensation from a flowing vapor onto isothermal axisymmetric bodies. *Journal of Thermophysics and Heat Transfer* 6: 581-591.

Kastanek, F. 1971. Numerical simulation technique for vertical drainage from a soil column. *Journal of Hydrology* 14:213-232.

Kim, K.H., and A.A. Teixeira. 1997. Predicting internal temperature response to conduction-heating of odd-shaped solids. *Journal of Food Engineering* 20(1): 51-63.

Klerk, A.D. 2003. Liquid holdup in packed beds at low mass flux. *AICHE Journal* 49(6): 1597-1600.

Kramer, G.J. 1998. Static liquid hold-up and capillary rise in packed beds. *Chemical Engineering* 53(16): 2985-2992.

Kushalkar, K.B., and V.G. Pangarkar. 1990. Liquid holdup and dispersion in packed columns. *Chemical Engineering Science* 45(3): 759-763.

Lago, M., and M. Araujo. 2001. Capillary rise in porous media. *Physica A* 289:1-17.

Lenz, M.K., and D.B. Lund. 1994. Temperature distributions during heat/hold processing of food. *Journal of Food Science* 38: 630-632.

Lienhard, J.H., and V.K. Dhir. 1974. Laminar film condensation on non-Isothermal and arbitrary heat-flux surfaces and on fins. *J. Heat Transfer* 96(2):197-203.

Liu, Y. S. 1994. Mathematical modeling of particulate two-phase tube flow applicable to aseptic processing. PhD diss. University Park, PA.: Penn State University, Department of Agricultural and Biological Engineering.

Lu, N., and W. J. Likos. 2004. Rate of capillary rise in soil. *Journal of Geotechnical and Geoenvironmental Engineering* 130(6): 646-656.

Masciopinto, C., G. Passarella, M. Vurro. 1994. Numerical simulation for the evaluation of the free surface history in porous media. Comparison between two different approaches. *Advances in Engineering Software* (21): 149-157.

Massey, B., J. Ward-Smith. 2006. 8thed. *Mechnics of Fluids*. New York, NY.: Taylor & Francis.

McKenna, A. B., and G. S. Tucker. 1991. Computer modelling for the control of particulate sterilization under dynamic flow conditions. *Food Control* 2(4): 224-233.

Mohamed, I.O. 2003. Computer simulation of food sterilization using an alternating direction implicit finite difference method. *Journal of Food Engineering* 60: 301-306.

National Instruments. 2009. What Is Data Acquisition? Auxtin, TX.: National Instruments Co. Available at http://www.ni.com/dataacquisition/whatis.htm. Accessed Feb. 2, 2009.

Omega. 2009. Introduction to Data Loggers. Available at http://www.omega.com/prodinfo/DataLoggers.html. Accessed 18 March 2009.

Oner, M.E. 2007. Continuous steam sterilization of apple slices. M.S thesis. University Park, PA.: Penn State University, Department of Agricultural and Biological Engineering.

Otero, L., and P.D. Sanz, 2003. Modeling heat transfer in high pressure food processing: a review. *Innovative Food Science and Emerging Technologies* 4:121-134.

Ott, R.L., and M. Longnecker. 2001. An Introduction to Statistical Methods and Data Analysis. 5th ed. Pacific Grove, CA.: Duxbury.

Pinczewski, W.V., and W.B.U. Tanzil. 1981. A numerical solution for the drainage of two-dimensional packed beds. *Chemical Engineering Science* 36: 1039-1043.

Puri, V.M., and R.C. Anantheswaran. 1993. The finite-element method in food processing: a review. *Journal of Food Engineering* 19: 247-274.

Popiel, C.O., and L. Boguslawski. 1975.Heat transfer by laminar film condensation on sphere surfaces. *Int. J. Heat Mass Transfer* 18: 1486-1488.

Raats, P.A.C., and W.R. Gardner. 1974. Movement of water in the unsaturated zone near a water table. In *Drainage For Agriculture*, 311-357. J.V. Schilfgaarde, ed. Madison, WI.: The American Society of Agronomy, Inc.

Radcliffe, D.E., and T.C. Rasmussen. Chapter 4: Soil Water Movement. In *Soil Physics Companion,* 85-122. A. W. Warrick, ed. Boca Raton, Fl.: CRC Press.

Rohsenow, W.M. 1956. Heat transfer and temperature distribution in laminar film condensation. *Trans. ASME* 78: 1645-1648.

Sabapathy, N. D. 2005. Heat and mass transfer during cooking of chickpea-measurements and computational simulation. PhD diss. Saskatoon, Saskatchewan: University of Saskatchewan, Department of Agricultural and Biological Engineering.

Saez, A.E., and R.G. Carbonell. 1985. Hydrodynamic parameters of gas-liquid concurrent flow in packed beds. *AIChE Journal* 32:52-62.

Saez, A.E., M.M. Yepez, C. Cabrera, and E.M. Soria. 1991. Static liquid holdup in packed beds of spherical particles. *AIChE Journal* 37(11):1733-1736.

Sater, V.E., and Octave Levenspiel. 1966. Two-phase flow in packed beds. Evaluation of axial dispersion and holdup by moment analysis. *Ind. Eng. Chem. Fundamen.* 5(1): 86-92.

Schubert, C.N., J.R. Lindner, and R.M. Kelly. 1986. Experimental methods for measuring static liquid holdup in packed columns. *AIChE Journal* 32(11): 1920-1923.

Scott, G., and P. Richardson. 1997. The application of computational fluid dynamics in the food industry. Trends in Food Science and Technology 8: 119-124.

Sheen, S., C.H. Tong, Y. Fu, and D.B. Lund. 1993. Lethality of thermal processes for food in anomalous-shaped plastic containers. *Journal of Food Engineering* 20(3): 199-213.

Shulman, H.L., C.F. Ullrich, and N. Wells. 1955. Performance of packed columns. I. total, static and operating holdups. *AIChE Journal* 1(2): 247-253.

Singh, R.P., and D.R. Heldman. *Introduction to Food Engineering*. 3rd ed. San Diego, CA.: Academic Press.

Sman, R.G.M. 2003. Simple model for estimating heat and mass transfer in regular-shaped foods. *Journal of Food Engineering* 60: 383-390.

Smith, P. G. 2003. *Introduction to Food Process Engineering*. New York, NY.: Kluwer Academic/Plenum Publishers.

Sun, D. and X. Zhu. 1999. Effect of heat direction on the numerical prediction of beef freezing processe*s. Journal of Food Engineering* 42: 45-50.

Sparrow, E.M., and J.L. Gregg. 1959. A boundary-layer treatment of laminar-film condensation. *Journal of Heat transfer. Trans. Amer. Soc. Mech. Engrs* 81: 13-18.

Specchia, V., and G. Baldi. Pressure drop and liquid holdup for two phase concurrent flow in packed beds. *Chemical Engineering Science* 32:515-523.

Stanek, V. 1994. *Fixed Bed Operations: Flow Distribution and Efficiency.* Vodickova, Czech: Academia.

Thom A. and C.J. Apelt. 1961. *Field Computations in Engineering and Physics.* London: D. Van Nostrand.

Thorvaldsson, K., and H. Janestad. 1999. A model for simultaneous heat, water and vapour diffusion. *Journal of Food Engineering* 40: 167-172.

Todsen, M. 1971. On the solution of transient free-surface flow problems in porous media by finite-difference methods. *Journal of Hydrology* 12:177-210.

Trautmann, N.M., and K.S. Porter. 2009. Water and the soil. Natural Resources Cornell Cooperative Extension. Available at: http://pmep.cce.cornell.edu/facts-slides-self/facts/wat-so-grw85.html. Accessed 11 May 2009.

Van Swaaij, W.P.M., J.C. Charpentier, and J. Villermaux. 1969. Residence time distribution in the liquid phase of trickle flow in packed beds. *Chemical Engineering Science* 24: 1083–1095.

Wadell, H. 1933. Sphericity and roundness of rock particles. *J Geol* 41:310-331.

Washburn, E.W. 1921. The dynamic of capillary flow. *Physical Review* 17(3): 273-283.

Walker, P.N. 2000. Segmented flow device. U.S. patent No. 5457513.

Walker, P.N. 2006. Personal communication. University Park, PA.: The Pennsylvania State University.

Walker, P.N., and R.B. Beelman. 2002. Segmented flow aseptic processing of PA crops: Mushrooms. A grant proposal submitted to the Pennsylvania Department of Agriculture. University Park, PA.: The Penn State University, Department of Agricultural and Biological Engineering.

Walker, P.N., and R.B. Beelman. 2005. Segmented flow aseptic processing of PA crops: apples. A grant proposal submitted to the Pennsylvania Department of Agriculture. University Park, PA.: Penn State University, Department of Agricultural and Biological Engineering.

Wang, L., and D. Sun. 2002. Modeling three-dimensional transient heat transfer of roasted meat during air blast cooling by the finite element method. *Journal of Food Engineering* 51: 319-328.

Wang, L., and D. Sun. 2003. Recent developments in numerical modeling of heating and cooling processes in the food industry – a review. *Trends in Food Science & Technology* 14: 408-423.

Wang, N., and J.G. Brennan. 1995. A mathematical model of simultaneous heat and moisture transfer during drying of potato. *Journal of Food Engineering* 24: 47-60.

Wang, Z.H. and G.H. Chen. 1999. Heat and mass transfer during low intensity convection drying. *Chemical Engineering Science* 54: 3899-3908.

Welt, B.A., A.A. Teixeira, K.A. Chau, M.O. Balaban, and D.E. Hintenlang. 1997. Explicit finite difference methods for heat transfer simulation and thermal process design. *Journal of Food Science* 62(2): 230-236.

Welti-Chanes, J., F. Vergara-Balderas, D.Bermudez-Aguirre. 2004. Transport phenomena in food engineering: basic concepts and advances. *Journal of Food Engineering* 67: 113-128.

Wen, D., and Y. Ding. 2006. Heat transfer of gas flow through a packed bed. *Chem. Eng. Sci.* 61: 3532-3542.

Wu, H., and P.N. Walker. 2008. Finite-difference analysis of heating of capillary fringe in steam processing. ASAE Paper No. 083787. Providence, RI.: ASAE.

Yang, J. W. 1973. Laminar film condensation on a sphere. *Journal of Heat Transfer* 95(2): 97-100.

Yang, W. 2003. Chapter 1. Particle characterization and dynamics. In *Handbook of Fluidization and Fluid-Particle Systems*, 1-29. W. Yang, ed. New York, NY.: Marcel Dekker, Inc.

Yang, Y. W., G. Zografi, and E. E. Miller. 1988. Capillary flow phenomena and wettability in porous media. *Journal of Colloid and Interface Science* 122(1): 24-34.

Yin, F., A. Afacan, K. Nandakumar, Karl T. Chuang. 2002.Liquid holdup distribution in packed columns: gamma ray tomography and CFD simulation. *Chemical Engineering and Processing* 41: 473-483.

Youngs, E.G. 1960. The drainage of liquids from porous media. *Journal of Geophysical Research* 65(12): 4025-4030.

Young, Y.P., A.N. Emery, and P.J. Fryer. 2002. Heat transfer to a model dough product during mixed regime thermal processing. *Trans IChemE* 80: 183-192.

APPENDIX A

OPERATING INSTRUCTIONS FOR QUANTACHROME MULTIPYCNOMETER AND PARTICLE DENSITY CALCULATION

A.1 Operating Instruction for Quantachrome Multipycnometer

1. Power – "on", allow 10-15 minutes for the pressure transducer to warm up and stabilize.

2. Select the correct REFERENCE VOLUME for the sample cell to be used. See the front panel for reference volume selection.

3. Fill the sample cup (about 3/4 full), insert it into the cell holder and replace the cover.

4. Open the "GAS OUT" and "GAS OUT RATE" control. Wait for a stable zero reading.

5. Close the "GAS OUT" toggle valve and set the meter to zero.

6. Turn the selector valve to "REF".

7. Open the "GAS IN" toggle valve, and pressurize to approximately 18 PSIG using the "GAS IN RATE" needle valve to control the rate of pressurization. Stop the flow by closing the "GAS IN" toggle valve.

8. Record the display reading after it has stabilized. This valve is "P1".

9. Turn the selector valve to "CELL".

10. Record the display reading after it has stabilized. This valve is "P2".

11.   Vent the pressure slowly to prevent blowing powder out of the cell, by

opening the "GAS OUT" toggle valve with the "GAS OUT RATE"

control slightly open.

12.   Calculate the true powder volume.

A.2 Particle Density Calculation

The govening equation for calculating particle density is

$$V_p = V_c - V_R \left(\frac{P_1}{P_2} - 1 \right)$$

Eq. **1.1**

Where

V_p = volume of powder

V_c = volume of sample cell

V_R = reference volume

P_1 = pressure reading after pressurizing the reference volume

P_2 = pressure reading after including V_c

APPENDIX B

DATA AND STATISTICAL ANALYSIS FOR CHARACTERISTICS OF PACKED BEDS

B.1 Statistical Analysis for Bulk Densities of Glass Beads.

Table **B-1**: Result of one-way ANOVA for Bulk Density versus Particle Diameter.

```
Source                 DF      SS      MS      F      P
Particle Diameter       2   1690.2   845.1   23.87  0.000
Error                   9    318.7    35.4
Total                  11   2008.9


S = 5.951    R-Sq = 84.14%   R-Sq(adj) = 80.61%



                              Individual 95% CIs For Mean Based on
                              Pooled StDev
Level   N     Mean   StDev  ----+---------+---------+---------+-----
2 mm    4  1566.53   3.90                             (----*-----)
3 mm    4  1557.70   8.24                    (-----*-----)
5 mm    4  1538.13   4.81   (-----*----)
                            ----+---------+---------+---------+-----
                             1536      1548      1560      1572


Pooled StDev = 5.95
```

B.2 Static Holdup Measured for Different Sizes of Glass Beads Using Different Base Weight.

Table **B-2**: Static holdup measured for 2 mm glass beads and calculated with mass-difference method.

Dry Weight (kg)	Wet Weight (kg)	Water weight (kg)	Water weight difference (kg)	Volumetric static holdup (m3/m3)	Average value of static holdup(kg)	Mean Value of Static Holdup
5	5.094	0.094				
5	5.093	0.093	---	---	---	
5	5.092	0.092				
5	5.094	0.094				
1	1.024	0.024	0.07	0.027195		
1	1.024	0.024	0.069	0.0268065	0.0266	0.0251
1	1.026	0.026	0.066	0.025641		
1	1.025	0.025	0.069	0.0268065		
2	2.046	0.046	0.048	0.024864		
2	2.05	0.05	0.043	0.022274	0.0236	
2	2.048	0.048	0.044	0.022792		
2	2.047	0.047	0.047	0.024346		

Table **B-3**: Static holdup measured for 3 mm glass beads and calculated with mass-difference method.

Dry Weight (kg)	Wet Weight (kg)	Water weight (kg)	Water weight difference (kg)	Volumetric static holdup (m3/m3)	Average value of static holdup(kg)	Mean Value of Static Holdup
5	5.096	0.096				
5	5.098	0.098	---	---	---	
5	5.095	0.095				
5	5.093	0.093				
1	1.019	0.019	0.077	0.0299145		
1	1.018	0.018	0.08	0.03108	0.0296	0.0291
1	1.019	0.019	0.076	0.029526		
1	1.021	0.021	0.072	0.027972		
2	2.04	0.04	0.056	0.029008		
2	2.042	0.042	0.056	0.029008	0.0286	
2	2.04	0.04	0.055	0.02849		
2	2.039	0.039	0.054	0.027972		

Table **B-4**: Static holdup measured for 5 mm glass beads and calculated with mass-difference method.

Dry Weight (kg)	Wet Weight (kg)	Water weight (kg)	Water weight difference (kg)	Volumetric static holdup (m3/m3)	Average value of static holdup(kg)	Mean Value of Static Holdup
5	5.093	0.093				
5	5.095	0.095	---	---	---	
5	5.094	0.094				
5	5.093	0.093				
1	1.016	0.016	0.077	0.029914		
1	1.015	0.015	0.08	0.03108	0.0300	0.0300
1	1.018	0.018	0.076	0.029526		
1	1.017	0.017	0.076	0.029526		
2	2.039	0.039	0.054	0.027972		
2	2.038	0.038	0.057	0.029526	0.0299	
2	2.036	0.036	0.058	0.030044		
2	2.031	0.031	0.062	0.032116		

B.3 Statistical Analysis of Static Holdup in Different Packed Beds

Table **B-5**: Paired t-test for static holdup calculated by two different methods.

```
Paired T for VSH_2mm_4kg - VSH_2mm_3kg

              N      Mean      StDev    SE Mean
VSH_2mm_4kg   4   0.026612   0.000673   0.000336
VSH_2mm_3kg   4   0.023569   0.001233   0.000617
Difference    4   0.003043   0.001017   0.000508


95% CI for mean difference: (0.001425, 0.004661)
T-Test of mean difference = 0 (vs not = 0): T-Value = 5.99  P-Value = 0.009
```

B.4 Statistical Analysis of Dynamic Holdup in 5 mm Glass Beads

The original data is shown in Table **B-6**. Three trails were tested . "2.5-2.0" stands for the DH in 0.5 kg packed bed calculated by subtracting DH in 2.0 kg from 2.5 kg packed bed.

Table **B-6**: Original data of DH in packed beds of 5 mm glass beads at different mass flow rate (shown as flowmeter scale).

scale	TRAIL 1			TRAIL 2			TRAIL 3			AVERAGE		
	2.50-2.0	3.0-2.0	3.5-2.0	2.50-2.0	3.0-2.0	3.5-2.0	2.50-2.0	3.0-2.0	3.5-2.0	2.50-2.0	3.0-2.0	3.5-2.0
0	0.002	0.005	0.004	0.004	0.004	0.003	0.004	0.004	0.007	0.003	0.004	0.005
5	0.012	0.011	0.009	0.010	0.009	0.011	0.010	0.008	0.011	0.011	0.009	0.010
10	0.012	0.013	0.012	0.014	0.013	0.013	0.014	0.012	0.013	0.013	0.013	0.013
15	0.012	0.014	0.017	0.014	0.018	0.016	0.016	0.015	0.016	0.014	0.016	0.016
20	0.016	0.019	0.021	0.018	0.021	0.018	0.018	0.017	0.019	0.017	0.019	0.019
25	0.024	0.023	0.021	0.024	0.023	0.020	0.018	0.021	0.020	0.022	0.022	0.020
30	0.024	0.025	0.025	0.028	0.026	0.021	0.022	0.023	0.023	0.025	0.025	0.023
35	0.028	0.031	0.027	0.028	0.028	0.025	0.024	0.026	0.025	0.027	0.028	0.026
40	0.032	0.034	0.032	0.030	0.030	0.027	0.026	0.030	0.027	0.029	0.031	0.029
45	0.034	0.038	0.033	0.034	0.033	0.029	0.030	0.033	0.031	0.033	0.035	0.031
50	0.036	0.041	0.036	0.040	0.034	0.031	0.034	0.035	0.035	0.037	0.037	0.034
55	0.036	0.042	0.039	0.044	0.037	0.035	0.038	0.035	0.037	0.039	0.038	0.037
60	0.036	0.043	0.040	0.044	0.038	0.034	0.040	0.039	0.040	0.040	0.040	0.038

There are one response variable DH and two independent variables "Weight" and "Scale". For this question, the factor "Scale" might be a variable that can affect the relationship between the outcome of interest and other primary independent

variable "Weight". "Scale" can be used as a covariate (C8057, 2009) to reduce the residuals. An ANOVA model with a covariate is called an analysis of covariance (ANCOVA) (C8057, 2009).

The outcome of interest for this question is the Dynamic Holdup, so the data can be restructured in the Minitab as Table **B-7**. The variable name is first set as "Weight". Thus the factor "Weight" has 3 levels.

Table **B-7**: Data reconstruction in Minitab for DH in 5 mm glass beads.

↓	C1	C2-T	C3
	DH	Weight	scale
1	0.0020000	2.50-2.0	0
2	0.0120000	2.50-2.0	5
3	0.0120000	2.50-2.0	10
4	0.0120000	2.50-2.0	15
5	0.0160000	2.50-2.0	20
6	0.0240000	2.50-2.0	25
7	0.0240000	2.50-2.0	30
8	0.0280000	2.50-2.0	35
9	0.0320000	2.50-2.0	40
10	0.0340000	2.50-2.0	45
11	0.0360000	2.50-2.0	50
12	0.0360000	2.50-2.0	55
13	0.0360000	2.50-2.0	60
14	0.0050000	3.0-2.0	0
15	0.0110000	3.0-2.0	5
16	0.0130000	3.0-2.0	10
17	0.0140000	3.0-2.0	15
18	0.0190000	3.0-2.0	20
19	0.0230000	3.0-2.0	25
20	0.0250000	3.0-2.0	30
21	0.0310000	3.0-2.0	35
22	0.0340000	3.0-2.0	40
23	0.0380000	3.0-2.0	45
24	0.0410000	3.0-2.0	50
25	0.0420000	3.0-2.0	55

ANCOVA has two more important considerations than ANOVA:

First, the covariate should be independent with the treatment effect.

195

Second, the relationship between the response variable and the covariate should not differ across the groups. (Homogeneity of regression slopes).

Firstly, the relationship between DH and scale was tested. The output shown in Table **B-8** was linearly correlated. In other words, for each treatment ("2.5kg-2kg", "3kg-2kg" and "3.5kg-2kg"), the regression lines between DH and Scale have the same slope. Since the regression slopes for different treatments are parallel, we can compare the differences among treatments by adjusting to a common level of the scale variable.

Table **B-8**: Regression output of DH versus scale.

Regression Analysis: DH versus scale

```
The regression equation is
DH = 0.00657 + 0.000574 scale


Predictor          Coef     SE Coef      T       P
Constant     0.0065698   0.0004086   16.08   0.000
scale        0.00057407  0.00001156  49.67   0.000


S = 0.00233886   R-Sq = 95.5%   R-Sq(adj) = 95.5%
```

Then the homogeneity was tested to see whether the three curves Figure **4-13** can be treated as one single curve.

The following residual plots in Figure **B-1** show nothing unusual. Thus, the assumptions of the ANCOVA are met.

The output of ANCOVA shows the p-value is 0.063>0.05, as highlighted in yellow in Table **B-9**, indicating that the null hypothesis can't be rejected so homogeneity is concluded.
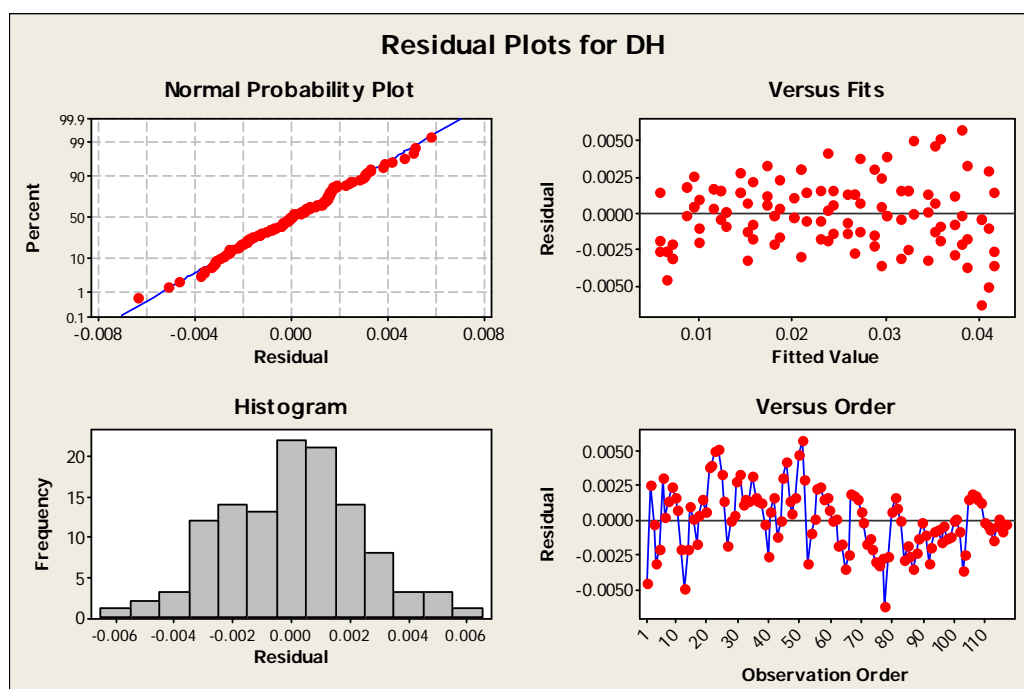
Figure **B-1**: Residual plots for dynamic holdup (DH) in 5 mm glass beads.

Table **B-9**: Partial Output of ANCOVA for 5 mm glass beads.

```
Analysis of Variance for DH, using Adjusted SS for Tests

Source    DF     Seq SS      Adj SS      Adj MS        F       P
scale      1  0.0134955   0.0134955   0.0134955  2546.07   0.000
Weight     2  0.0000301   0.0000301   0.0000151     2.84   0.063
Error    113  0.0005990   0.0005990   0.0000053
Total    116  0.0141246


S = 0.00230229   R-Sq = 95.76%   R-Sq(adj) = 95.65%
```

APPENDIX C

EXPERIMENT RESULTS FOR STEAM PROCESSING OF PACKED BEDS WITH SATURATED STEAM
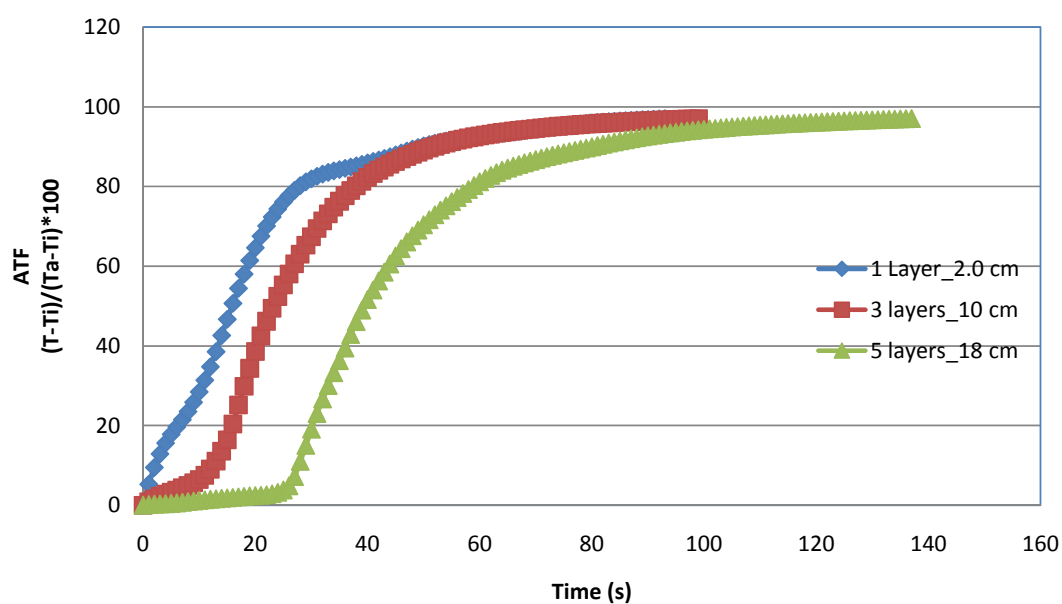
Figure **C-1**: ATF of the bottom probe (1.0 cm height) for 3 mm glass beads. Curves end at where ATF=97. 1 layer_20 cm means 1 layer of glass beads with 2.0 cm bed height.

The time taken for the bottom probe to reach where ATF=97% was

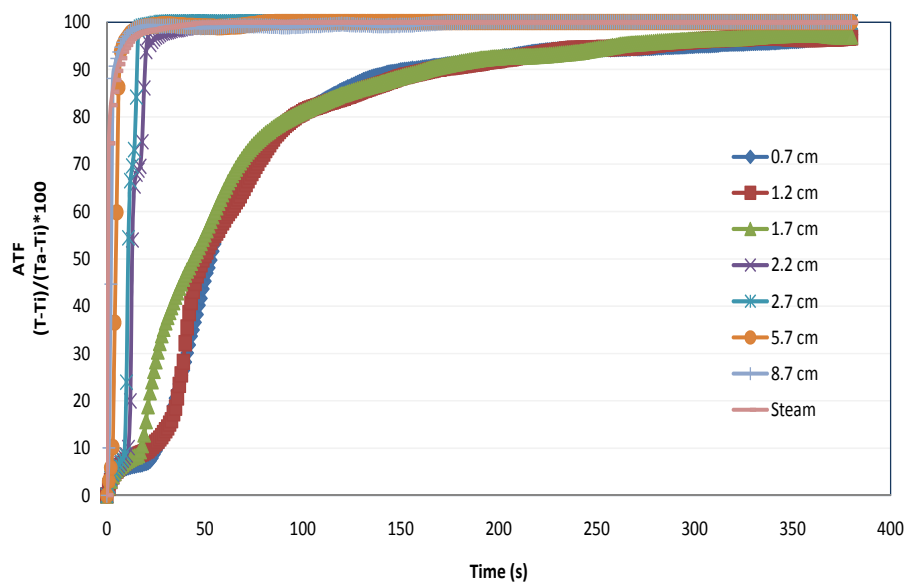approximately 90 s for 1 layer, 100 s for 3 layers, and 140 s for 5 layers.
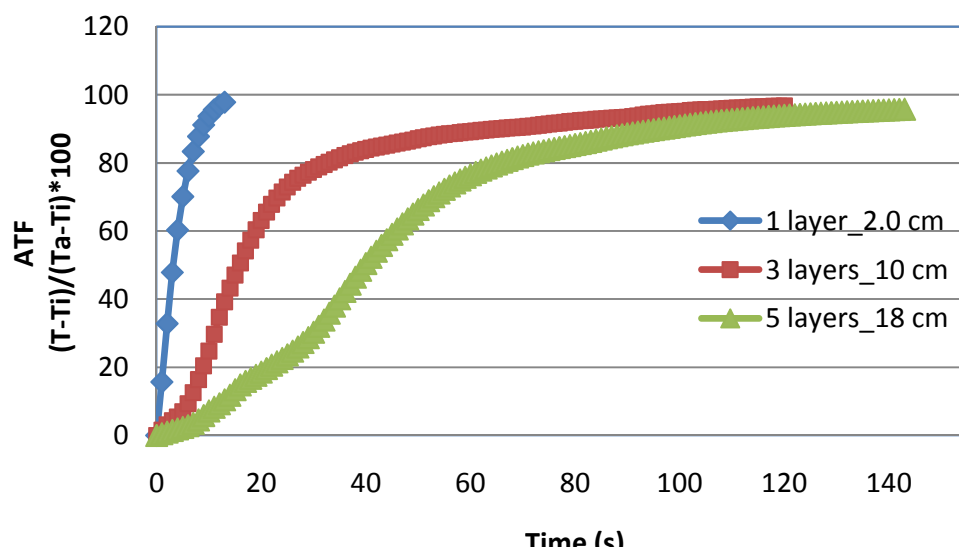
Figure **C-2**: ATF of the bottom probe (1.0 cm height) for 5 mm glass beads. Curves end at where ATF=97. 1 layer_20 cm means 1 layer of glass beads with 2.0 cm bed height.

The time taken for the bottom probe to reach where ATF=97% was 13 s for 1 layer, 120 s for 3 layers, and 140 s for 5 layers.

Figure **C-3**: Temperature History at different positions from bottom to top of 1.2 kg packed bed (11 cm height) from 2 mm glass beads. Data was ended at where the last curve reached to ATF=97.
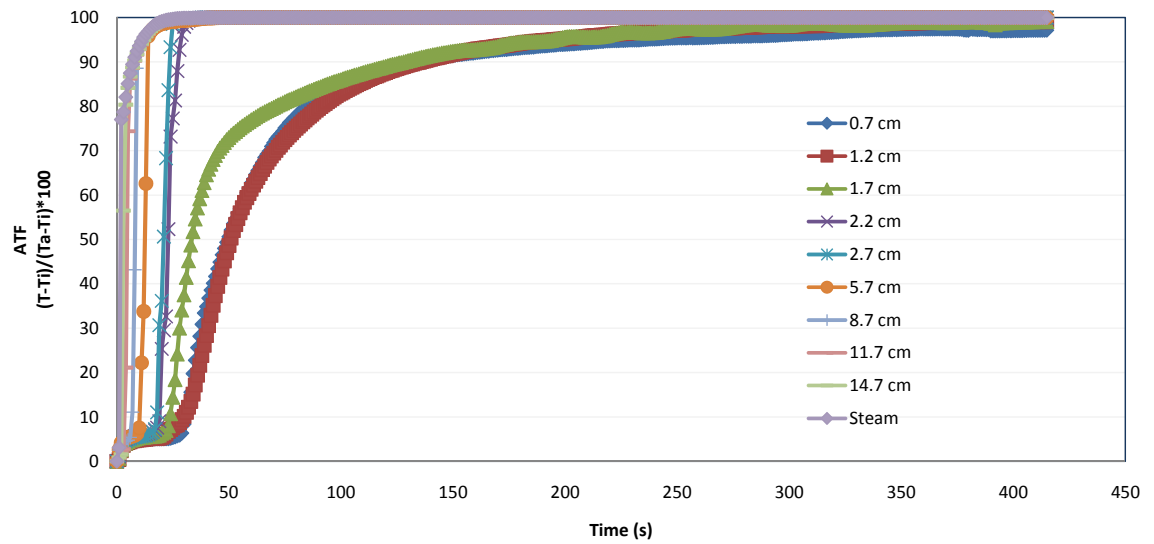
Figure **C-4**: Temperature History at different positions from bottom to top of 18 cm height (2 kg) packed bed from 3 mm glass beads. Data was ended at where the last curve reached to ATF=97.
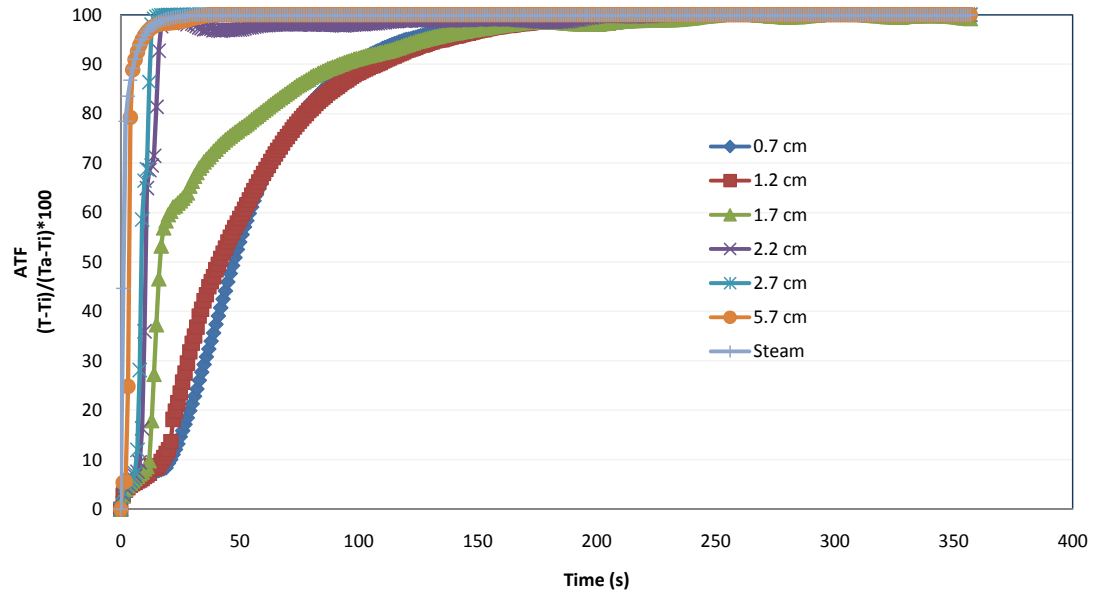
Figure **C-5**： Temperature History at different positions from bottom to top of 11 cm height (1.2 kg) packed bed from 3 mm glass beads. Data was ended at where the last curve reached to ATF=97.
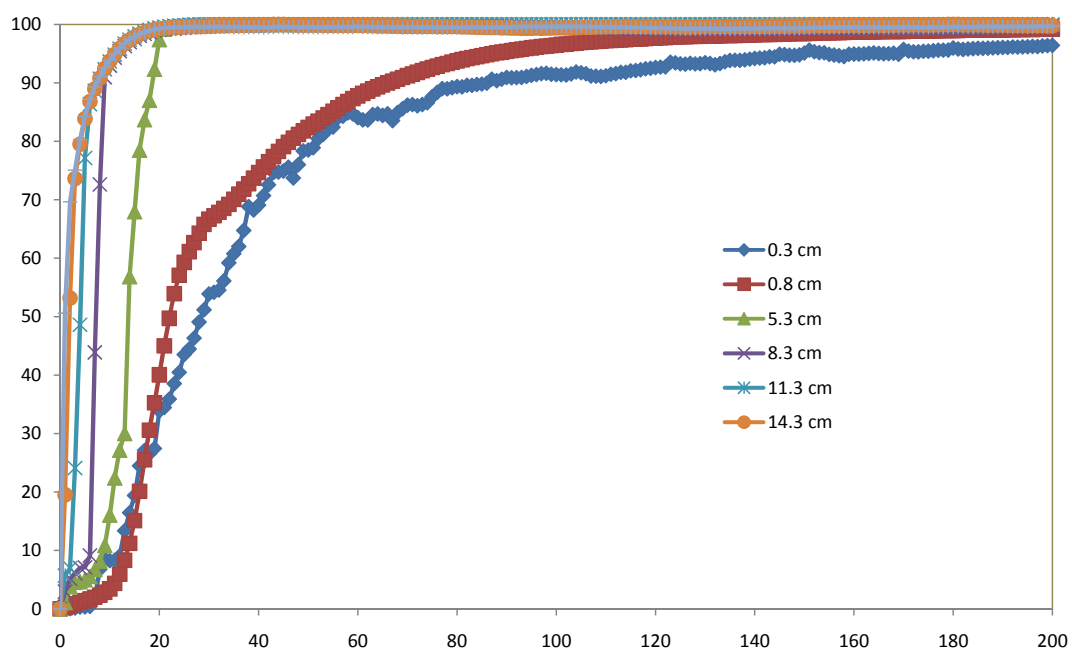
Figure **C-6**: Temperature History at different positions from bottom to top in packed bed with 18 cm height from 5 mm glass beads. Data was ended at where the last curve reached to ATF=97.
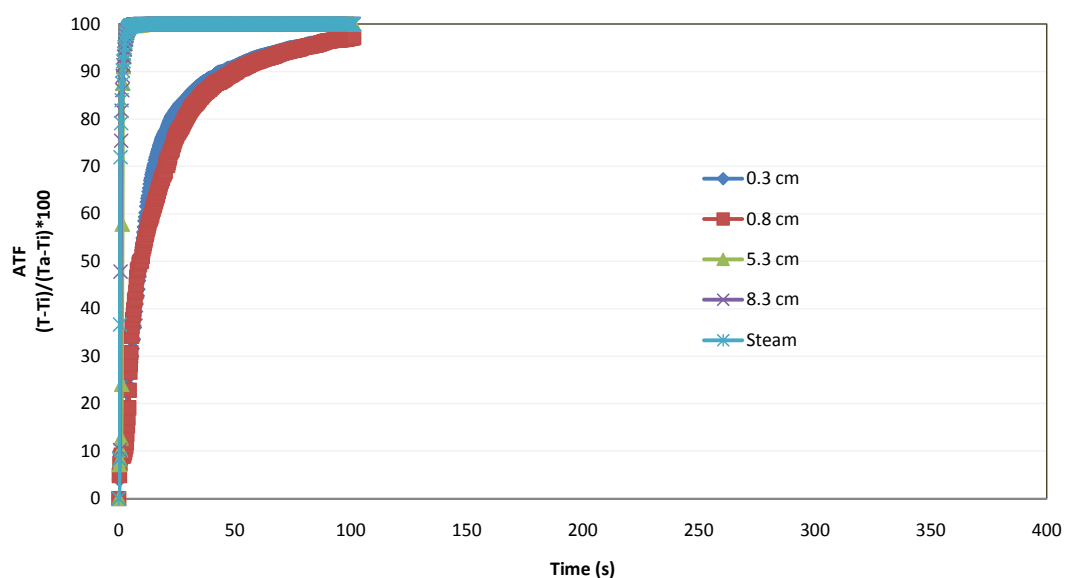
Figure **C-7**: Temperature History at different positions from bottom to top of 11 cm height packed bed (1.2 kg) from 5 mm glass beads. Data was ended at where the last curve reached to ATF=97.
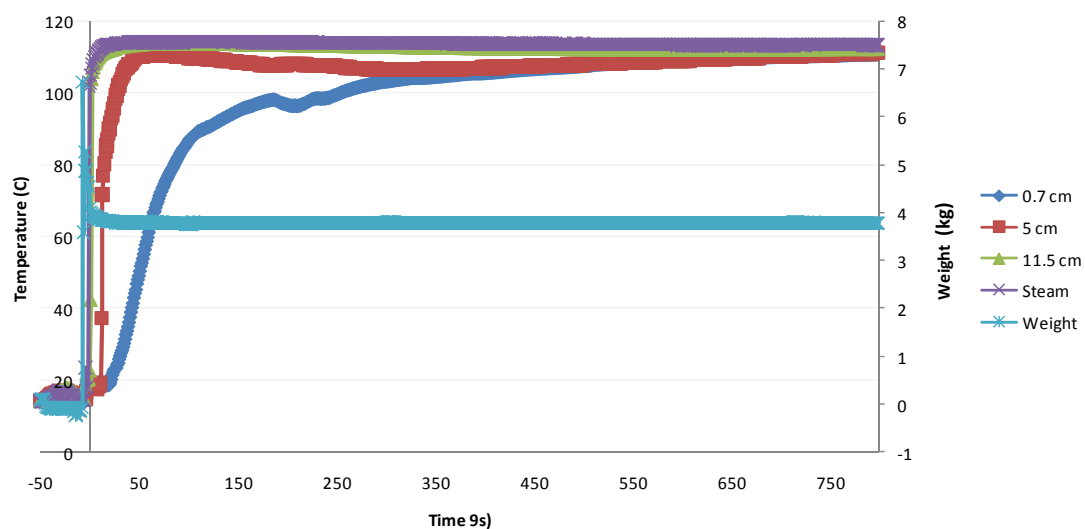

Figure **C-8**: Simultaneous measurement of temperature and weight in 18 cm high packed bed. Glass Beads size: 3 mm. Data is plotted from -50 to 800 s with time zero being when water table falls to bed surface.
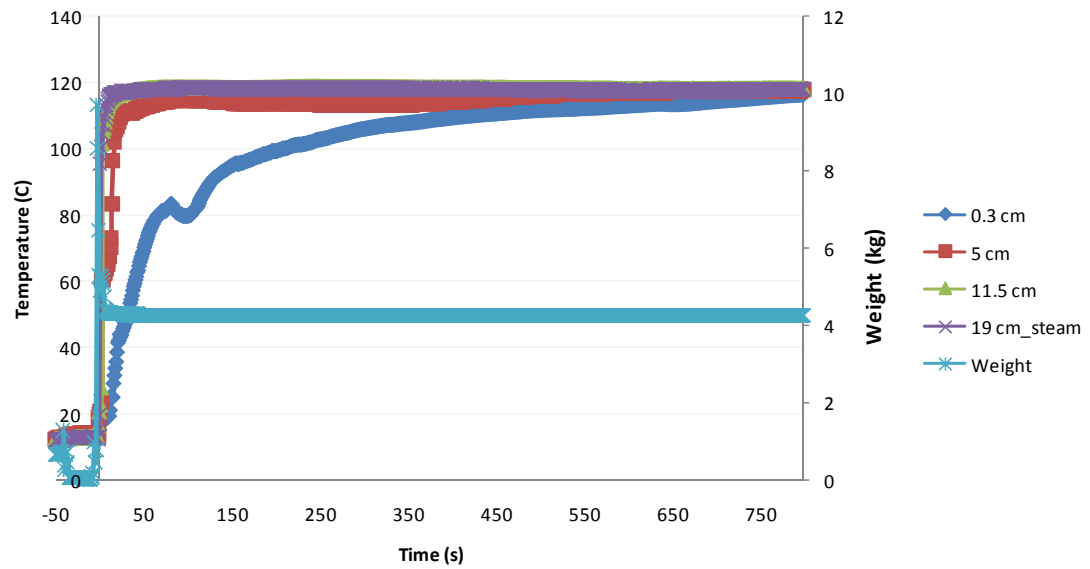
Figure **C-9**: Simultaneous measurement of temperature and weight in 18 cm high packed bed. Glass Beads size: 5 mm. Data is plotted from -50 to 800 s with time zero being when water table falls to bed surface.

APPENDIX D

MODEL VERIFICATION FOR MASS FLOW IN PACKED BED

D.1 Bed Depth of 27 cm
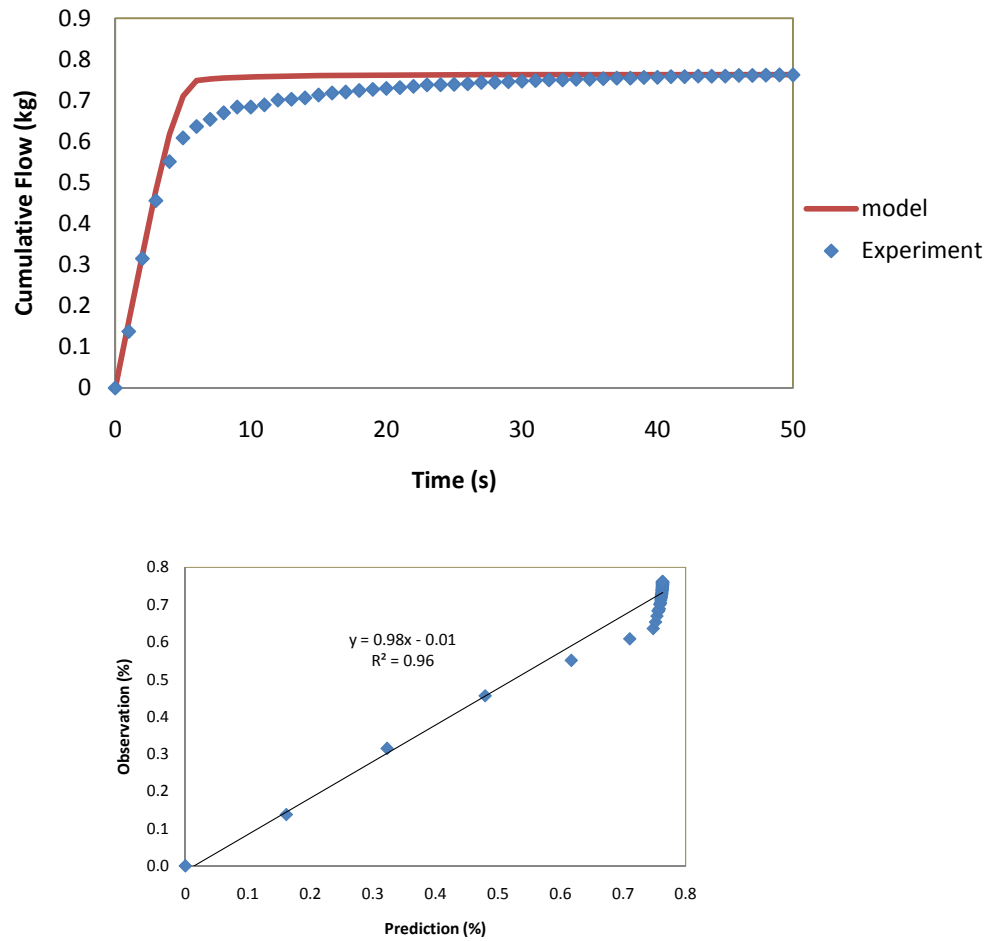
D.1.1 Cumulative Mass Flow in Packed Bed

Figure **D-1**: Comparison between predicted and observed data for cumulative water flow through 27 cm depth of packed bed from 3 mm glass beads. RMSE= 0.04%.
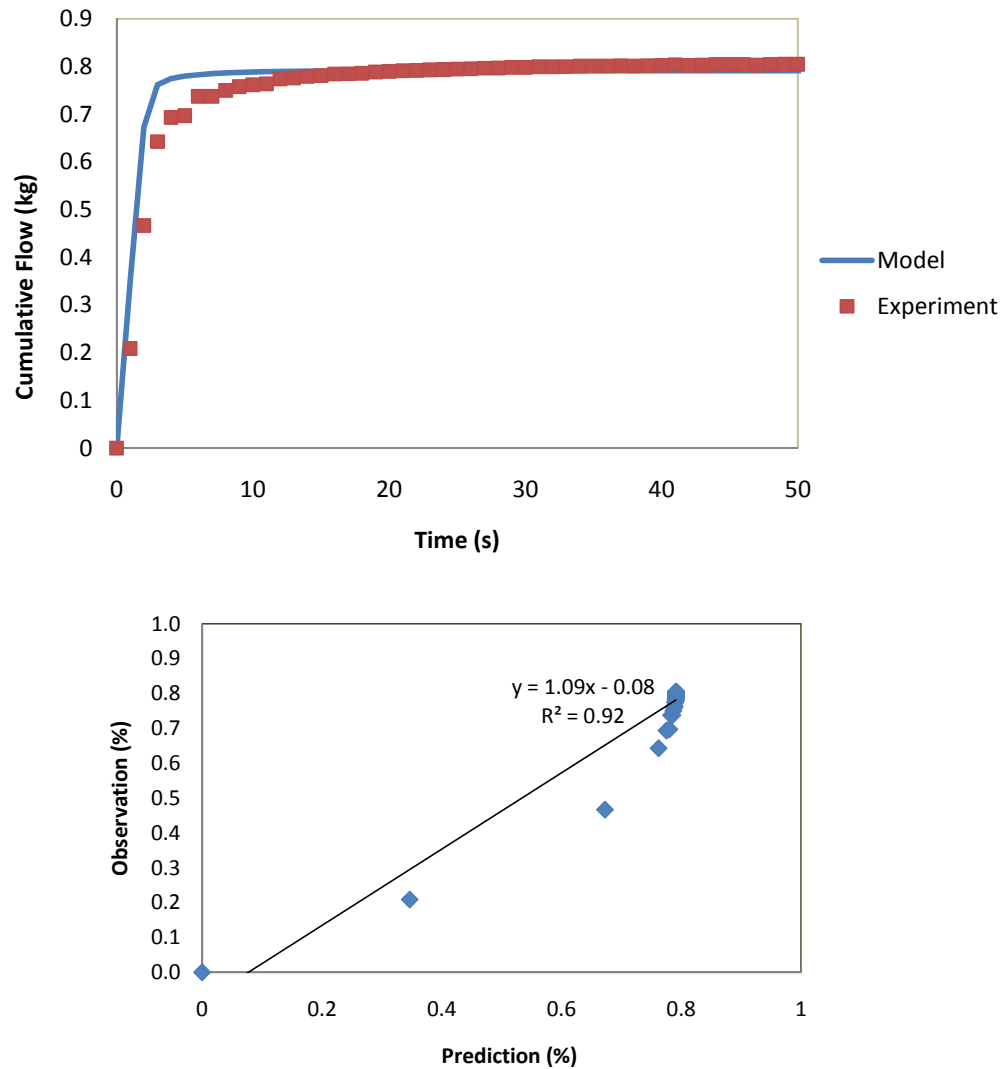
Figure **D-2**: Comparison between predicted and observed data for cumulative water flow through 27 cm depth of packed bed from 5 mm glass beads. RMSE= 0.04%.
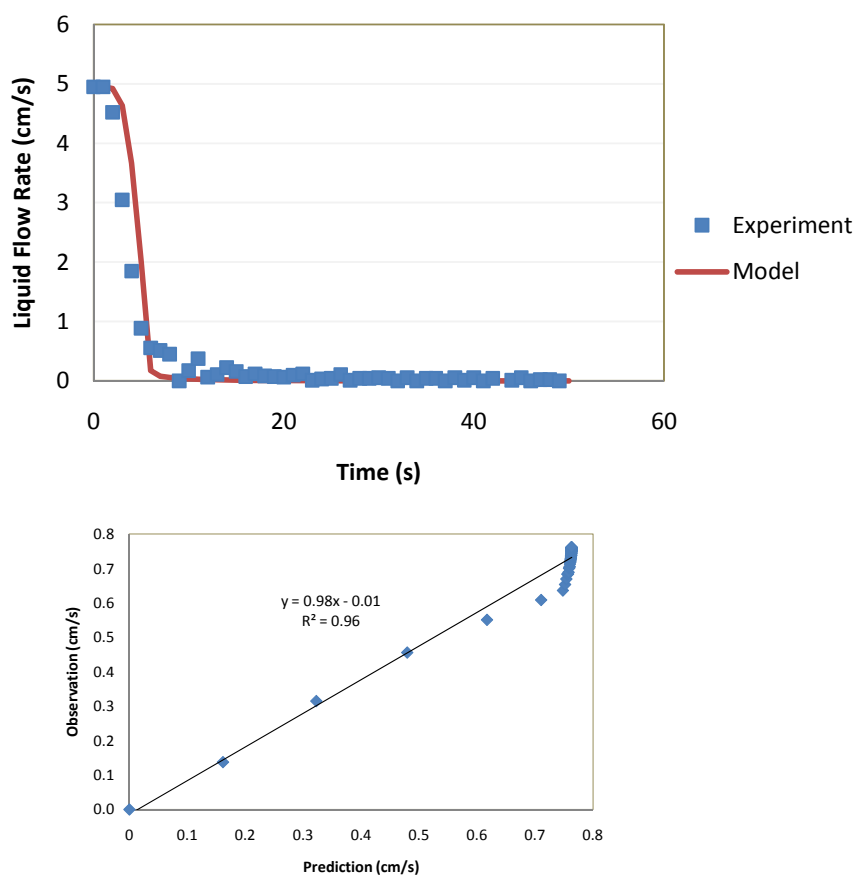
D.1.2 Mass Flow Velocity in Packed Bed

Figure **D-3**: Comparison of liquid flow velocity versus time from predicted and observed data in 27 cm depth of packed beds of 3 cm glass beads. RMSE=0.40 cm/s.

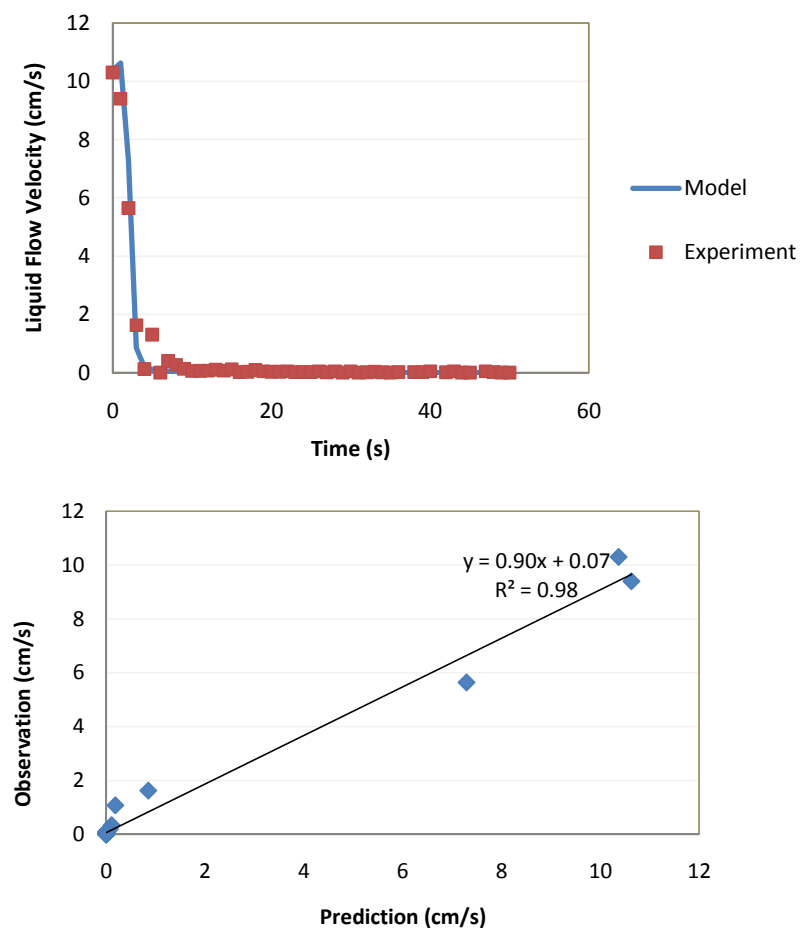Figure **D-4**: Comparison of liquid flow velocity versus time from predicted and observed data in 27 cm depth of packed beds of 5 cm glass beads. RMSE=0.34 cm/s.

D.2 Bed Depth of 18 cm

D.2.1 Cumulative Mass Flow

Figure **D-5**: Comparison between predicted and observed data for cumulative water flow through 18 cm depth of packed bed from 3 mm glass beads. RMSE=0.45kg.
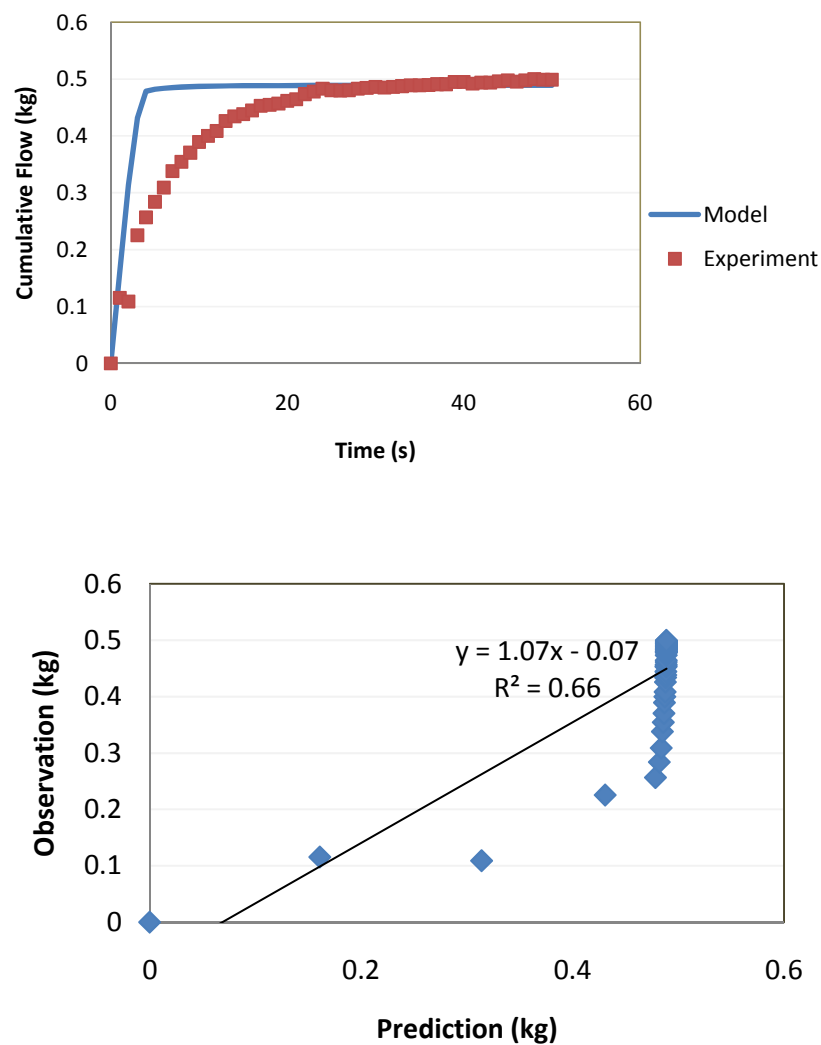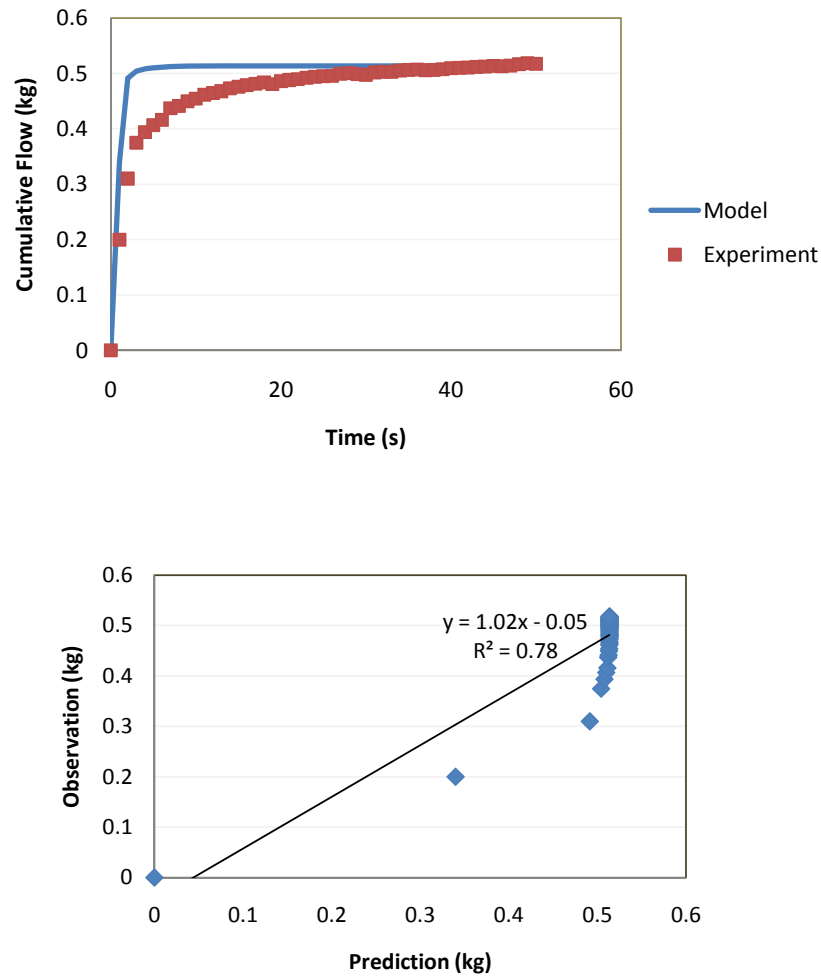
Figure **D-6**: Comparison between predicted and observed data for cumulative water flow through 18 cm depth of packed bed from 5 mm glass beads. RMSE=0.05 kg.

D.3 Mass Flow Rate

Figure **D-7**: Comparison of liquid flow velocity versus time from predicted and observed data in 18 cm depth of packed bed from 3 cm glass beads. RMSE=0.30 cm/s.
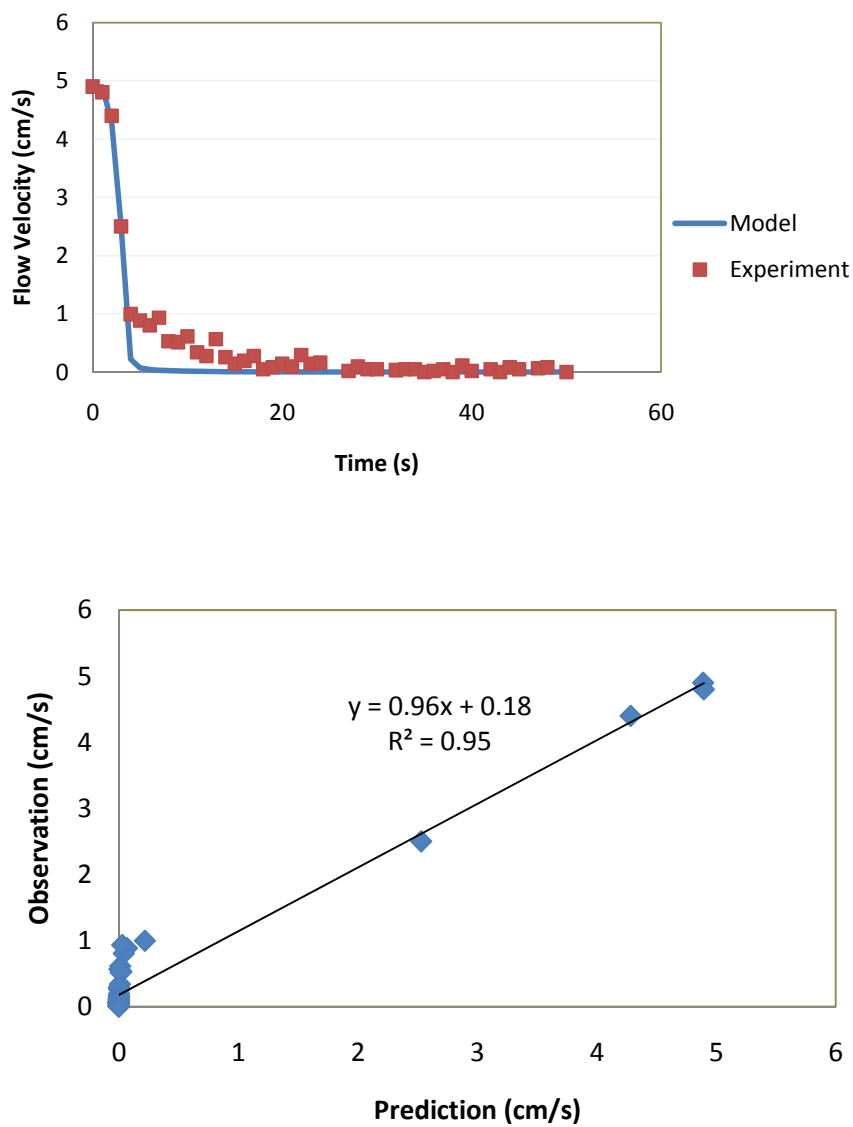
Figure **D-8**: Comparison of liquid flow velocity versus time from predicted and observed data in 18 cm depth of packed bed from 5 cm glass beads. RMSE=0.58 cm/s.
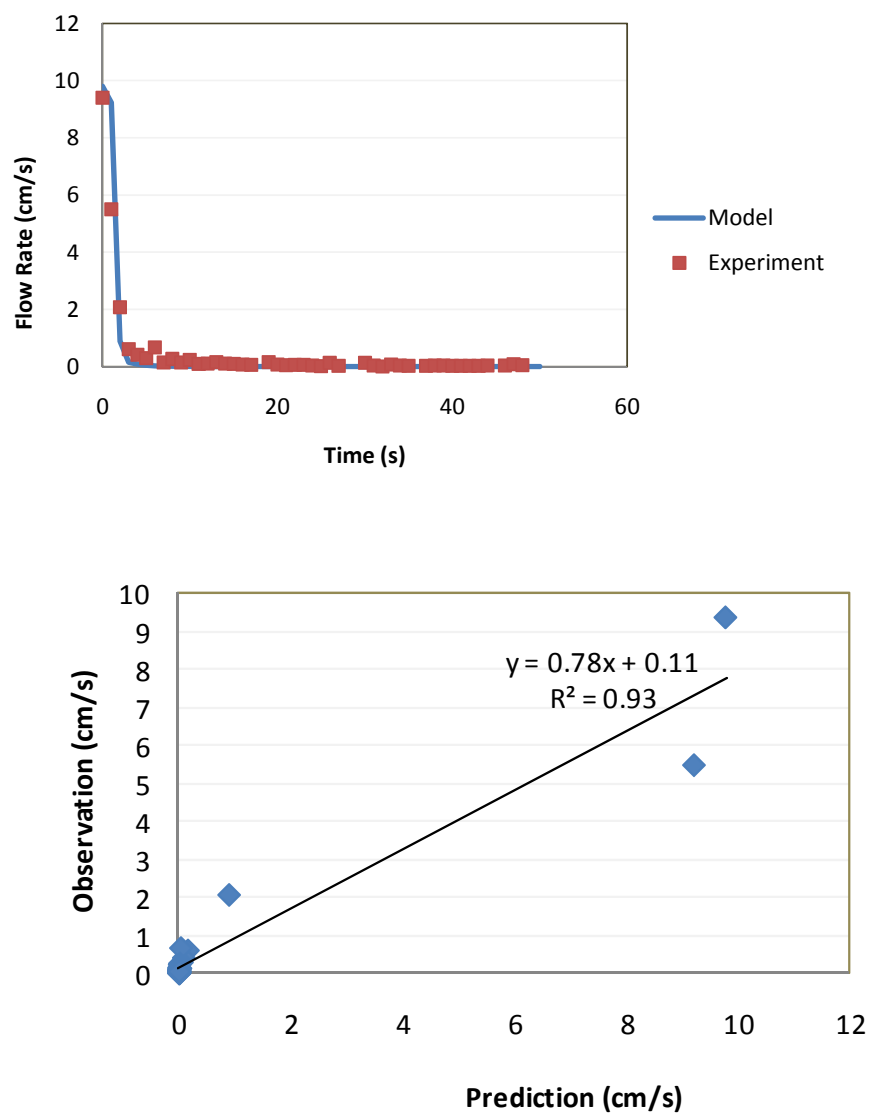
APPENDIX E

PARTIAL LIST OF PARAMETER VALUES FOR FINITE-DIFFERENCE MODEL

Table **E-1**: Parameters for UFZ (for 2 mm glass beads) in Finite Difference Model.

Variable Name	Symbol	Value										Unit	Equation
Height of unsaturated zone	Hu	0.1758										m	=H-Hc
Volume per layer	VL	6.23034E-05										m3	=Hu*Ac/Nl
Initial water volume per layer	MiL	2.86505E-05										m3	=Vl*por
Initial water weight per layer	Win	0.02744144										m	=MiL*rhol
Shell number of particle	Nsh	10											
Shell thickness	dr	0.00025										m	=Dp/Nsh/2
Number of glass beads per layer	NgbL	514.1793093											=Vl*(1-por)/Vp
Outside radius	Ro	0.0025	0.002	0.002	0.002	0.002	0.001	0.001	8E-04	5E-04	3E-04	m	
Inside Radius	Ri	0.00225	0.002	0.002	0.002	0.001	0.001	8E-04	5E-04	3E-04	0	m	
Outside area of shell	Ash	7.85398E-05	6E-05	5E-05	4E-05	3E-05	2E-05	1E-05	7E-06	3E-06	8E-07	m2	
Mass per shell	Msh	5.10291E-05	4E-05	3E-05	2E-05	2E-05	1E-05	7E-06	4E-06	1E-06	2E-07	kg	

Table **E-2**: Thermo-dynamic parameters of CF in Finite Difference Model.

Variables	Symbol	Value	Unit
effective stagnant thermal conductivity	Kef	1.4506	$W/m^2{\cdot}K$
effective thermal diffusivity of CF	alphae	9.12043E-04	m^2/s
heat capacity of mixture	Cpm	1590.441905	$J/kg{\cdot}K$
Elemental height of capillary fringe	dy	0.0006	m
Density of mixture	Rhom	1994.448175	kg/m^3

VITA

Haijun Wu

Education

Ph.D. in Agricultural and Biological Engineering, 12/2009
The Pennsylvania State University, University Park, PA

M.S. in Biological Engineering, 06/2003
South China University of Technology, Guangzhou, P.R. China

B.S. in Fermentation Engineering, 07/1997
Shandong Institute of Light Industry, Jinan, P.R. China

Employment

Graduate Assistant, Agricultural and Biological Engineering Dept.,
The Pennsylvania State University, University Park, PA.
08/2005 – 05/2009

R&D, Heinz-Meiweiyuan (Guangzhou) Food Co., Ltd
Guangzhou, P.R. China
06/2003 – 08/2005

QC, Shenzhen Tsingtao Beer Asahi Co., Ltd
Shengzhen, P.R. China
03/2000 – 08/2000

Shandong Foreign Economic School
Yantai, P.R. China
07/1997 – 09/1999